Acidification of the Nordic Seas~~Acidification~~

Filippa Fransner[1], Friederike Fröb[1,2], Jerry Tjiputra[3], Nadine Goris[3], Siv K. Lauvset[3], Ingunn Skjelvan[3], Emil Jeansson[3], Abdirahman Omar[3], Melissa Chierici[4], Elizabeth Jones[4], Agneta Fransson[5], Sólveig R. Ólafsdóttir[6], Truls Johannessen[1], and Are Olsen[1]

[1]Geophysical Institute, University of Bergen, and Bjerknes Centre for Climate Research, Bergen, Norway
[2]Max Planck Institute for Meteorology, Hamburg, Germany
[3]NORCE Norwegian Research Centre, Bjerknes Centre for Climate Research, Bergen, Norway
[4]Institute of Marine Research, Fram Centre, Tromsø, Norway
[5] Norwegian Polar Institute, Tromsø, Norway
[6]Marine and Freshwater Research Institute, Reykjavík, Iceland

Correspondence: Filippa Fransner (filippa.fransner@uib.no)

Abstract.

~~With prevailing low temperatures,~~ Due to low calcium carbonate saturation states, and deep winter mixing ~~, and cold-water coral reefs~~that brings anthropogenic carbon to the deep ocean, the Nordic Seas ~~is~~ and their cold-water corals are vulnerable to ocean acidification. Here, we present a detailed investigation of changes in pH and aragonite saturation ~~, and its impact on cold-water corals,~~ in the Nordic Seas ~~,~~ from pre-industrial times to 2100, by using *in situ* observations, gridded climatological data, and Earth System Model (ESM) projections ~~. From pre-industrial to present, the Nordic Seas surface pH has dropped by 0.06 on average, and the aragonite saturation horizon has moved from a depth of 2500 meter to 2000m, which is well below the cold-water coral habitats. Between 1981 and 2019 pH decreased by, on average, 0.10 in the Nordic Seas surface waters. The pH drop, mainly driven by an uptake of anthropogenic CO$_2$, is significant all over~~ for three different future scenarios.

During the period of regular ocean biogeochemistry observations from 1981-2019 the pH decreased with rates of 2-3 10^{-3} yr^{-1} in the upper 200 m of the Nordic Seas~~, except in the Barents Sea Opening. We also find that the acidification has penetrated relatively deep, in some regions~~. In some regions, the pH decrease can be detected down to 2000 m ~~. This has~~ depth. This resulted in a ~~significant decrease in~~ decrease of the aragonite saturation state, which ~~are~~ now is close to undersaturation in the depth layer of 1000-2000 m~~in the modern ocean. Model projections indicate an additional surface ocean pH decrease of 0.1-0.4 until the year of 2100. In the high-emission scenario, RCP8~~. The model simulations suggest the pH of the Nordic Seas to decrease at an overall faster rate than the global ocean from preindustrial to 2100, bringing the Nordic Seas pH closer to the global average. In the esmRCP8.5 ~~, the entire~~ scenario, the whole water column is projected to be undersaturated ~~in aragonite by~~ with respect to aragonite at the end of the ~~century, threatening Nordic Seas' cold-water corals and their ecosystems. Under the emission-driven RCP4~~21st century, endangering all cold water corals of the Nordic Seas. In the esmRCP4.5 scenario~~the saturation horizon is~~, the deepest cold water coral reefs are projected to be ~~lifted to 400-800 m by the end of this century, endangering the deepest living cold-water corals~~exposed to undersaturation. Exposure of all cold-water corals to corrosive waters can only be avoided ~~under the emission-driven RCP2~~with marginal under the esmRCP2.6 scenario.

Over all time scales, the main driver of the pH drop is ~~an~~ the increase in dissolved inorganic carbon, ~~which to some extent is opposed by increasing alkalinity. Temperature and~~ followed by temperature. Thermodynamic salinity effects are of secondary importance. We find substantial changes in alkalinity and dissolved inorganic carbon as a result of the salinification of the Atlantic Water during all time periods, and as a result of an increased freshwater export in polar waters in past and future scenarios. However, the net impact of this change in freshwater content on pH is negligible, as the effect of the freshwater-driven alkalinity change is cancelled out by the effect of the freshwater-driven change in dissolved inorganic carbon that has an opposite effect on pH. The effect of the salinification in the western Nordic Seas, and the increasing freshwater export in the eastern Nordic Seas, on pH are therefore negligible.

1 Introduction

Since 1850, human activities have released 650 ± 65 Gt of carbon to the atmosphere, of which about 25% ~~have~~ has been taken up by the oceans (Friedlingstein et al., 2020) where it has been added to the pool of dissolved inorganic carbon (C_T). The increasing C_T has resulted in surface seawater pH decline of approximately 0.1 in the global ocean from pre-industrial to present-days, which corresponds to an approximately 30% increase in hydrogen ion (H^+) concentration (e.g., Doney et al., 2009; Gattuso and Hansson, 2011; Jiang et al., 2019). ~~This ocean acidification is~~ Furthermore, the decreasing pH also causes a reduction in the calcium carbonate ($CaCO_3$) saturation state (Ω). It hence poses a serious threat to ~~many marine organisms, in particular those having shells and skeletons consisting of calcium carbonate (~~marine organisms that have shells or structures consisting of $CaCO_3$~~)~~, such as pteropods and corals (Guinotte et al., 2006; Turley et al., 2007; Manno et al., 2017; Doney et al., 2020; Doo et al., 2020)~~as the pH drop also leads to a reduction in the $CaCO_3$ saturation state (Ω) of seawater~~. Depending on the CO_2 concentration pathway, future projections suggest further reductions of surface ocean pH of 0.1~~-0.4~~ -0.3 from the 1990s until the end of the 21st century ~~from the 1990s~~ (Bopp et al., 2013). While global average acidification rates for surface waters, both from pre-industrial times to ~~present~~ present-day and as projected for the future~~have been dealt with~~, are investigated in several studies (e.g. Caldeira and Wickett, 2003; Raven et al., 2005; Kwiatkowski et al., 2020), less is known about acidification rates on regional scales, especially below the surface.

The Nordic Seas, comprised of the Greenland, Iceland and Norwegian seas (Fig. 1) and bounded by the Fram Strait in the north, the Barents Sea Opening to the northeast and the Greenland-Scotland Ridge in the south, are of particular interest when it comes to ocean acidification due to ~~its~~ their specific dynamic, biogeochemical and ecosystem characteristics. The surface circulation pattern ~~(e.g. Blindheim and Østerhus, 2013; Våge et al., 2013) is characterised by the~~ of the Nordic Seas (e.g. Blindheim and Østerhus, 2013; Våge et al., 2013) is dominated by the relatively warm, saline Atlantic waters that flow northward as the Norwegian Atlantic Current in the east, mainly constrained to the Norwegian Sea, and relatively cold and fresh waters of Arctic origin flowing southward as the East Greenland Current in the west. ~~The surface waters are undersaturated~~

~~in pCO$_2$, i. e. their~~ In the Greenland and Iceland Seas, deep and intermediate water masses are formed through open-ocean convection (Våge et al., 2015; Brakstad et al., 2019). Some of these water masses ultimately overflow the Greenland-Scotland Ridge and feed into the North Atlantic Deep Water helping to sustain the lower limb of the Atlantic Meridional Overturning Circulation (AMOC, Dickson and Brown, 1994; Våge et al., 2015; Chafik and Rossby, 2019). The surface water pCO$_2$ is generally lower than that of the atmosphere, making ~~them~~ the Nordic Seas important sinks for atmospheric CO$_2$. This undersaturation ~~comes as a result of~~ results from several processes, including ~~strong~~ primary production, cooling of northward flowing Atlantic waters, and the inflow of pCO$_2$ undersaturated waters from the Arctic Ocean ~~(Olsen et al., 2008; Ólafsson et al., 2020b). In the Greenland and Iceland seas, deep and intermediate water-masses are formed through open-ocean convection. Some of these water-masses ultimately overflow the Greenland-Scotland Ridge and feed into the North Atlantic Deep Water and consequently help to sustain the lower limb of the Atlantic Meridional Overturning Circulation (AMOC, Dickson and Brown, 1994; Våge et al., 2015; Ch~~
~~The strong connection between surface and deep waters that is created through this~~ (Anderson and Olsen, 2002; Takahashi et al., 2002; Ólaf
Although the Nordic Seas are an overall sink for atmospheric CO$_2$, the direct uptake of anthropogenic CO$_2$ through air-sea CO$_2$ exchange is limited. Instead, there is a large advective supply of excess anthropogenic CO$_2$ from the south (Anderson and Olsen, 2002; Olse
contributes to the acidification. Part of the anthropogenic CO$_2$ that enters the Nordic Sea's surface waters is brought to deep waters through the deep water formation, ~~would ultimately lead to early and relatively large detection of anthropogenic carbon and acidification in the deep waters of the Nordic Seas and North Atlantic (Tjiputra et al., 2010; Perez et al., 2018), which could have negative impacts on their cold-water coral reefs. Due to~~ from where it is slowly advected to the North Atlantic Ocean (Tjiputra et al., 2010; Perez et al., 2018). The deep reaching anthropogenic CO$_2$, in combination with the prevailing low temperatures ~~, the Nordic Seas already have naturally~~ that give low saturation states of CaCO$_3$ (Ólafsson et al., 2009; Skjelvan et al., 2014), ~~making their~~ make the cold-water coral reefs of the Nordic Seas particularly exposed to ocean acidification(Kutti et al., 2014).

There has been extensive research on changes in the carbonate system and pH in the Nordic Seas, facilitated by the many research and monitoring cruises in the area ~~(e.g., Bellerby et al., 2005; Olsen et al., 2006; Ólafsson et al., 2009; Skjelvan et al., 2008; Chieric~~
~~Acidification~~ (e.g., Olsen et al., 2006; Ólafsson et al., 2009; Skjelvan et al., 2008; Chierici et al., 2012; Skjelvan et al., 2014; Jones et al., 2
Between the 1980s and 2010s, the pH has been shown to decrease with rates of -0.0023 to -0.0041 y^{-1} ~~have been observed~~ in surface waters, which is greater than expected from the increase in atmospheric CO$_2$ alone (Ólafsson et al., 2009; Skjelvan et al., 2014). This is consistent with the many observations that have indicated a weakening of the pCO$_2$ undersaturation of the Nordic Seas surface waters, i.e., that surface ocean pCO$_2$ ~~, which is closely related to pH,~~ has risen faster than the atmospheric pCO$_2$ (Olsen et al., 2006; Skjelvan et al., 2008; Ólafsson et al., 2009), ~~i. e. a weakening of the p~~over the past decades. The future pH of the Nordic Seas have been assessed with different modelling approaches (Bellerby et al., 2005; Skogen et al., 2014, 2018). Bellerby et al. (2005) investigated the impact of climate change on the Nordic Seas CO$_2$ system under a doubling of the atmospheric CO$_2$ ~~undersaturation~~ to a value of 735 ppm. It was done by combining observed relationships between the inorganic CO$_2$ system and temperature and salinity, with output of ocean physics from the Bergen Climate Model. They found the pH to decrease by about 0.3, with the largest decrease taking part in the polar waters of the eastern Nordic Seas. For the future scenario A1B (see Meehl et al., 2007), which assumes approximately 700ppm atmospheric CO$_2$ by the year 2100,

Skogen et al. (2014) found that the pH of the Nordic Seas surface waters ~~might have occurred the past decades. Studies on present and future pH~~ decreases by 0.19 between 2000 and 2065, and that the aragonite saturation horizon shoals by 1200 m. They estimated C_T to be the overall driver of this acidification. Skogen et al. (2018) looked into future changes in the Nordic Seas ~~using both a regional and an Earth System Model have also been published (Skogen et al., 2014, 2018)~~biogeochemistry under the Representative Concentration Pathway 4.5 (RCP4.5) scenario, a stabilization future scenario used within Climate Model Intercomparison Project Phase 5 (CMIP5 Taylor et al., 2012), and found the surface pH to drop by 0.18 between 1995 and 2070.

All the studies mentioned above have been focusing on selected periods of time and scenarios, using specific datasets. There is, ~~however,~~ to our knowledge, no ~~previous work assessing acidification rates~~ work assessing pH changes and their drivers from the pre-industrial until the end of the 21st century, under different scenarios, using both observational and modelling data~~.~~

, and that provides a detailed regional perspective on the various drivers. In this study, we fill this gap by examining past, ~~present~~ present-day, and projected future ~~ocean acidification rates and changes in~~ changes in pH and aragonite saturation in the Nordic Seas, over the full water column and in different regions, by using the best available information for the various time periods. This includes a combination of *in situ* observations, gridded climatological data, and Earth System Model (ESM) projections ~~. To get a better understanding of the processes behind the acidification rates, we decompose the pH changes into their thermodynamic and chemical drivers~~for different future scenarios.

1.1 ~~pH Drivers - Theoretical Background~~

2 Drivers of pH and saturation states - Theoretical Background

The rising atmospheric CO_2 concentration ~~increases the pCO_2 difference between the atmosphere and the ocean; i.e. the oceans become more undersaturated in CO_2 with respect to the atmosphere, which~~ results in a flux of CO_2 from the atmosphere into the ocean. ~~When~~ In the ocean CO_2 ~~dissolves in seawater, it~~ reacts with water to form carbonic acid (H_2CO_3)~~:~~

$$CO_2 + H_2O \rightleftharpoons H_2CO_3$$

, which then dissociates into bicarbonate (HCO_3^-) and hydrogen ions (H^+)~~:~~

$$H_2CO_3 \rightleftharpoons HCO_3^- + H^+$$

. A large part of the resulting H^+ is neutralized by carbonate ions (CO_3^{2-}) that have been supplied to the ocean by the weathering of carbonate and silicious minerals~~:~~

$$CO_3^{-2} + H^+ \rightleftharpoons HCO_3^-$$

. Together, this forms the following equilibria:

$$CO_2 + H_2O \rightleftharpoons H_2CO_3 \tag{1}$$

$$H_2CO_3 \rightleftharpoons HCO_3^- + H^+ \tag{2}$$

$$CO_3^{-2} + H^+ \rightleftharpoons HCO_3^- \tag{3}$$

Combined, the concentration of CO_2~~($CO_{2(aq)}$)~~, H_2CO_3, HCO_3^-, and CO_3^{2-}, constitute the concentration of dissolved inorganic carbon (C_T)~~, while total alkalinity (A_T) is mostly determined by HCO_3^-, and CO_3^{2-} (carbonate alkalinity)~~. In seawater, approximately 90% of C_T exists in the form of HCO_3^-, 9% as CO_3^{2-} and 1% as CO~~$_{2(aq)}$~~$_2$.

As seen from Equations 1 - 3, the dissolution of CO_2 in seawater results in an increase in H^+ concentration, which leads to a decrease in pH~~,~~. On total scale, pH is defined as:

$$pH = -log_{10}([H^+]+[HSO_4^-]) \tag{4}$$

where HSO_4^- is sulphate. Apart from C_T, ~~seawater pH is also controlled~~ pH is influenced by temperature, salinity, and total alkalinity (A_T~~. The qualitative, instantaneous, effects of an increase in each property are shown in Table 1~~). A_T is mostly determined by HCO_3^- and CO_3^{2-} (carbonate alkalinity). Temperature and salinity ~~only~~ affect pH by altering the dissociation constants and thus the partitioning of C_T between its different constituents. ~~A_T is the sum of the concentration of bases (proton acceptors) in the seawater.~~ The relation between C_T and A_T influences ~~the~~ pH by affecting the buffer capacity of seawater. ~~Note that the relations in Table 1 are the instantaneous, or thermodynamic, effects from a change in these properties, and~~ The qualitative, direct effects of an increase in each property are shown in Table 1. Note that this Table does not consider indirect effects on pH, for example from the change in air-sea fluxes that will follow ~~,~~ from e.g.~~from ,~~, a temperature driven pCO$_2$ change (e.g. Jiang et al., 2019; Wu et al., 2019).

Table 1. Direction of ~~instantaneous~~ direct effects of an increase in temperature, salinity, C_T and A_T on pH and Ω.

Driver	pH	Ω
Temperature	-	+
Salinity	-	-
C_T	-	-
A_T	+	+

Equations ~~2 and 3 can be summarized as:~~

~~$H_2CO_3 + CO_3^{2-} \longrightarrow 2HCO_3^-$~~

~~showing that the dissolution of~~ 1 to 3 show that an increase in anthropogenic CO_2 ~~in seawater~~ and C_T results in a reduction in CO_3^{2-}. This ~~further~~ affects the saturation state of $CaCO_3$ (Ω), defined as:

$$\Omega = \frac{[Ca^{2+}][CO_3^{2-}]}{K_{sp}}, \tag{5}$$

where K_{sp} is the solubility product. When Ω is less than one, the water becomes corrosive and $CaCO_3$ ~~exists in two different forms in seawater:~~ starts to dissolve. The two most abundant forms of $CaCO_3$ in seawater are calcite and aragonite. ~~Aragonite is more soluble than calcite, with a higher K_{sp}.~~ The saturation state of aragonite (Ω_{Ar}) is ~~therefore~~ lower than that of calcite (Ω_{Ca}) ~~at a given place and time. When Ω is less than one, the water is corrosive and $CaCO_3$ dissolves.~~ as aragonite is more soluble than calcite, equating to a higher K_{sp}.

~~Equation 5 shows that lower concentrations of CO_3^{2-}, as induced by uptake of anthropogenic CO_2 and increase in C_T, result in a reduction in the saturation state.~~ The impact of C_T on the saturation state is ~~also~~ seen in the spatial distribution of Ω in the surface ocean, which broadly follows temperature gradients (e.g. Orr, 2011; Jiang et al., 2019). The reason behind this temperature dependency is the higher CO_2 solubility of colder waters~~that give them the capacity to absorb more CO_2 at a given atmospheric pCO_2, which decreases the CO_3^{2-} concentration~~. Consequently, cold waters ~~also~~ have a relatively low Ω_{Ar} and Ω_{Ca} and are ~~thus~~ more vulnerable to acidification. ~~Apart from C_T,~~ Ω is also influenced by A_T, temperature and salinity, as shown in Table 1.

The sensitivity of pH and Ω to ~~uptake of~~ an anthropogenic CO_2 increase is dependent on the buffer capacity of the seawater ~~that is largely determined by the concentration of carbonate ions CO_3^{2-}~~(e.g. Sarmiento and Gruber, 2006; Orr, 2011). Waters with ~~higher concentrations of CO_3^{2-}~~a higher buffer capacity, i.e.~~a higher buffer capacity,~~ higher concentrations of CO_3^{2-}, have the capability of converting a larger fraction of the absorbed CO_2 into bicarbonate. A smaller fraction remains as dissolved CO_2, implying a smaller increase in the seawater pCO_2. These waters therefore have the capability of absorbing more CO_2 for any given increase in atmospheric pCO_2 (assuming a uniform increase in pCO_2 between ~~water-masses~~water masses), which also implies a larger decline in $CaCO_3$ saturation state. ~~The drop in pH~~ pH is, on the ~~other hand, is larger~~ contrary, decreasing more in waters with lower ~~CO_3^{2-} concentration as they have less ability to neutralise the carbonic acidsince their buffer capacity is lower~~buffer capacity as they are less effective in neutralising carbonic acid.

3 Data~~and methods~~

3.1 ~~Data~~Observational data

3.1.1 ~~Observational data~~

~~This study makes use of~~ As observational data, we used C_T, A_T, temperature, salinity, phosphate, and silicate data collected between 1981 and 2019 during dedicated research cruises, at two time-series stations, and in the framework of the Norwegian program "Monitoring ocean acidification in Norwegian waters". Sampling locations are shown in Fig. 1.

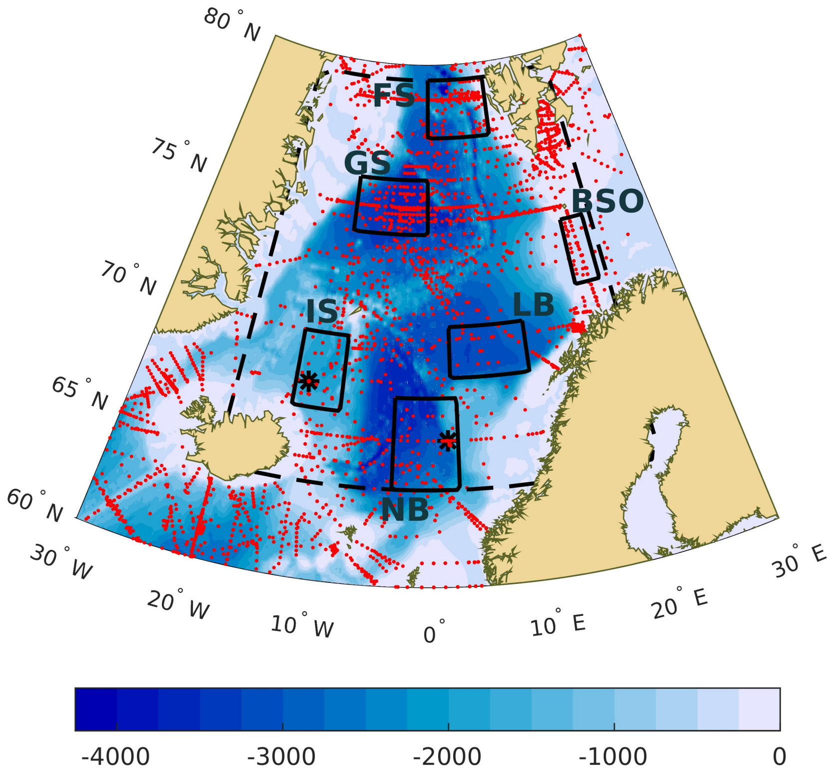

Figure 1. Map of the Nordic Seas with sampling locations (~~magenta~~red). Also shown are the locations of the six regions where trends have been analyzed separately (rectangles)~~;~~, that is BSO: Barents Sea Opening; FS: ~~Eastern~~ eastern Fram Strait; GS: Greenland Sea; IS: Iceland Sea; LB: Lofoten Basin ~~;~~ and NB: Norwegian Basin. The dashed line marks the borders of the area that we define as the Nordic Seas. The asterisk markers in the Norwegian Basin and the Iceland Sea show the positions of Ocean Weather station M and the Iceland Sea time-series station, respectively. The filled contours illustrate the bathymetry at 250 m intervals.

Data from 28 research cruises (Brewer et al., 2010; Anderson et al., 2013a, b; Anderson, 2013a, b; Bellerby and Smethie, 2013; Johannessen and Golmen, 2013; Johannessen, 2013a, b; Johannessen and Simonsen, 2013; Johannessen and Olsen, 2013; Johannessen et al., 2013c, a, b; Jones et al., 2013; Olsen et al., 2013; Olsen and Omar, 2013; Omar and Olsen, 2013; Omar and Skogseth, 2013; Omar, 2013; Pegler et al., 2013; Skjelvan et al., 2013; Wallace and Deming, 2014; Lauvset et al., 2016; Tanhua, 2017; Jeansson et al., 2018; Marcussen, 2018; Schauer et al., 2018) in the Nordic Seas were extracted from the GLODAPv2.2019 data product, which provides bias-corrected, ~~cruise based~~cruise-based, interior ocean data (Olsen et al., 2019). The GLODAPv2 data product is considered consistent ~~to~~ among cruises within 0.005 for salinity, 2% for silicate , 2% for phosphate, and 4 μmol kg^{-1} for both C$_T$ and ~~4 μmol kg^{-1} for~~ A$_T$ (Olsen et al., 2019).

~~The time-series~~ Time-series data are from ~~the Norwegian Sea (~~Ocean Weather Station M ~~) and~~ in the Norwegian Sea, and from the Iceland Sea. The data from the Ocean Weather Station M, located at 66 °N and 2 °E, have been described in Skjelvan et al. (2008). At this station, sampling at 12 depth levels between surface and seabed (2100 m) was carried out each month between 2002 and 2009, and 4-6 times each year between 2010 and 2019. ~~Here~~For these data, the uncertainty related to the ~~sample data~~ measurements is 0.001 for salinity, 0.7 μmol kg^{-1} for silicate, 0.06 μmol kg^{-1} for phosphate, and 2 μmol kg^{-1} for C_T and ~~2 μmol kg^{-1} for~~ A_T. The time-series station in the Iceland Sea, covering the period of 1985-2019, is situated at 68 °N and 12.67 °W. It is visited approximately 4 times a year and samples are taken at 10-20 depth levels between surface and seabed (1900 m). The uncertainty related to the ~~sampled data~~ measurements at this station is 0.005 for salinity, 2% for silicate, 2% for phosphate, and 4 μmol kg^{-1} for both C_T and ~~4 μmol kg^{-1} for~~ A_T. These data have been described in Ólafsson et al. (2009).

The data from the program "Monitoring ocean acidification in Norwegian waters" ~~covers the period 2011-2019 (2011-2012 Tilførselsprogrammet and 2013-2019 Havforsuringsprogrammet) and are based on water column stations along repeat~~ were sampled in the full water column along repeated sections in the Nordic Seas ~~(Chierici et al., 2012, 2013, 2014, 2015, 2016, 2017; Jones et a~~ ~~Analytical methods for C_T and A_T follow the Dickson et al. (2007) and accuracy and precision is controlled by Certified Reference Materials (CRM), and by participation in international intercomparison studies (e.g. Bockmon and Dickson, 2015)~~in the period 2011-2019 (Chierici et al., 2012, 2013, 2014, 2015, 2016, 2017; Jones et al., 2018, 2019, 2020). The uncertainties related to the sampled data is 0.005 for salinity, 0.1 for silicate, 0.06 for phosphate, 2 μmol kg^{-1} for both C_T and ~~2 μmol kg^{-1} for~~ A_T.

Data ~~for the Eastern~~ from the eastern Fram Strait were collected on cruises with RV Helmer Hansen within the CarbonBridge project, and on cruises with RV Lance (Chierici et al., 2019b) organized by the Norwegian Polar Institute.

~~For~~ Analytical methods for C_T and A_T, in all datasets described above (for GLODAP after the mid 1990s), follow Dickson et al. (2007) a the accuracy and precision is controlled by Certified Reference Materials (CRM), and by participation in international intercomparison studies (e.g. Bockmon and Dickson, 2015).

For estimates of atmospheric CO_2 ~~data~~change, we used the annual mean atmospheric CO_2 mole fraction (xCO_2) from the Mauna Loa updated records, downloaded from www.esrl.noaa.gov/gmd/ccgg/trends/. Although the absolute values of atmospheric xCO_2 varies with latitude, the growth rates are the same across the globe.

3.1.1 ~~Model data~~

3.2 Gridded climatological data

Climatological distributions of pH and Ω_{Ar} were calculated from C_T, A_T, temperature, salinity, phosphate and silicate in the mapped GLODAPv2 data product (Lauvset et al., 2016). Pre-industrial pH was determined by subtracting the GLODAPv2 estimate of anthropogenic carbon from the mapped climatology of present (i.e., 2002) C_T (Lauvset et al., 2016). We assumed that the changes in the temperature, salinity and A_T of the Nordic Seas are of minor importance for changes in pH between pre-industrial times and present-day. The GLODAPv2 estimate of anthropogenic carbon have been calculated using the transit time distribution (TTD) approach. We note that we use the GLODAPv2 estimate of pre-industrial pH only for comparison with the ESM data, specifically in Fig. 4 (5.2).

3.3 Earth System Model data

For the estimates of past and future ocean acidification and saturation states under various climate scenarios, we ~~used output of~~ primarily used output from the fully coupled Norwegian Earth System Model ~~(NorESM1-ME, Bentsen et al., 2013; Tjiputra et al., 2013, 20~~ ~~well as outputs of an ensemble of ESMs that participated in the Coupled Model Intercomparison Project Phase 5 (CMIP5, Taylor et al., 2012~~ interactive atmospheric CO_2 (NorESM1-ME, Bentsen et al., 2013; Tjiputra et al., 2013, 2016). NorESM1-ME includes the dynamical isopycnic vertical coordinate ocean model MICOM (Bleck and Smith, 1990) and the Hamburg Oceanic Carbon Cycle model (HAMOCC5, Maier-Reimer et al., 2005), adapted to the isopycnic ocean model framework. ~~The~~ HAMOCC5 ~~model~~ simulates lower trophic ecosystem processes up to the zooplankton level, including primary production, remineralization and predation, and full water column inorganic carbon chemistry. ~~While the simulations of NorESM1-ME are used to get a process understanding, the ESM ensemble is used to get an estimate of model uncertainty. We chose emission-driven historical and future scenarios, rather than concentration driven ones, as only those capture the full impact of carbon cycle feedbacks (Booth et al., 2013). Specifically, we utilise~~ For our assessment, we utilised emission-driven historical ~~experiments~~ simulations for the period from 1850 to 2005 and ~~emission-driven future scenarios~~ future scenarios simulations for the period from 2006 to 2100, with focus on ~~Representative Concentration Pathways~~ RCP's 2.6, 4.5 and 8.5 (RCP2.6, RCP4.5, and RCP8.5; Meinshausen et al., 2011; van Vuuren et al., 2011a). RCP2.6 represents a mitigation scenario, RCP4.5 a stabilization scenario and ~~RCP 8.5~~ RCP8.5 a high-emission scenario. ~~While NorESM1-ME outputs are available for future scenarios with low to high emissions (RCP2~~For the emission-driven runs used here, the corresponding scenarios are named esmRCP2.6, ~~RCP4~~esmRCP4.5 and ~~RCP8~~esmRCP8.5~~), the~~. Because the emission-driven simulations prognostically simulate the atmospheric CO_2 concentration, there is normally a deviation between the atmospheric CO_2 concentrations in the esmRCP's and those prescribed in the RCP's (e.g. Friedlingstein et al., 2014). The deviation between the simulated atmospheric CO_2 concentration by NorESM1-ME and the prescribed one, and its effect on pH, is shown in Table S1 in the supplementary material. Prior to experiments, NorESM1-ME has undergone an extended spin-up procedure (>1000 years). The changes in pH, in all considered depth layers, is minor (more than one order of magnitude less) in the preindustrial control simulation compared to the historical run and the future scenarios, indicating that the impact of model drift on our results is negligible .

As a means of uncertainty assessment, we use the outputs from an ensemble of emission-driven ESMs that participated in CMIP5 ~~data-portals only contains ESM outputs for the future scenario with high emissions (RCP8.5, referred to as ‘esmrcp85’ within the data-portal). We therefore utilised~~ (Taylor et al., 2012). We chose emission-driven rather than concentration-driven scenarios, as they include the feedback of the carbon cycle on the physical climate (Booth et al., 2013) and thus give a more comprehensive estimate of the effect of model-related uncertainties on climate projections, and in particular on atmospheric CO_2, ocean carbon uptake and ocean acidification. It is well known that the inter-model spread is larger in emission-driven scenarios than in concentration-driven ones (Booth et al., 2013; Friedlingstein et al., 2014). While NorESM1-ME ~~to inform about variations in future pH-changes that are dependent on the presumed future emission strength, and our ESM-ensemble~~

~~to inform about model-dependent uncertainties in those pH-changes, albeit only~~ outputs are available for low to high future emission scenarios, the CMIP5 data-portals only contains emission-driven ESM outputs for the high ~~emission scenario~~future emission scenario (esmRCP8.5). Our ESM-ensemble ~~contains~~ consists of all ESMs that ~~have participated in~~ participated in the experiment 'esmrcp85' and RCP8.5, and whose output is publicly available in one of the CMIP5 data portals and contains all variables needed for our analysis. This results in an ensemble of ~~7 ESMs:~~ 6 ESMs; 1) CESM1(BGC) (The Community Earth System Model, version 1 - Biogeochemistry, Long et al., 2013), 2) CanESM2 (second-generation Canadian earth system model, Arora et al., 2011)) , 3) GFDL-ESM2G (Geophysical Fluid Dynamics Laboratory Earth System Model with Modular Ocean Model, version 4 component, Dunne et al. 2013a; 2013b), 4) GFDL-ESM2M (Geophysical Fluid Dynamics Laboratory Earth System Model with Generalized Ocean Layer Dynamics (GOLD) component, Dunne et al. 2013a; 2013b), 5) IPSL-CM5A-LR (L'Institut Pierre-Simon Laplace Coupled Model, version 5A, low resolution, Dufresne et al., 2013), and 6) MPI-ESM-LR (Max Planck Institute Earth System Model, low resolution, Giorgetta et al., 2013). Both for NorESM1-ME and ~~7) MRI-ESM1 (Meteorological Research Institute-Earth System Model v1, Yukimoto et al., 2011). For~~ our model ensemble, we only investigate one realisation of each scenario.

3.3.1 ~~Gridded climatological data~~

~~Climatological distributions of pH and Ω_{Ar} were calculated from the data of C_T, A_T, temperature, salinity, phosphate and silicate included in the mapped GLODAPv2 data product (Lauvset et al., 2016). The GLODAPv2 climatology of C_T is normalized to the year of 2002. It is important to mention that the GLODAPv2 climatology along the northern Greenland coast is mainly based on data from one cruise in 1993, and is therefore likely not representative for the long-term mean. We also determined pre-industrial pH by subtracting the GLODAPv2 estimate of anthropogenic carbon from the mapped climatology of present C_T (Lauvset et al., 2016) for comparison with the pre-industrial state estimate from NorESM1-ME. When doing so we assumed that the changes in the temperature, salinity and A_T of the Nordic Seas are of minor importance. The GLODAPv2 estimate of anthropogenic carbon hase been calculated with the the transit time distribution (TTD). He et al. (2018) published a thorough analysis of the different sources of uncertainty in this method, and concluded that the overall uncertainty is 7.8-13.6%. Combining this with the mapping errors Lauvset et al. (2020) estimate that the global ocean anthropogenic carbon inventory calculated from the mapped fields is 167±29 PgC. Note that the GLODAPv2 mapped pre-industrial climatology is referenced to an atmospheric CO_2 level of 280 ppm, and not to a specific time period or year. These data are only used in Fig. 4.~~

3.3.1 ~~Cold-water coral positions~~

3.4 Cold-water coral positions

To estimate the potential impact of the Nordic Seas acidification on cold-water corals, we used habitat positions in longitude and latitude from EMODnet Seabed Habitats (www.emodnet-seabedhabitats.eu) together with information on depth from ETOPO1 (NOAA National Geophysical Data Center, 2020).

3.5 ~~Methods~~

4 Methods

4.0.1 ~~Spatial drivers~~

4.1 Spatial drivers of pH and saturation states

To ~~elucidate the~~ identify drivers of observed spatial variability of surface pH and Ω_{Ar}~~distribution as extracted from the Nordic Seas in the GLODAPv2 climatology, we performed a correlation analysis with the drivers listed in Table 1. When it comes to C_T and A_T, one has to look at the combined effect, i.e. C_T/A_T. A potential correlation does not necessarily mean that there is a mechanistic relation, but can be a consequence of the contrasting properties of the Atlantic and polar waters. Therefore, in an attempt to better understand the effect of each driver~~, we calculated pH and Ω_{Ar} by ~~step by step introducing the spatially varying climatologies of the drivers~~ using spatially varying GLODAPv2 climatologies of specific drivers in Table 1, while keeping all other drivers constant (set to the spatial mean value of the Nordic Seas surface waters). ~~First, we calculated~~ Because the relation between C_T and A_T is a proxy for the buffer capacity, we decided to look at their combined effect on pH, meaning that both changes in C_T and A_T are included in the calculations. Their combined effect we from now on refer to as C_T+A_T. First, pH and Ω_{Ar} ~~by using the spatially varying temperature climatology , and keeping all other variables constant~~ were calculated with temperature being the only spatially varying climatology (pH(T), Ω_{Ar}(T)). Thereafter, we ~~repeated the same exercise with the~~ used spatially varying temperature, C_T and A_T climatologies to ~~get~~ calculate pH(T, C_T, A_T) and Ω_{Ar}(T, C_T, A_T). Finally, ~~we added~~ the salinity variability ~~to get~~ was added to estimate pH(T, C_T, A_T,S) and Ω_{Ar}(T, C_T, A_T, S). ~~We started with temperature because it has an initial thermodynamic effect on pH and~~ To estimate the constribution of each driver, the pH and Ω_{Ar} ~~, and a subsequent, secondary, effect from the resulting air-sea CO_2 exchange and change in C_T/A_T. Salinity was chosen as the last variable due to the minor effect it has on~~ fields calculated with the different spatially varying drivers were thereafter correlated with the actual pH and Ω_{Ar} ~~.~~

4.1.1 ~~pH changes and its drivers~~

~~It is important to keep in mind that changes in pH represents a relative change, and that pH trends are therefore not directly comparable across water-masses with large differences in mean pH (Fassbender et al., 2021). In these cases, it is preferable to evaluate changes in H^+ concentration that represents an absolute change (Kwiatkowski and Orr, 2018). However, pH variations in~~ of the Nordic Seas~~are relatively small, and we have therefore decided to use pH in this study~~.

~~Present~~

~~Measurements of~~

4.2 Temporal drivers of pH change

4.2.1 Present-day observational change

Measurements of temperature, salinity, C_T, and A_T ~~, temperature, salinity~~ (Figs. ~~S1-S4)phosphate~~ S1-S4), phosphate, and silicate from the data sets described in Sect. 3.1.1 were used to calculate pH ~~(on total scale)~~ and Ω_{Ar}, ~~at in situ temperature and pressure,~~ using CO2SYS for MATLAB (Lewis and Wallace, 1998; van Heuven et al., 2011). pH was calculated on total scale at at in situ pressure and temperature. Wherever nutrient data were missing, silicate and phosphate concentrations were set to 5 μmol kg^{-1} and 1 μmol kg^{-1}, respectively, which are representative values for the Nordic Seas. For the CO2SYS calculations~~we used~~ , the dissociation constants of Lueker et al. (2000), the bisulfate dissociation constant of Dickson (1990) and the borate-to-salinity ratio of Uppström (1974) were used. This ratio has recently been shown to be suitable for the western Nordic Seas (Ólafsson et al., 2020a).

~~Present day~~ Present-day trends (1981-2019) in pH, and Ω_{Ar} were determined for six different regions in the Nordic Seas: the Norwegian Basin (NB), the Lofoten Basin (LB), the Barents Sea Opening (BSO), ~~Eastern~~ eastern Fram Strait (FS), the Greenland Sea (GS) and the Iceland Sea (IS) (Fig. 1). These regions were chosen ~~not only~~ based on the data-availability~~(they are~~ , being centered around stations and sections where repeated measurements are taken~~)~~, but also ~~in order~~ to get a representation of the main surface ~~water-masses~~ water masses of the Nordic Seas. ~~The~~ In the surface, the Norwegian Basin, Lofoten Basin, and Barents Sea Opening are ~~all under the influence of~~ influenced by relatively warm and salty northward flowing Atlantic Water, while the Greenland and Iceland ~~seas are more~~ Seas are influenced by relatively cold and fresh southward flowing polar waters. ~~The Fram Strait is an area that in the surface is under influence of Atlantic Water in the eastern part,~~ As the Fram Strait surface is influenced by Atlantic and polar waters~~in the western part. In order to minimize the aliasing effects of latitudinal and longitudinal gradients, the geographical range of each region was kept as small as possible. For example, the boundaries of~~ , we constrain the Fram Strait box ~~are constrained~~ to the east ~~, in order~~ (hereinafter referred to as eastern Fram Strait) to ensure that ~~this mostly represents the influence of Atlantic Waters, and we therefore refer to is as the Eastern Fram Strait.~~ it mostly represents Atlantic Waters. The geographical range of each regional box is kept small so that aliasing effects of latitudinal and longitudinal gradients are minimized.

Regional trends were computed from annual means for five different depth intervals (0-200, 200-500, 500-1000, 1000-2000, and 2000-4000 m) using linear regression. ~~Although summer mixed layer depths generally isshallower than 200 m, a thickness of~~ The relatively thick upper layer was chosen to keep all depths influenced by the seasonal cycle in one layer, that is, to minimize the number of layers where the trends may be affected by seasonal undersampling. As the winter mixed layer reaches approximately 200 ~~m was used for the surface layer since this~~ m (e.g. Skjelvan et al., 2008), this depth sets the approximate lower limit for the ~~influence~~ impact of seasonal variations~~associated with, e.g., primary production (e.g. Skjelvan et al., 2008)~~. The significance of the trends (at 95% confidence level), were determined from the p-value of the t-statistic ~~,~~ (as implemented in MATLAB's fitlm function). For the comparison of trends, ~~we determined~~ 95% confidence intervals of the slopes were determined by the use of the Wald method (as implemented in MATLAB's fitlm and coefCI functions).

The observed long-term changes in pH were decomposed into contributions from changes in temperature (T), salinity (S), C_T and A_T (Figs. ~~S1-S4~~S1-S4, and Tables S2-S5), following the ~~proceedure~~ procedure of Lauvset et al. (2015). First, the effect of each of these processes on the CO_2 fugacity (fCO_2) is determined following Takahashi et al. (1993)~~and Metzl et al. (2010)~~:

$$\frac{dfCO_2}{dt} = \frac{\partial fCO_2}{\partial T}\frac{dT}{dt} + \frac{\partial fCO_2}{\partial S}\frac{dS}{dt} + \frac{\partial fCO_2}{\partial C_T}\frac{dC_T}{dt} + \frac{\partial fCO_2}{\partial A_T}\frac{dA_T}{dt} \tag{6}$$

~~Second~~The long-term mean values for the sensitivities (the fCO_2 partial derivatives) were approximated as in Fröb et al. (2019). Changes in A_T and C_T are driven by biogeochemical processes, transport, mixing and dilution or concentration by freshwater fluxes, which is in direct proportion to the dilution or concentration of salinity. The freshwater-effect can be separated by introducing salinity-normalized C_T (sC_T) and A_T (sA_T) (Keeling et al., 2004; Lovenduski et al., 2007):

$$sC_T = \frac{S_0}{S}(C_T - C_0) + C_0; \qquad sA_T = \frac{S_0}{S}(A_T - A_0) + A_0 \tag{7}$$

Here we set S_0 to 35 (Friis et al., 2003) and used the intercept of Eq. 6 and 7 in Nondal et al. (2009) as the non-zero freshwater end-member (A_0 and C_0). Substituting A_T and C_T in Eq. 6 by Eqs. 7 yields:

$$\frac{\partial fCO_2}{\partial C_T}\frac{dC_T}{dt} = \frac{sC_T - C_0}{S_0}\frac{\partial fCO_2}{\partial C_T}\frac{dS}{dt} + \frac{S}{S_0}\frac{\partial fCO_2}{\partial C_T}\frac{dsC_T}{dt} \tag{8}$$

$$\frac{\partial fCO_2}{\partial A_T}\frac{dA_T}{dt} = \frac{sA_T - A_0}{S_0}\frac{\partial fCO_2}{\partial A_T}\frac{dS}{dt} + \frac{S}{S_0}\frac{\partial fCO_2}{\partial A_T}\frac{dsA_T}{dt} \tag{9}$$

Subsequently, the magnitude of each fCO_2 driver is converted to $[H^+]$ by using Henry's law ($[CO_2] = k_0 \times fCO_2$) and the expression for $d[H^+]/d[CO_2]$ ~~(equation 1.5.87 Zeebe and Wolf-Gladrow, 2001)~~from equation 1.5.87 (Zeebe and Wolf-Gladrow, 2001):

$$\frac{d[H^+]}{dt} = \frac{d[H^+]}{d[CO_2]}\frac{k_0 \times dfCO_2}{dt} \tag{10}$$

Finally, ~~we converted it~~ H^+ in equation 10 was converted to pH by acknowledging that ~~$dpH = -(H^+ln(10))^{-1}dH^+$.~~

~~We additionally made a decomposition of the A_T and C_T drivers into a freshwater component and a biogeochemical component (Supplementary material, Sect. 1). The freshwater drivers of A_T and C_T are typically of similar magnitude and opposite sign, and consequently cancel each other. We therefore decided to stay with the more simple decomposition as shown in Eq. 6. The only exception is discussed in Sect. 5.2~~$dpH = -([H^+]\ln(10))^{-1}d[H^+]$. Here we consider the sulphate in Eq. 4 to be negligible, and did therefore not include it.

To ~~understand~~ control whether the observed pH changes are consistent with the changes in atmospheric CO_2, we additionally determined the pH change that can be expected in seawater where the pCO_2 perfectly tracks the atmospheric pCO_2 (pH_{perf})

~~was determined~~ for each region. This was achieved by adding the observed change in atmospheric xCO_2 to the local mean $p$$CO_2$ for the first year with observations, and then calculating the pH with CO2SYS with the local temperature, salinity, A_T, phosphate and silicate and their respective changes as inputs. We ~~did not make any~~ applied no corrections for water vapour and atmospheric pressure ~~because~~ as the rates of change for xCO_2 and pCO_2 are ~~the same~~proportional. Any deviation between observed pH change and pH_{perf} is a consequence of changes in seawater $p$$CO_2$ that are smaller/larger than in the atmosphere, i.e., a change in the air-sea $p$$CO_2$ difference.

~~**Past and future**~~

4.2.2 Model- and observation-based past and future changes

As described in Sect. 2, the total change in pH and saturation states does not only depend on local changes in C_T, A_T, temperature, salinity, and nutrients, but also on the initial buffer capacity of the seawater. ~~ESMs are~~ For the calculation of past and future pH changes, we use ESM data, which is usually biased, i.e., there is an offset between modelled fields and reality and this also holds for the buffer capacity. In particular, NorESM1-ME has high A_T and low C_T relative to observations in deep waters, leading to ~~a~~ biased high pH (Fig. ~~S5~~S5) and saturation states (not shown). To alleviate this bias in our analysis of past and future pH and Ω_{Ar}, we applied the modelled ~~rates of~~ change of temperature, salinity, C_T, A_T, phosphate and silicate to the gridded GLODAPv2 climatology. ~~From this~~ Here, the modelled change between pre-industrial, present-day and future were calculated as differences between 10-year means; i.e., 1850-1859, 1996-2005 and 2090-2099, respectively. We note that we could not center our present-day 10-year mean around the year 2002 to which the GLODAPv2 climatology is normalized as the future scenarios start in 2006. After we obtained past and future states of ~~these properties , which were used to calculate the~~ the properties listed above, we calculated past and future pH, Ω_{Ar} and Ω_{Ca} in CO2SYS. Similar procedures have been used by Orr et al. (2005) and Jiang et al. (2019) ~~for the calculation of future pH . The modelled rates of change from present to future and past to present were calculated as the difference between the time period of 2090-2099 and 1996-2005,~~ to calculate future pH. Additionally, we used this methodology to calculate the drivers of past-to-present and ~~1996-2005 and 1850-1859 (10-year means)~~ present-day-to-future pH changes, following the methodology described in the previous section. Here we used a value of zero for the freshwater end members A_0 and C_0 as NorESM1-ME does not include any riverine input of A_T and C_T.

To estimate the impact of acidification on the cold-water corals of the Nordic Seas, we calculated the mean saturation state in our region east of 0 °E, and south of 64 °N, for P.I., present day and for the future under the esmRCP2.6, ~~respectively. Because the historical runs end at 2005, and thereafter are branched into future scenarios, we could not center our 10 year means around 2002, the year to which the GLODAPv2 climatology is normalized~~esmRCP4.5 and esmRCP8.5 scenarios. The exclusion of the western and northern parts was done to constrain the mean to the Atlantic Water where the cold-water corals are located. The saturation horizon was defined as the deepest vertical grid cell where $\Omega_{Ar} > 1$.

In order to facilitate a comparison with other model-based acidification studies, we have chosen to present the past and future changes for the surface ocean (i.e., 0 m) in Sect. 5.3 and 5.5. However, in Sect. 5.2, where the observed changes of the upper

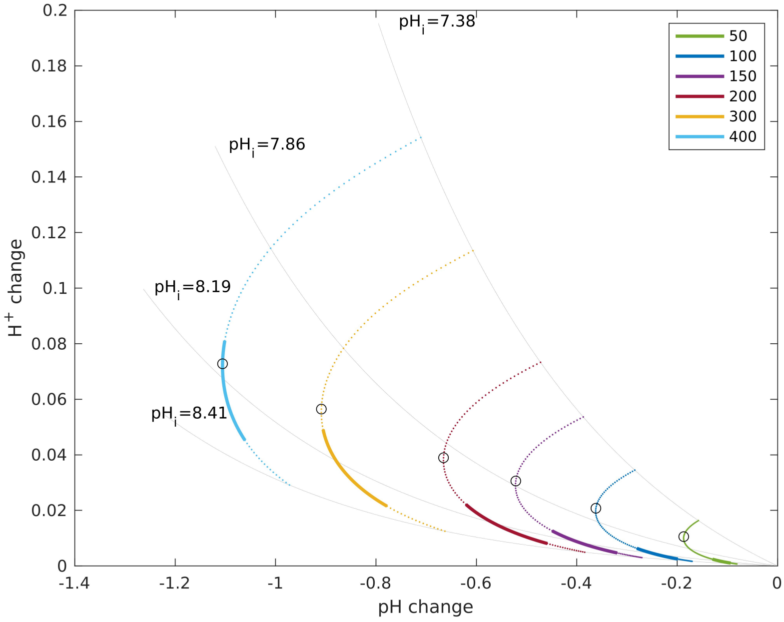

Figure 2. H^+ change plotted against pH change for six different increases in C_T (colored lines), for a range of initial pH. The upper and lower ends of the colored lines represents an initial pH of 7.38, and 8.41, respectively. The bold part of the lines represents the pH range in the Nordic Sea surface water in the GLODAPv2 climatology. The circles are plotted at the initial pH where the initial and final C_T over A_T ratio are centered around 1.

200 m are put into perspective to past and future changes, we have calculated and presented the model mean over the upper 200 m.

~~The methodology for calculating pHdrivers described in the previous section was also used for calculating the drivers of past (1850-1859 to 1996-2005) and future (1996-2005 to 2090-2099) pHchanges, using the changes in temperature, salinity~~

4.3 pH or H^+ change?

In a recent publication, Fassbender et al. (2021) recommend to analyze changes in H^+ concentrations in addition to changes in pH, when comparing pH trends across water masses with different initial pH. The underlying reason is that a change in pH represents a relative change, and that it is possible to obtain the same pH changes across water masses with different change in H^+ concentration. We estimated the sensitivity of our results to the choice between pH and H^+ by plotting the change in H^+ concentration against the change in pH, ~~A~~for a given change in C_T ~~and~~ at various initial pH. The different initial pH were obtained by varying the C_T over A_T ratio, and the calculations were done with a temperature and salinity of 5°C and 35, respectively. For a given increase in C_T below 200 μmol kg^{-1}, we see that the relationship between the H^+ and pH change is approximately linear in the Nordic Seas. The maximum C_T ~~data from NorESM1-ME output together with the climatological~~

~~values from GLODAPv2~~change in this study amounts to 170 μmol kg^{-1} in the surface waters under the esmRCP8.5 scenario. The choice between pH or H$^+$ therefore has little impact on our results. The linear relationship breaks down, if pH decreases as a result of an increasing C$_T$ over A$_T$ ratio. The maximum pH change takes place at the buffer minimum, which is close to where C$_T$=A$_T$, approximately at (pK1+pK2)/2 (Frankignoulle, 1994; Fassbender et al., 2017; Middelburg et al., 2020), which in our example is at pH 7.6. The linear relationship between the H$^+$ and pH change does therefore not hold for pH ranges where relatively low initial pH values are included, as is the case for the examples in Fassbender et al. (2021), as well as for larger C$_T$ changes. In these cases it is more appropriate to use H$^+$ for diagnosing ocean acidification.

4.3.1 ~~Uncertainty analysis~~

4.4 Uncertainty analysis

There are several sources of uncertainties (σ) involved in our calculations of pH and Ω: measurement uncertainty (σ_{mes}), mapping uncertainty (σ_{map}) for the gridded product, and uncertainties related to dissociation constants (σ_{Kx}) used in the CO2SYS calculations. To estimate the total uncertainties in our calculations of pH and Ω~~resulting from these~~, we used the ~~uncertainty~~ error propagation routine in the MATLAB version of CO2SYS (Orr et al., 2018). The uncertainties in the input parameters (A$_T$, C$_T$, temperature, salinity, phosphate and silicate) were set to σ_{mes} for the single measurements, and $\sqrt{\sigma_{mes}^2+\sigma_{map}^2}$ for the mapped product ~~and for the~~ as well as for past and future estimates. As σ_{mes} ~~we used the estimated uncertainties~~ and σ_{map}, the product consistency from Olsen et al. (2019), and ~~for σ_{map} we used the mapping uncertainty~~ the mapping error (3D field) from Lauvset et al. (2016), were used, respectively. The correlation between uncertainties in A$_T$, C$_T$ were set to 0. ~~Including a~~ This is a reasonable assumption given that C$_T$ and A$_T$ are measured on different instruments using different analytical methodologies. In addition, including a positive correlation term would decrease the ~~uncertainty, and possibly overestimating the uncertainty is preferable to including a poorly constrained correlation term (Lauvset et al., 2020)~~overall uncertainty and we prefer a potential overestimation. For the dissociation constants ~~we used~~ the default uncertainties in ~~CO2SYS~~the errors.m function were used. From here on, the calculated uncertainties will be presented as ~~σ_1~~σ_{point} for discrete data, when σ_{Kx} and σ_{mes} are included, and ~~σ_2~~σ_{field} for 3D data, when σ_{Kx}, σ_{mes} and σ_{map} are included.

For the observations described in Section 3.1.1, the mean, maximum and minimum uncertainties (~~σ_1) in~~ σ_{point}) for our calculations of pH, Ω_{Ar}, Ω_{Ca} and pCO$_2$ ~~obtained from the uncertainty propagation~~ are listed in Table 2. Variations in the uncertainties arise from variations in temperature and salinity, which impact the uncertainty of dissociation constants. ~~As discussed in Orr et al. (2018), random and systematic uncertainties~~ While systematic uncertainties would tend to cancel out when calculating trends (i.e.,comparing measurements from the same location but from different times), ~~unless there are substantial changes in the local salinity and temperature~~random uncertainties would not (Orr et al., 2018). Therefore, to estimate to what extent these uncertainties could impact our trend estimates, we further investigated whether there is any trend in the uncertainties~~(Figs. S6-S7)~~. This is discussed in Sect. 5.4.

For the GLODAPv2 estimate of pre-industrial C$_T$ there is an additionnal uncertainty coming from the TTD method that was used to calculate the anthropogenic CO$_2$. He et al. (2018) published a thorough analysis of the different sources of uncertainty in this method, and concluded that the overall uncertainty is 7.8-13.6%. Combining this with the mapping errors, Lauvset et al. (2020) estim that the global ocean anthropogenic carbon inventory calculated from the mapped fields is 167±29 PgC. This results in an uncertainty of 0.02 in the pre-industrial Nordic Seas upper layer pH.

Table 2. Uncertainties (~~σ_T~~σ_{point}, mean, max and min) in pH, Ω_{Ar}, Ω_{Ca} and pCO$_2$ (μatm), calculated from the individual observations described in Section 3.1.1.

	mean	max	min
pH	0.017	0.022	0.014
Ω_{Ar}	0.085	0.174	0.037
Ω_{Ca}	0.134	0.271	0.058
pCO$_2$	14.387	53.608	5.901

In ~~our observational data~~the trends of the uppermost layer (0-200 m), there is also an uncertainty ~~in the annual mean estimates~~ related to seasonal undersampling. Most samples (about 60% in total) from the data sets described in Sect. 3.1.1 were collected during spring and summer (April-September, Figs. ~~S8-S13~~S8 -S13). The uneven sampling frequency of different seasons introduces uncertainty in the annual means of the uppermost ocean layer, and can ~~bias the~~ lead to biases in our trend estimates. Unfortunately, there are not enough data to allow for ~~deseasonalization~~ de-seasonalization in order to remove such potential biases. ~~To~~ Therefore, to get an idea of the effect of seasonal undersampling we ~~additionnaly~~ additionally calculated trends by using annual means containing samples from the productive season only, both for a longer period (April-September~~, and~~) to include both the spring bloom and the summer production, and for a shorter period (June-August~~, only~~), to include only the summer season.

~~Because a large part of this study~~ Modelled future projections are uncertain due to incomplete understanding or parameterization of fundamental processes, as well as different and unknown future carbon emission scenarios (Frölicher et al., 2016). Because this study primarily focuses on process understanding and the driving factors behind pH change, we do not consider model uncertainty in Sect. ~~5~~5.3,5.5, and 5.2.2, where the drivers of pH ~~change~~ changes in the model projections are analysed~~, here we only use the combined uncertainties of measurements and mapping.~~

~~In~~ . However, in Sect. 5.1, where the future aragonite saturation horizon is presented, we ~~additionally take into account model and scenario uncertainty. Modelled future projections are uncertain due to incomplete understanding or parameterization of fundamental processes, as well as different and unknown future carbon emission scenarios (Frölicher et al., 2016). We note that internal climate variability is an additional source of uncertaintythat we do not take into account in this study~~do account for model uncertainty. The model dependent uncertainty, here defined as the model spread, of the future saturation horizon ~~, under the emission-driven RCP8~~under the esmRCP8.5 scenario, ~~is~~ was estimated by adding the modelled change in C$_T$ and A$_T$ for each model of our ESM-ensemble to the GLODAPv2 climatologies. ~~Here we neglect the~~ Model differences in changes of temperature, salinity, phosphate and silicate are neglected because they are minor in comparison to the effect of the changes in C$_T$ and A$_T$ (~~Sect. 5.2).~~ This is further discussed in Sect. 5.2.2). Internal climate variability is an additional source of model uncertainty that we do not explicitly account for in this study. However, a large part of this variability is eliminated because we use 10 year means for the future and past estimates of pH.

5 ~~Results~~

5 Results and discussion

~~pH evolution, averaged over the Nordic Seas surface waters (0-200 m), from 1850 to 2100, separated into past (1850-1980), present (1981-2019) and future (2020-2100). Black dots with error bars show the observed annual mean pH, with standard deviations (due to spatial/seasonal variations), determined from all available observations in the Nordic Seas shown in Fig. 1. The solid black line shows the trend calculated from the observations. The gray, red, yellow and blue solid lines show NorESM1-ME output for emission-driven historical and future (RCP8.5, RCP4.5 and RCP2.6) simulations, respectively, where the shading depicts the spatial variation (standard deviation). Note that this figure illustrates the actual modelled pH data, and not the modelled rates of change applied to observational data. The dashed lines show the evolution of global surface ocean pH from the same simulations. The black asterisk (1850) with error bars show an estimate of the pre-industrial mean pH with spatial standard deviation, derived from the GLODAPv2 mapped product as described in Sect. 3.2. The numbers in black and blue show the calculated and significant linear trend with standard errors from the observations and the model, respectively, for the period of 1981-2019.~~

~~Before going into regional details of pH changes, we will give an overview of surface pH changes from 1850 to 2100 (Fig. 4). To be consistent with our regional analysis in Sect. 5.4, the surface layer is taken as the top 200 m. The pre-industrial estimates of the average Nordic Seas surface pH in GLODAPv2 and NorESM1-ME (from year 1850) are in good agreement (within the spatial standard deviations), with mean values of 8.21±0.02~~ This Section is organized as follows: we will start to describe the present distribution of pH and ~~8.22±0.02, respectively. From 1850~~ Ω_{Ar} and its drivers (Section 5.1). In Section 5.2, we give an overview of pH changes from pre-industrial to ~~1980, NorESM1-ME simulates an average pH decline of 0.06 in the Nordic Seas. For the period between 1981 and 2019, the modelled pH encompasses the observed one (within the spatial standard deviations), except for a few years, showing that the pH of the Nordic Seas surface water is reasonably well simulated. The pH trend estimated from the observations for this period, -2.64±0.31 10^{-3} yr^{-1}, is not significantly different (at the 95% confidence level)from the modelled pH trend, -2.21±0.04 10^{-3} yr^{-1}. Because the pH calculated from observational data is based on discrete samples with incomplete spatial and temporal coverage, its representatives for the entire Nordic Seas can be questioned, and we cannot expect an exact agreement with the model.~~

~~As expected, the future evolution of surface water pH in the Nordic Seas depends strongly on the CO$_2$ emission scenario (Fig. 4) . Under the high-CO$_2$ emission RCP8.5 scenario, NorESM1-ME simulates the pH to decrease by 0.40 between 2020 and 2100, to an average value of 7.66±0.02 by the end of the century (model ensemble range: 7.59-7.79, Fig. S5). For the RCP4.5 scenario, which corresponds roughly to the currently pledged CO$_2$ emission reductions under the Paris agreement, the surface pH is simulated to drop by about 0.15, reaching an average value of 7.93±0.01. In the RCP2.6 scenario, where the CO$_2$ emissions are kept within what is needed to limit global warming to 2 °C (van Vuuren et al., 2011b), pH reaches its~~

Table 3. Spatial correlation (r) and explained variance (r^2, in paranthesis) between pH and pH(T), pH(T,C_T,A_T) and pH(T,C_T,A_T, S), and between Ω_{Ar} and Ω_{Ar}(C_T,A_T), Ω_{Ar}(C_T,A_T, T) and Ω_{Ar}(C_T,A_T, T, S) in the Nordic Seas surface (0 m) waters. Numbers in bold indicate significant correlation.

Drivers	(T)	(T,C_T,A_T)	(T,C_T,A_T,S)
pH	**0.58** (0.34)	**0.94** (0.89)	**1.00** (1.00)
Ω_{Ar}	**0.85** (0.73)	**1.00** (1.00)	**1.00** (1.00)

~~lowest value of 8.02±0.02 in the middle of the century, before it increases again to reach a value of 8.03±0.01 by the end of the century. This peak and decline is related to the overshoot profile of the atmospheric CO_2 concentration, with a maximum value of 443 ppm in mid-century followed by net negative emissions that subsequently decrease the atmospheric CO_2 down to 421 ppm in~~ 2100.

~~In 1850, the simulated Nordic Seas average surface pH is 0.11 units higher than the global average, which is related to the undersaturation of CO_2 in the surface waters of the Nordic Seas (Jiang et al., 2019). Note that our global average is lower than the one estimated by, e.g., Jiang et al. (2019) for the surface ocean due to our 200 m thick surface layer. The difference between the global ocean and the Nordic Seas is decreasing with time and by the end of the century the Nordic Seas surface pH is 0.03, 0.07 and 0.08 pH units higher than the global average in the RCP8.5~~Thereafter we describe regional changes from pre-industrial to present-day (Section 5.3), present-day changes (Section 5.4), ~~RCP4.5 and RCP2.6 scenarios, respectively. This is most likely partly due to the colder waters of the Nordic Seas,which gives them a lower buffer capacity,and partly due to a faster warming in the high latitude oceans related to polar amplification (Dai et al., 2019),which would give a faster decrease in the Nordic Seas pH compared to the global mean. Additionally,in RCP8.5,there is an increase in the pCO_2 undersaturation of the global ocean that increases the global average pH~~ changes from present-day to future (~~Fig. S14) .~~Section 5.5) and assess its impacts on cold-water corals (Section 5.1). In Section 5.2 we analyze the drivers of pH change in the different time periods.

5.1 ~~Present distribution of pH and Ω saturation states~~

5.1 Present-day spatial distribution of pH and Ω saturation states

Due to the contrasting properties of ~~the Atlantic waters(~~Atlantic waters, here defined as waters with salinity > 34.5~~)~~, (Malmberg and Désert, polar waters (defined as the waters with salinity < 34.5 detached from the Norwegian coast) that meet and mix in the Nordic Seas, there are large spatial gradients in ~~its surface~~ surface (0 m) temperature, salinity and chemical properties (Fig. ~~S15~~3 and S14). The Atlantic Water, located in the eastern part of the Nordic Seas, is characterized by higher temperature, salinity, and A_T, while polar waters are colder and fresher with lower A_T. This results in a decrease in temperature, salinity, and A_T from ~~south and east to north and west~~southeast to northwest. Within the Atlantic water ~~,~~ there is a tendency of increasing C_T ~~increases~~ with decreasing temperature~~,~~. This is largely as a consequence of the increased CO_2 solubility in colder water~~. The~~, i.e., a cooling of a water mass result in an increase in C_T ~~associated with polar waters~~due to an uptake of CO_2 from the

~~Maps of present day surface pH (a) and Ω_{Ar} (b). The solid line in (a) mark the the border between Atlantic Water (salinity>34.5) and polar waters (salinity<34.5). pH and Ω_{Ar} plotted against variations induced by temperature (c,d), temperature and C_T/A_T (e,f) and temperature, C_T/A_T and salinity (g,h) in pH and Ω_{Ar}, calculated as described in Section 4.1 in Atlantic Water (red) and polar waters (blue). Each circle represents a value from a single grid.~~

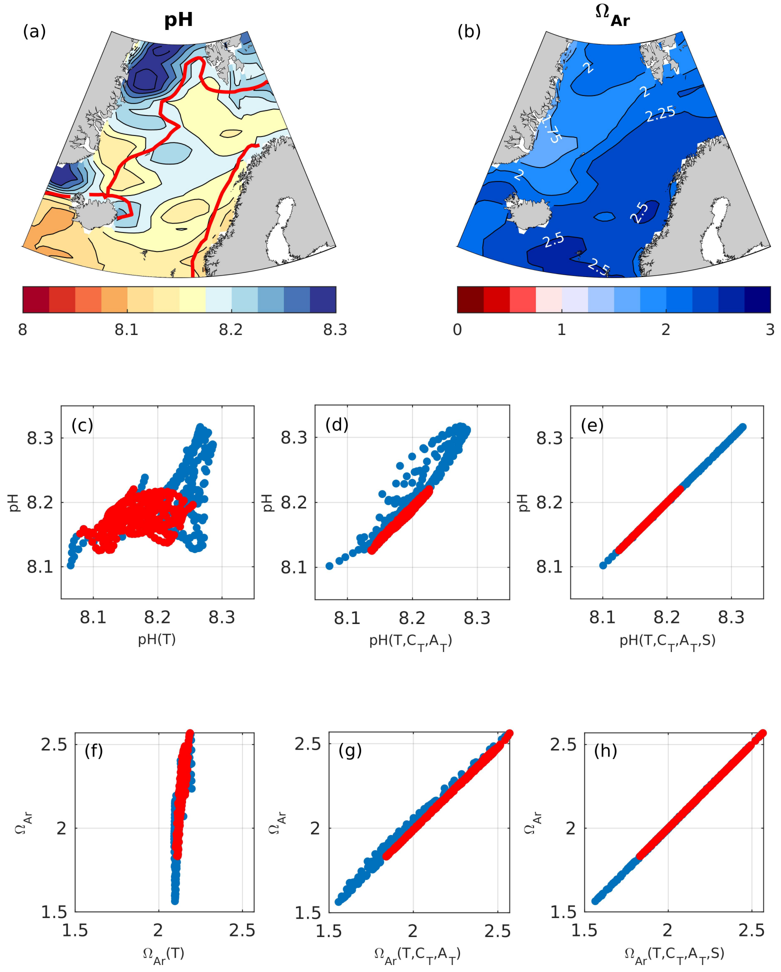

Figure 3. Maps of present-day surface (0 m) pH (a) and Ω_{Ar} (b). The solid red line in (a) mark the border between Atlantic Water (salinity>34.5) and low salinity waters (salinity<34.5). The low saline waters include Norwegian coastal waters (constrained to the Norwegian coast) and polar waters (constrained to the north-western part of the domain). pH and Ω_{Ar} plotted against variations induced by temperature (c,f), temperature and $C_T + A_T$ (d,g) and temperature, $C_T + A_T$ and salinity (e,h) in pH and Ω_{Ar}, calculated as described in Section 4.1 in Atlantic Water (red) and low salinity waters (blue). Each circle represents a value from a single grid cell.

atmosphere. In polar waters, C_T is lower than ~~that of Atlantic waters~~ in Atlantic waters due to the lower pCO_2 (Fig. S14)), and also as a result of the large freshwater export from the Arctic Ocean that dilutes not only C_T, but also A_T and salinity.

The surface pH in the Nordic Seas increases from ~~the~~ Atlantic waters to ~~the~~ polar waters (Fig. 3). ~~There is a significant, strong (R<-0.5), negative correlation with all drivers, i.e. pH decreases with increasing temperature, salinity, C_T and A_T (Table ?? and Fig. S16). Here, only the negative correlation with A_T is nonphysical, i.e. we would expect an increasing pH with an increasing A_T (Table 1). The correlation with C_T/A_T is insignificant. Because the drivers are not orthogonal, it is impossible to rule out the contribution of each driver by just looking at these correlations, and we can only conclude that there is a strong water-mass dependency in the spatial distribution of these variables.~~

~~From the correlation between the pH and~~ The correlation between the pH and the pH calculated with spatially varying temperature only (pH(T)~~, we note~~), keeping all other drivers constant, is 0.58. This means that temperature-induced variations (through the thermodynamic effect) are able to explain 34% of the spatial variability in pH (Fig. 3 ~~). The range in pH(T) values (8.06 - 8.29) is very close to the observed one (8.10-8.32), indicating that temperature alone can give rise to the observed pH-range.~~ and Table 3). Adding C_T ~~and~~ +A_T ~~to the picture~~ and salinity contributions explains an additional 55% ~~(temperature, C_T and A_T explain all together 89%), and are therefore important contributors to spatial variations in pH~~and 11%, ~~in~~ respectively, of the spatial variability in pH. The effect of salinity is largest in the low-salinity regions, i.e., in polar waters and the Norwegian coastal waters. In contrast to what is suggested by directly correlating ~~these variables (Table ??). This shows~~ pH and C_T+A_T (Table S9), the results in Table 3 show that C_T+A_T are important contributors to spatial variations in pH. This indicates that the influence of C_T and A_T on pH is masked out by temperature variations in Table~~??~~ S9 and Fig. ~~S16~~S15, which can be explained by the two cancelling effects that temperature has on pH ~~described in Jiang et al. (2019)~~(Jiang et al., 2019). For example, while the instantaneous, thermodynamic ~~,~~ effect of a drop in temperature leads to a pH increase, it also ~~gives rise to a decrease~~ results in a drop in $p\mathrm{CO}_2$~~that leads to a~~, which subsequently leads to an anomalous CO_2 uptake from the atmosphere~~, which subsequently increases the C_T/A_T ratio and decreases the pH. In the Nordic Seas, the spatial pH variations strongly correlate with surface $p\mathrm{CO}_2$ (R=-0.99, Table ??), which range between 185 and 342 μatm and is lower than the atmospheric $p\mathrm{CO}_2$ of 373 μatm (in year 2002, to which these data are normalized). This undersaturation is partly a result of the large heat release to the atmosphere and cooling of the sea surface, and shows that the sea surface CO_2 did not yet equilibrate with the atmosphere. Because most of the data have been used to produce these climatologies are from the productive season, there is probably also a contribution from primary production to this undersaturation. There is also a negative correlation between~~. This increases the C_T/A_T ratio~~and temperature, indicating that CO_2 uptake has been taking place. The temperature effect on pH in the Nordic Seas is therefore a combination of the instantaneous thermodynamic effect, and the effect of the subsequent CO_2 exchange and the resulting increase in the C_T/A_T ratio. The strong relation between pH and $p\mathrm{CO}_2$, which also has been observed for the global ocean (Jiang et al., 2019), suggests that the processes responsible for the spatial pH variations in the Nordic Seas are heat fluxes and production/remineralization of organic matter. On top of temperature, C_T and A_T, the addition of salinity explains the last 11% of the spatial variability in pH. The effect of salinity is the largest in the low-saline regions, i.e in the polar waters and in the Norwegian coastal current~~, which in turn causes a drop in pH that counteracts the initial thermodynamic affect.

The saturation state Ω_{Ar} show an opposite pattern to pH, with low saturation states in polar waters, and high saturation states in Atlantic Water. ~~The Ω_{Ar} distribution is strongly correlated with C_T/ A_T (R=-0.99) (Fig. 3,f) and temperature (R=-0.86). This is related to the strong relation between Ω_{Ar} and C_T/ A_T to the climatological temperature distribution and its impacts on the CO_3^{2-} concentration (for which C_T/ A_T is a proxy), as described in Section 2. As for pH, temperature has two effects on Ω_{Ar}, but in contrast to pH where these effects are counteracting, they reinforce each other for Ω_{Ar}.~~ From Fig. 3,d, it becomes clear that the temperature effect on the solubility of Ω_{Ar} (Ω_{Ar}(T)) only ~~can~~ explain 11% of the observed Ω_{Ar} range, although it is able to explain 98% of the variability. When adding C_T+ A_T contributions, the observed range in Ω_{Ar} is reproduced, and 100% of the variability is explained. C_T+A_T strongly influences Ω_{Ar}, because with decreasing C_T to A_T ratio, the CO_3^{2-} concentration decreases as well. The C_T to A_T ratio itself strongly correlates with temperature as the CO_2 solubility increases with decreasing temperature and vice versa (S9). The strong correlation ~~with temperature~~ between Ω_{Ar} and temperature (Table S9) is therefore largely a result of the temperature effect on C_T~~/~~ +A_T, and as such, the CO_3^{2-} concentration, (Sect. 2 and Orr (2011); Jiang et al. (2019)). ~~When adding C_T/ A_T to the picture, the observed range in Ω_{Ar} is reproduced, and 100% of the variability is explained. Salinity~~ Thermodynamic salinity induced variations only have a minor contribution to the spatial variations in Ω_{Ar} ~~. As~~ (less than 1%), and, as for pH, the effect of salinity is more prominent in the low salinity-regions.

~~Spatial correlation between various chemical and physical properties in the Nordic Seas surface waters. Numbers in bold indicate significant correlation. pH Ω_{Ar} pCO_2 C_T/A_T Temperature **-0.58 -0.86 0.66 -0.79** Salinity **-0.68 0.46 0.71 -0.35**C_T **-0.75** -0.07 **0.74** 0.07A_T **-0.64 0.63 0.69 0.5**C_T/A_T -0.02 **-0.99** -0.09 pCO_2 **-0.99 -0.23**~~

5.2 Overview of modelled and observed pH changes from pre-industrial to the end of the 21st century

Here we give an overview of upper layer, taken to be the upper 200 m for both model and observations, pH changes in the Nordic Seas from 1850 to 2100 (Fig. 4). Note that in this section we use the actual modelled pH data, and not the modelled change applied to observational data, and use this as an opportunity to evaluate the model's performance. The pre-industrial average Nordic Seas surface pH estimated in GLODAPv2, using an atmospheric CO_2 of 280 ppm, and NorESM1-ME, using year 1850 with an atmospheric CO_2 of 284 ppm, are in good agreement, with mean values of 8.21±0.02 and 8.22±0.02, respectively. From 1850 to 1980, the emission-driven NorESM1-ME simulates an average pH decline of 0.06 in the Nordic Seas, while the concentration-driven run simulates a drop of 0.05 (Fig S5). The difference is caused by the slightly too strong increase of atmospheric CO_2 from 1850-1980 in the emission-driven run, and is on the same order of magnitude as the estimated pH uncertainty in the observational data (Table 2) and in the GLODAPv2 pre-industrial pH estimate in the Nordic Seas (Sect. 4.4). For the period between 1981 and 2019, the modelled pH largely encompasses the observed one (within the spatial standard deviations), showing that the pH of the Nordic Seas surface water is reasonably well simulated. The pH trend estimated from the observations for this period, -2.64±0.31 10^{-3} yr^{-1}, is not significantly different (at the 95% confidence level) from the modelled pH trend, -2.21±0.04 10^{-3} yr^{-1}. Because the pH calculated from observational data is based on discrete samples with a limited spatial and temporal coverage, its representativeness for the entire Nordic Seas is questionable, and we do not expect an exact agreement with the model. For example, the stronger trend obtained from the observational data might be a result of the samples in the beginning of the period being biased to regions with higher pH.

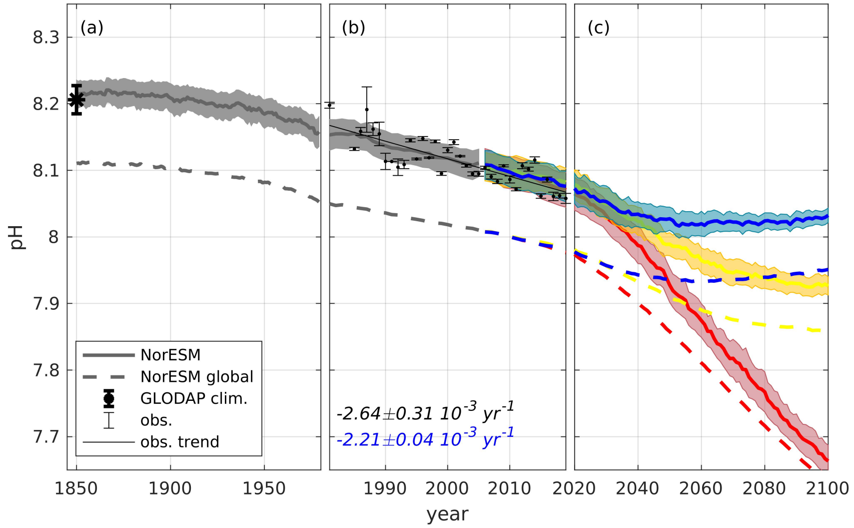

Figure 4. ~~Spatial correlation~~ pH evolution, averaged over the Nordic Seas surface waters (~~r~~0-200 m)~~and explained variance (r^2, in paranthesis) between pH and pH~~from 1850 to 2100, separated into past (~~T~~1850-1980), ~~pH~~present-day (~~T,C_T,A_T~~1981-2019) and ~~pH~~future (~~T~~2020-2100). Black dots with error bars show the observed annual mean pH, ~~C_T~~with standard deviations (due to spatial/seasonal variations), ~~A_T~~determined from all available observations in the Nordic Seas as shown in Fig. 1. The solid black line shows the trend calculated from these observations. The gray, ~~S)~~red, yellow and ~~between Ω_{Ar}~~ blue solid lines show NorESM1-ME output for emission-driven historical and ~~Ω_{Ar}~~future (~~C_T~~esmRCP8.5, ~~A_T~~esmRCP4.5 and esmRCP2.6) simulations, ~~Ω_{Ar}(C_T,A_T~~respectively, ~~T~~where the shading depicts the spatial variation (standard deviation). Note that this figure illustrates the actual modelled pH data, and ~~Ω_{Ar}~~not the modelled change applied to observational data. The dashed lines show the evolution of global surface ocean pH from the same simulations. The black asterisk (~~C_T,A_T, T, S~~1850) ~~in~~ with error bars show an estimate of the ~~Nordic Seas surface waters~~pre-industrial mean pH with spatial standard deviation, derived from the GLODAPv2 mapped product as described in Sect. ~~Numbers~~ 3.2. The numbers in ~~bold indicate~~ black and blue show the calculated and significant ~~correlation~~linear trend with standard errors from the observations and the model, respectively, for the period of 1981-2019.

~~Drivers pH (T)pH (T, C_T, A_T) pH (T, C_T, A_T, S) pH **-0.58** (0.34)**-0.94** (0.89) **1.00** (1.00)Drivers Ω_{Ar}(T)Ω_{Ar}(T, C_T, A_T) Ω_{Ar}(T, C_T, A_T, S) Ω_{Ar} **0.85** (0.73)**1.00** (1.00)**1.00** (1.00)~~

The future evolution of upper layer pH in the Nordic Seas depends strongly on the CO_2 emission scenario (Fig. 4). In the esmRCP2.6 scenario, where the CO_2 emissions are kept within what is needed to limit global warming to 2 °C (van Vuuren et al., 2011b), pH drops by 0.04 from 2020 to 2099, and reaches a value of 8.03±0.01. Note that in this scenario there is a peak and decline, related to the overshoot profile of the atmospheric CO_2 concentration, with a minimum pH value in mid-century. For the esmRCP4.5 scenario, which corresponds roughly to the currently pledged CO_2 emission reductions under the Paris agreement, the surface pH is simulated to drop by about 0.15, reaching an average value of 7.93±0.01 by the end of the 21st century. Under the high-CO_2 esmRCP8.5 scenario, NorESM1-ME simulates the pH to decrease by 0.40 between 2020 and 2099 to an average value of 7.67±0.02. This equals a pH decline of approximately to -5.00 10^{-3} yr^{-1}.

The model related uncertainty in the esmRCP8.5 scenario, measured as the inter-model spread of the pH in 2099, displays a pH range of 7.59-7.79, Fig. S5). The model uncertainty in the emission-driven ensemble is, as expected, larger than in the concentration-driven ensemble where the pH spans a range of 7.71-7.75 in 2099. The intermodel-spread in the emission-driven runs is reduced if only considering the pH change (Table S6). This shows that a large part of the uncertainty is removed if only considering the pH change as we do in the following sections in this study.

The simulated Nordic Seas average upper layer pH is 0.11 higher than the global average in 1850, which is related to the undersaturation of CO_2 in the surface waters of the Nordic Seas (Jiang et al., 2019). Our global average pH is about 0.1 lower than that estimated by, e.g., Jiang et al. (2019) for the surface ocean due to our consideration of a 200 m thick upper layer. The difference between the simulated upper layer pH of the global ocean and the Nordic Seas is decreasing with time. By the end of the 21st century, the Nordic Seas upper layer pH is 0.03, 0.07 and 0.08 higher than the global average for the esmRCP8.5, esmRCP4.5 and esmRCP2.6 scenarios, respectively. This is partially a result of the colder waters of the Nordic Seas, which gives them a lower buffer capacity. Additionally, in esmRCP8.5, there is an increase in the pCO_2 undersaturation of the global ocean that increases the global average pH (Fig. S16). Other factors driving this decreasing pH difference between the global ocean and the Nordic Seas can be differential heating. A quantitative assessment of the drivers is beyond the scope of this paper.

5.3 ~~Changes~~ Modelled pH and Ω_{Ar} changes from pre-industrial to ~~present~~present-day

~~Maps of surface pH and~~ In this Section and the following, we present temporal changes in pH and Ω_{Ar} ~~distributions, and their changes from pre-industrial to present (calculated from the gridded GLODAPv2 data and rates of change from the NorESM1-ME emission-driven historical run as described in Section 4.2), are shown in Fig. 5. The~~. Note that results for the modelled changes are referring to the 0 m surface, unlike the 0-200 m depth range that we use for the upper layer in Sect. 5.2 and 5.4.

From pre-industrial to present, the spatial pattern of changes in surface pH and Ω_{Ar} are similar (Fig. 5). The strongest decreases, reaching -0.12 and -0.55, respectively, are found in Atlantic ~~waters~~ Water along the Norwegian coast both for pH and Ω_{Ar}. The smallest change is found in polar waters ~~. The reasons behind these patterns of change will be discussed in Section 5.2.~~

(see more in depth discussion in Sect. 5.2.2). The corresponding maps for H^+ (Fig. S17) show a similar spatial distribution as for pH. Due to the longer ventilation time scales of deeper waters, the pH decrease weakens with depth. As shown in the section across 70°N (Fig. 6), waters below 2500 m are nearly unaffected. While the entire water column remains saturated with respect to calcite, the saturation horizon (Ω=1) of aragonite shoaled from a mean depth of 2200 m (uncertainty range: 2100-2400 m) during pre-industrial, to a present-day mean depth of 2000 m (uncertainty range: 1700-2300 ~~) min present times~~m), across this specific section. Note that these depths were obtained from the contour interpolation when creating Fig. 6, which has a finer vertical resolution than the GLODAPv2 climatology.

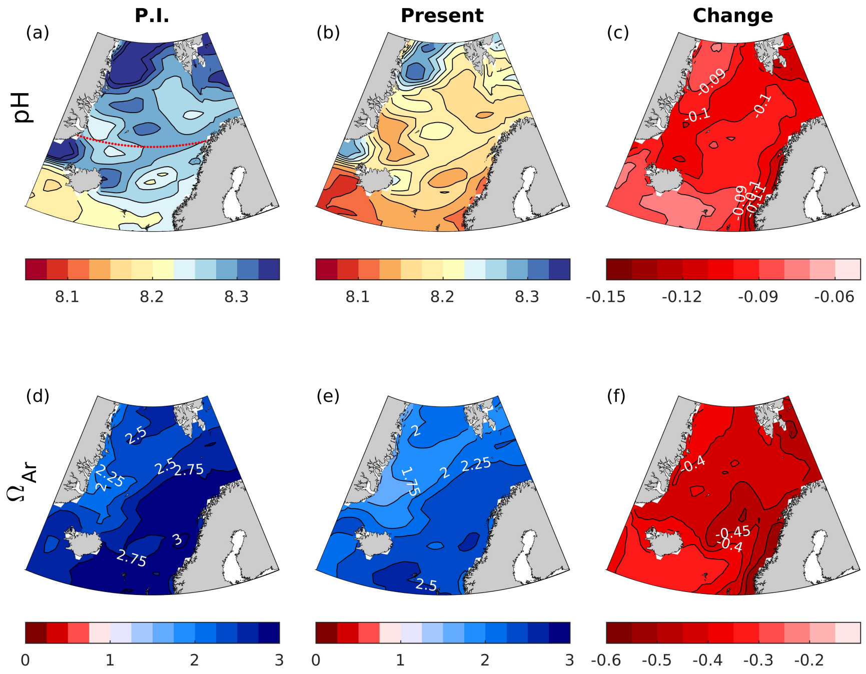

Figure 5. Maps of surface water (0 m) pH and Ω_{Ar} for pre-industrial (P.I., 1850-1859), ~~present times~~ present-day (1996-2005), and the change in between the two periods. The maps were calculated from the GLODAPv2 gridded climatologies (Lauvset et al., 2016) applying the simulated changes by NorESM1-ME, as explained in Sect. 4.2. The dotted ~~black~~ red line in (a) show the location of the ~~crossection~~ cross-section presented in Fig. 6~~.~~.

5.4 ~~Present day~~ Observed present-day changes ~~(1981-2019)~~in pH and Ω_{Ar}

Table 4. pH trends ± standard error (10^{-3} yr^{-1}) calculated from the data presented in Fig. 7. Bold numbers indicate that the trends are significantly different from zero.

Depth (m)	NB	LB	BSO	FS	GS	IS
0-200	**-3.04±0.32**	**~~-2.4~~-2.40±0.23**	-1.67±0.77	**-2.53±0.74**	**-2.19±0.37**	**~~-3.1~~-3.10±0.30**
200-500	**-2.22±0.32**	**-1.89±0.31**	-1.05±0.82	**-1.49±0.42**	**-1.61±0.22**	**-2.51±0.27**
500-1000	**-1.17±0.27**	**-2.27±0.46**		-1.09±0.52	**-1.52±0.18**	**-1.84±0.29**
1000-2000	**-0.65±0.22**	~~-0.8~~-0.80±0.40		-0.55±0.81	**-1.36±0.15**	**-1.3±0.21**
2000-4000	0.46±0.55	-0.22±0.51		-0.03±0.69	-0.31±0.23	

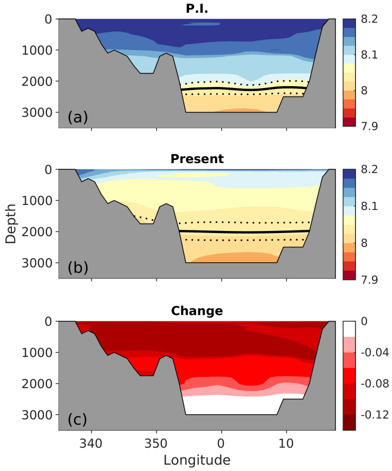

Figure 6. Zonal cross sections (at 70 °N) of pre-industrial (1850-1859) and present pH (1996-2005), and the change between the two periods. The solid black line shows the saturation horizon of aragonite (Ω_{Ar}=1). The dashed lines shows the associated uncertainties(~~σ^2~~ σ_{field}).

Table 5. Ω_{Ar} trends ± standard error (10^{-3} yr^{-1}) calculated from the data presented in Fig. 8. Bold numbers indicate that the trends are significantly different from zero.

Depth (m)	NB	LB	BSO	FS	GS	IS
0-200	**-11.97±3.25**	**-8.45±1.18**	**-8.29±3.54**	**-11.61±3.13**	-4.05±3.21	**-11.20±2.22**
200-500	**-5.57±2.51**	-1.76±2.17	3.94±3.01	-2.06±1.60	**-3.19±0.61**	**-6.37±0.74**
500-1000	**-4.28±1.25**	-5.55±3.38		-1.11±1.46	**-2.98±0.52**	**-4.52±0.71**
1000-2000	**-3.49±1.24**	0.03±1.76		0.65±3.08	**-2.98±0.59**	**-2.57±0.50**
2000-4000	3.67±1.82	0.33±1.57		1.13±1.53	0.53±0.80	

Regional trends in observed seawater pH between 1981 and 2019 for ~~the~~ five different depth intervals are presented in Fig. 7 and Table 4. The corresponding trends in H$^+$ are shown in Fig. ~~S17 and Table S7. In surface waters~~ S18 and Table S10. In the upper layer (0-200 m), significant trends of 2-3 10^{-3} yr^{-1} are found in all basins except for the Barents Sea Opening. The uncertainties (standard errors) of these trends are ~~approximately~~ between ±~~0.3~~ 0.2 and ±0.8 10^{-3} yr^{-1}. Due to the difference in sampled years, we cannot robustly compare the magnitude of trends between the basins. ~~The~~ Skjelvan et al. (2014) also found significant trends in upper 200 m pH of the Norwegian and Lofoten basins and of the Greenland Sea for the period of 1981-2013. Our estimated trend in the Norwegian Basin of -3.04 ± 0.32 10^{-3} yr^{-1} is weaker than ~~the~~ their -4.1 10^{-3} yr^{-1} trend~~estimated for the period 1981-2013 by Skjelvan et al. (2014)~~, which can be a result of different sampling period and slightly different definition of regions. However, our trend ~~estimate~~ estimates in the Greenland Sea and Lofoten Basin of -2.19 ± 0.37 10^{-3} yr^{-1} and -2.40 ± 0.23 10^{-3} yr^{-1}, respectively, agrees well with ~~their~~ the trend of -2.3 10^{-3} yr^{-1} that they calculated for both regions. The non-significant trend we find in the Barents Sea Opening is also in agreement with the results

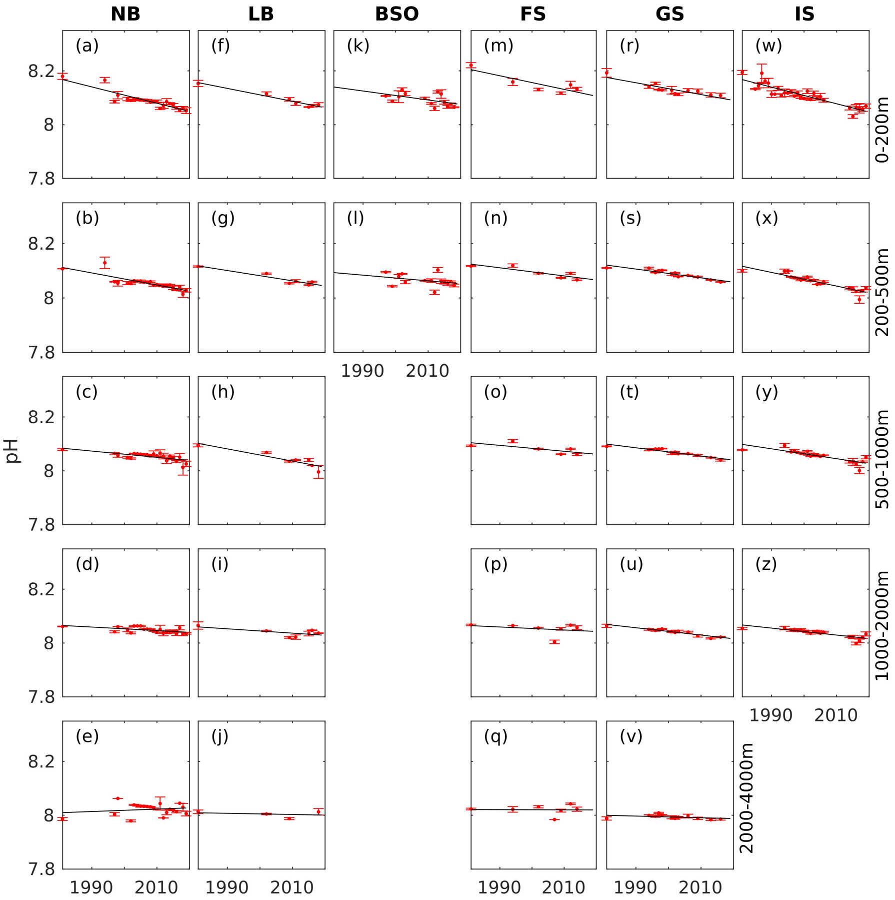

Figure 7. Annual mean pH (red dots) with standard deviation (error bars) in the different basins, at five different depth ~~levels~~intervals, calculated as described in Sect. 4.2. The solid black line show the trend estimate from the linear regression.

of Skjelvan et al. (2014). In contrast to their results, we obtained a significant trend in the eastern Fram Strait, which may be a result of the larger time span of our dataset. As expected from the generally longer ventilation time scales of deep waters, the trends in pH ~~declines with depth(but see Sect. 5.5)~~decline with depth. Significant trends are detected down to 2000 m in the ~~Norwegian Basin, and in the Greenland and Iceland seas~~Greenland Sea, in agreement with Skjelvan et al. (2014), but also in the Iceland Sea and in the Norwegian Basin. In the Lofoten Basin and ~~Eastern~~ eastern Fram Strait, ~~however,~~ the decrease in pH is significant down to the 1000 m and 500 m layers, respectively. ~~In the shallow Barents Sea Opening there is~~ As for the upper layer, no significant trend ~~below the surface layer~~ is found in the 200-500 m layer in the shallow Barents Sea Opening.

Trends of aragonite saturation states are shown in Fig. 8 and Table 5. As for pH, the ~~rates~~ rate of change is strongest in ~~surface waters~~the upper layer. For Ω_{Ar}, the ~~rates of decline are~~ decline is in the order of 10^{-2} yr^{-1} and significant in all regions except for the Greenland Sea. The weak decline in the Greenland Sea surface layer is a result of a smaller increase in C_T in combination with relatively strong increases in A_T and temperature, which counteracts the effect of C_T on the saturation

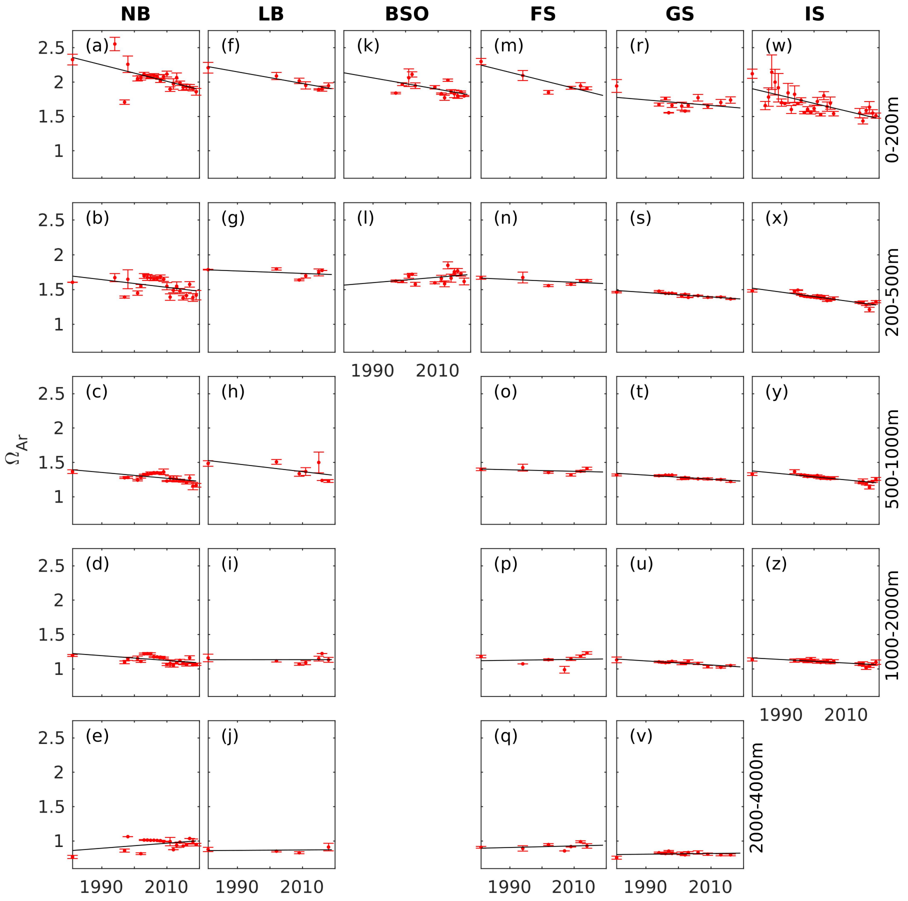

Figure 8. Annual mean Ω_{Ar} (red dots) with standard deviation (error bars) in the different basins, at five different depth intervals, calculated as described in Sect. 4.2.The solid black line show the trend estimate from the linear regression.

states (while the temperature amplifies pH declines, see Sect. ~~5.2~~2). The reduction in Ω_{Ar} is significant down to 2000 m in the Norwegian Basin and the Greenland and Iceland ~~seas~~Seas. In the other regions, no significant decline has occurred below the surface layer. In the depth layers considered, aragonite undersaturation occurs in the 2000-4000 m layer. The waters in the depth range 1000-2000 m are close to the limit of undersaturation. The smallest values in this layer are 1.05, 1.07, 0.99, 1.02, and 1.01, for the Norwegian Basin, Lofoten Basin, ~~Barents Sea Opening, Eastern~~ eastern Fram Strait, Greenland Sea and Iceland Sea, respectively. Considering the associated uncertainties of 0.06 (Table 2), this is indistinguishable from undersaturation in all regions except for the Lofoten Basin. ~~Only the waters between 2000-4000 m , which are already undersaturated in aragonite, are more or less unaffected~~In contrast to Skjelvan et al. (2014) who only found a significant negative trend in the upper 200 m layer of the Norwegian Basin, we are now, with the longer time series, able to state that there is a significant decrease in Ω_{Ar} in several regions and at several depth layers.

During ~~this period of time~~ the period 1981-2019, we detect trends in the uncertainties of pH and Ω_{Ar} (Figs. ~~S6 and S7)~~S6 and S7), reaching -0.04 10^{-3} yr^{-1} and 0.53 10^{-3} yr^{-1}, respectively. These are, however, about two orders of magnitude smaller than the trends in pH and Ω_{Ar}, and they do therefore not significantly impact ~~our estimated trends~~interpretation of our results.

~~Annual mean Ω_{Ar} (red dots) with standard deviation (error bars) in the different basins, at five different depth levels, calculated as described in Sect. 4.2.The solid black line show the trend estimate from the linear regression.~~

~~Ω_{Ar} trends $\pm$ standard error (10^{-3} yr^{-1}) calculated from the data presented in Fig. 8. Bold numbers indicate that the trends are significantly different from zero. Depth (m) NB LB BSO FS GS IS 0-200 **-11.97±3.25 -8.45±1.18 -8.29±3.54 -11.61±3.13** -4.05±3.21 **-11.20±2.22** 200-500 **-5.57±2.51** -1.76±2.17 3.94±3.01 -2.06±1.60 **-3.19±0.61 -6.37±0.74**500-1000 **-4.28±1.25** -5.55±3.38 -1.11±1.46 **-2.98±0.52 -4.52±0.71**1000-2000 **-3.49±1.24** 0.03±1.76 0.65±3.08 **-2.98±0.59 -2.57±0.50**2000-4000 3.67±1.82 0.33±1.57 1.13±1.53 0.53±0.80~~

5.5 ~~Future~~ Modelled pH and Ω_{Ar} changes from present-day to future

~~The future evolution of pH in the Nordic Seas depends strongly on the emission scenario (Fig. 4). Here we will present, in more detail, the future evolution of~~

In this section we go into regional details of future pH and Ω_{Ar} ~~under low and high emission scenarios, RCP2~~changes under the esmRCP2.6 and ~~RCP8~~the esmRCP8.5 ~~respectively, as simulated by NorESM1-ME~~scenarios. The results are presented for the surface (0 m), and not for the upper layer 0-200 m as in Sect. 5.2 and 5.4.

In ~~RCP2~~esmRCP2.6, ~~an additional~~ a pH decline of 0.06-0.11 in the surface waters is simulated between ~~present~~ present-day (1996-2005) and future (2090-2099) (Fig. 9c). The largest pH decreases are found in polar waters, leading to a weakening of the ~~zonal gradient in pH that we see in the present and pre-industrial periods. The surface~~ present-day zonal pH gradient. Surface Ω_{Ar} is ~~expected~~ projected to decrease by about 0.2-0.5 under esmRCP2.6, with the largest drops taking place in polar waters. Surface waters ~~are expected to~~ remain supersaturated with respect to both calcite and aragonite~~under RCP2.6. An interesting feature in this scenario, is that~~. Interestingly, the strongest ocean acidification occurs at depths of 1000-2000 m in this scenario (Fig. 10c), which leads to a shoaling of the aragonite saturation horizon to a depth of 1100 m (uncertainty range: 800-1200 m). This is discussed in more detail in Sect. ~~5.2~~5.2.2.

~~Maps of surface water pH and Ω_{Ar} for the present (1996-2005) and the RCP8.5 future (2090-2099), as well as the changes between the periods. The maps are drawn from the GLODAPv2 gridded climatologies combined with rates of change from the NorESM1-ME. The dotted black line in (a) show the location of the crossection presented in Fig. 10.~~

~~Under the RCP8~~Under the esmRCP8.5 scenario, ~~the pH in surface waters~~ surface pH drops by about 0.4-0.5 ~~from present, to a value of 7.6-7.9 in 2100~~ between present-day and future (Fig. 11), with the largest decreases ~~taking place~~ in polar waters. ~~The surface~~ Surface Ω_{Ar} ~~drop~~ drops by around 1.1-1.3. In contrast to ~~RCP2~~esmRCP2.6, the largest decline of Ω_{Ar} take place in the Atlantic Water. The reason behind this is discussed in Sect. 5.2.2. The strong ocean acidification in this scenario leads to a reversal of the pH ~~depth dependency so that~~ depth-dependency so that pH increases from surface to depth by the end of the ~~century pH increases from the surface to deep ocean~~ 21st century (Fig. 10c)~~, reflecting that the input of anthropogenic carbon~~

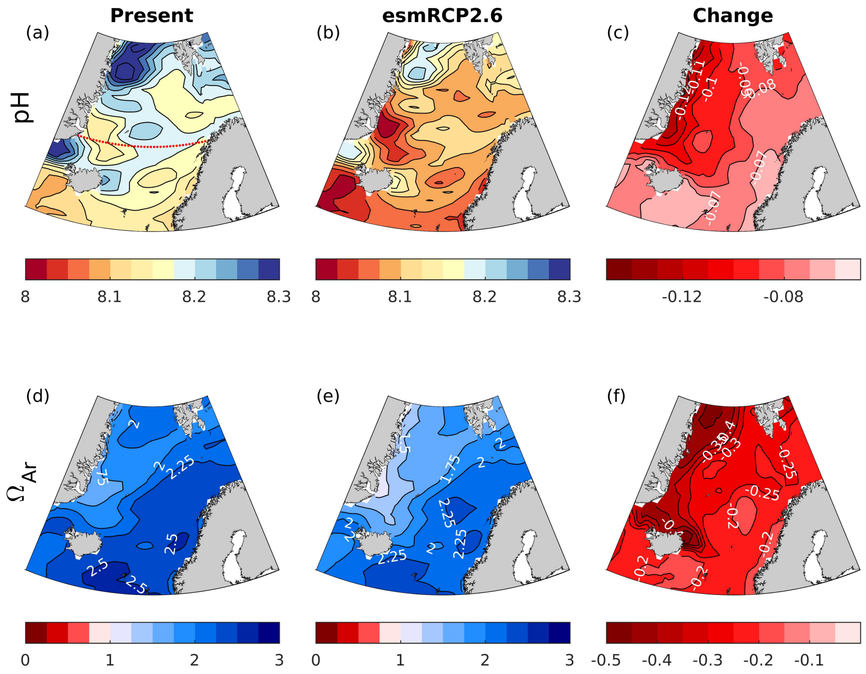

Figure 9. Maps of surface water (0 m) pH and Ω_{Ar} for the ~~present~~ present-day (1996-2005) and the ~~RCP2~~esmRCP2.6 future (2090-2099), as well as the changes between the periods. The ~~maps are drawn from~~ data-input of the maps is based on GLODAPv2 gridded climatologies combined with ~~rates of~~ the change from the NorESM1-ME. The dotted ~~black~~ red line in (a) show the location of the crossection presented in Fig. 10.

. Here, the anthropogenic carbon input at the surface overrides the effect of pressure and organic matter remineralization on the vertical pH gradient. The change in Ω_{Ar} is large enough to bring the entire water column, and consequently also the entire seafloor, to aragonite undersaturation. The only exception is a thin surface layer (above 30 ±10 m) in the Atlantic Water region. For all emission scenarios the spatial distribution of H^+ and its change (shown in Fig. S19 and Fig. S20) are similar to that of pH.

6 ~~Discussion~~

5.1 Implications for cold-water corals

Cold-water corals build their structures out of aragonite, which is the more soluble form of calcium carbonate. These corals can, to some degree, compensate for aragonite undersaturation in seawater by increasing their internal pH by 0.3-0.6 (McCulloch et al., 2012; Al For some time, they can therefore continue to calcify in waters with Ω_{Ar}<1. However, the calcification rates and breaking

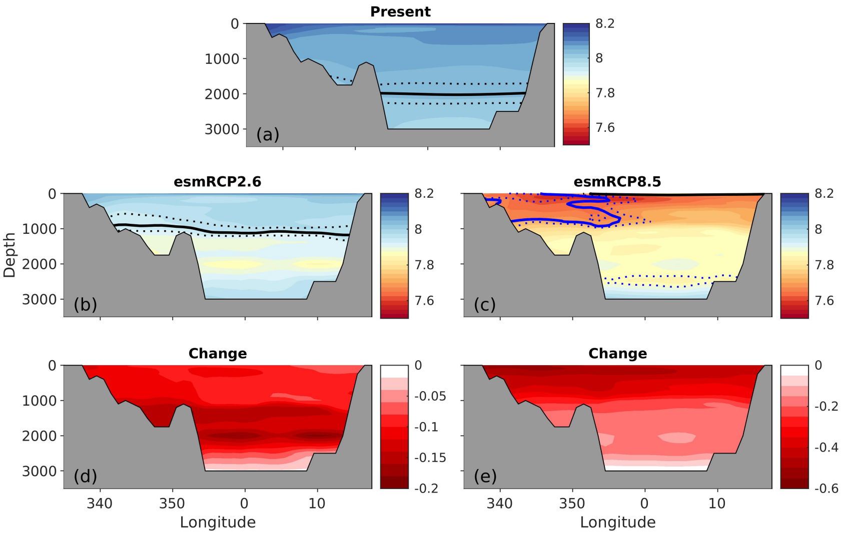

Figure 10. Zonal cross sections (at 70 °N) of ~~the~~ present (1996-2005) and future (2090-2099) pH under the emission-driven ~~RCP2~~esmRCP2.6 and ~~RCP8~~esmRCP8.5 scenarios, along with the change between the periods. The solid and dotted black lines show the saturation horizon of aragonite (Ω_{Ar}=1) with uncertainty (~~$\sigma 2$~~σ_{field}). The solid and dotted blue line show the corresponding for calcite (Ω_{Ca}=1).

strength of the structures of the most abundant coral organism, *Lophelia pertusa*, is reduced under such conditions (Hennige et al., 2015). Furthermore, dead coral structures, which compose the major part of the reefs, cannot resist corrosive waters and experience increased dissolution rates at Ω_{Ar}<1. Cold-water coral reefs, along with their ecosystems, are consequently likely to collapse if the water they live in becomes undersaturated with respect to aragonite. It has been estimated that about 70% of the deep sea corals globally will be below the aragonite saturation horizon by the end-of-the-century under high-emission-scenarios (Guinotte et al., 2006; Zheng and Cao, 2014).

Most of the reef sites that have been identified in the Nordic Seas (321 out of the 324 within the region defined in Fig. 1) are at depths of 0-500 m (Fig. 12, see also Buhl-Mortensen et al. (2015)). The aragonite saturation horizon estimated from the GLODAPv2 climatology for present climate is at 2000 m, with uncertainty range 1750-2500 m. Note that the uncertainty range of the depth of the saturation horizon is not equally distributed around the mean because the uncertainty analysis is done for the saturation state, from which the depth distribution is calculated. From the discrete measurements we also see that the waters in the depth range 1000-2000 m are close to being undersaturated with respect to aragonite (Sect. 5.4). For the time being, the saturation horizon is thus well below the majority of the cold-water corals in the Nordic Seas.

In the esmRCP2.6 scenario, NorESM1-ME projects that the aragonite saturation horizon will shoal to 900 m (uncertainty: 800-1100 m), while in the esmRCP4.5 scenario the saturation horizon is projected to shoal to 600 m depth (uncertainty: 400-700 m) by the end of this century. This implies that the deepest observed reefs will be exposed to corrosive waters, and thus experience elevated costs of calcification and dissolution of dead structures. The majority (315 out of 324) of the

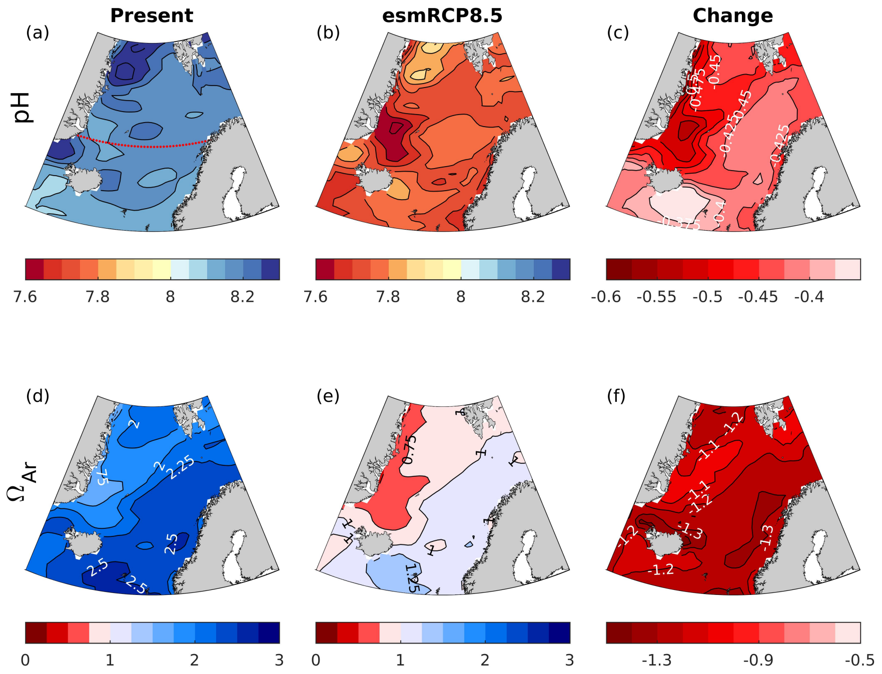

Figure 11. Maps of surface water (0 m) pH and Ω_{Ar} for the present (1996-2005) and the esmRCP8.5 future (2090-2099), as well as the changes between the periods. The data-input of the maps is based on GLODAPv2 gridded climatologies combined with the change from the NorESM1-ME. The dotted red line in (a) show the location of the crossection presented in Fig. 10.

coral sites in the Nordic Seas are, however, found at shallower depths than the projected saturation horizon with uncertainty, although the margins are small. Also García-Ibáñez et al. (2021) suggested that cold-water corals in the subpolar North Atlantic will be exposed to corrosive waters if the 2-degree goal (which is the aim of RCP2.6) is not met. In the esmRCP8.5 scenario, NorESM1-ME projects the whole water column below 20 m (uncertainty: 10-20 m) to be undersaturated with respect to aragonite at the end of this century, such that all cold-water coral reefs in the Nordic Seas will be exposed to corrosive waters. For esmRCP8.5 the NorESM1-ME results are consistent with our CMIP5 model ensemble that suggests the future saturation horizon lies in the range of 0 and 100 m. Comparison with the CMIP5 ensemble is not possible for esmRCP2.6 and esmRCP4.5 because few of the models have performed emission-driven runs under these scenarios. However, NorESM1-ME simulates one of the stronger pH-declines in all depth layers considered in Fig. S5 (Table S6), and has also been shown to be on the upper end of absorption of anthropogenic carbon in the Arctic Ocean (Terhaar et al., 2020a), suggesting that our estimates of the future saturation horizon lies in the shallower end of possible future states.

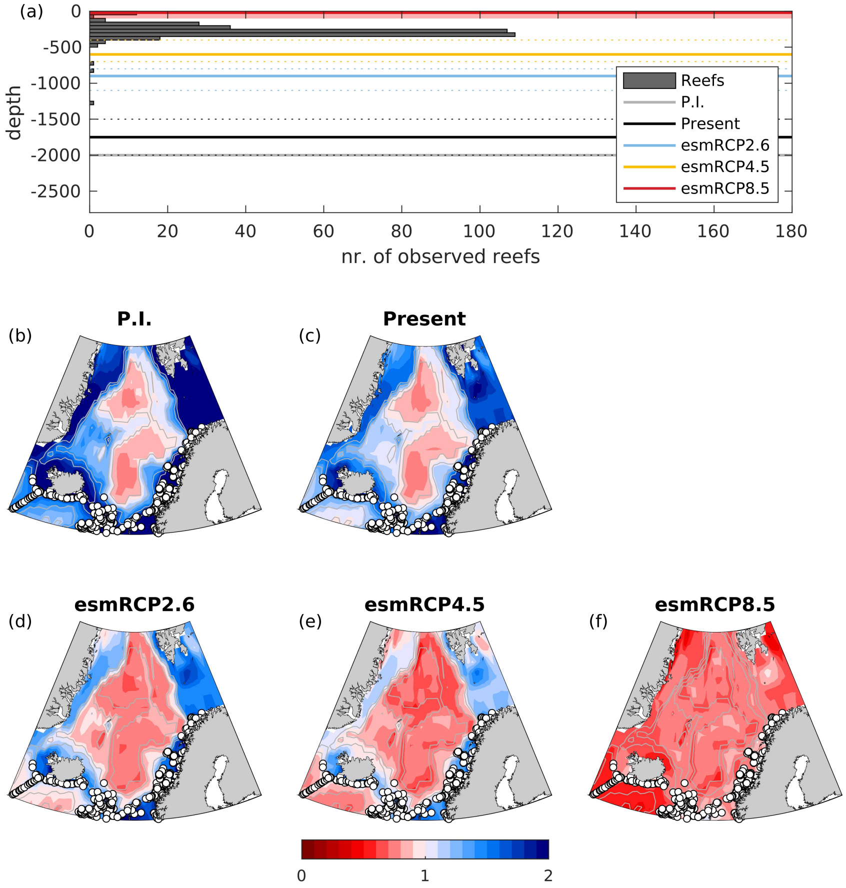

Figure 12. Number of observed reef sites per 50 m depth interval together with the aragonite saturation horizons (solid lines) in the Nordic Seas for past (1850-1879), present-day (1980-2005) and future (2070-2099) under the esmRCP2.6, esmRCP4.5 and esmRCP8.5 scenarios calculated from the GLODAPv2 climatology and NorESM1-ME simulations. The dashed lines show the uncertainty (σ_{field}). The red shading shows the projection uncertainty as estimated from our ESM ensemble for esmRCP8.5. (a) and maps showing aragonite saturation state of bottom waters (calculated from the GLODAPv2 climatology and NorESM1-ME simulations) together with positions of observed reefs (b-f).

5.2 Drivers of Ocean Acidification

5.2.1 Present-day drivers

To understand what has caused the observed pH changes presented in Sect. ~~5~~5.4, we decompose the trends into their different drivers ~~using Eq. 2 and subsequent transformation of fCO_2 to pH~~ as described in Sect. 4.2 (Fig. 13). In the ~~surface~~ upper layer (i.e.~~the upper 200~~ , 0-200 m) the pH decrease in the period 1981-2019 is in agreement (within 95% confidence) with the pH change expected from the increase in atmospheric CO_2, except for in the Norwegian Basin and the Iceland Sea where the trends

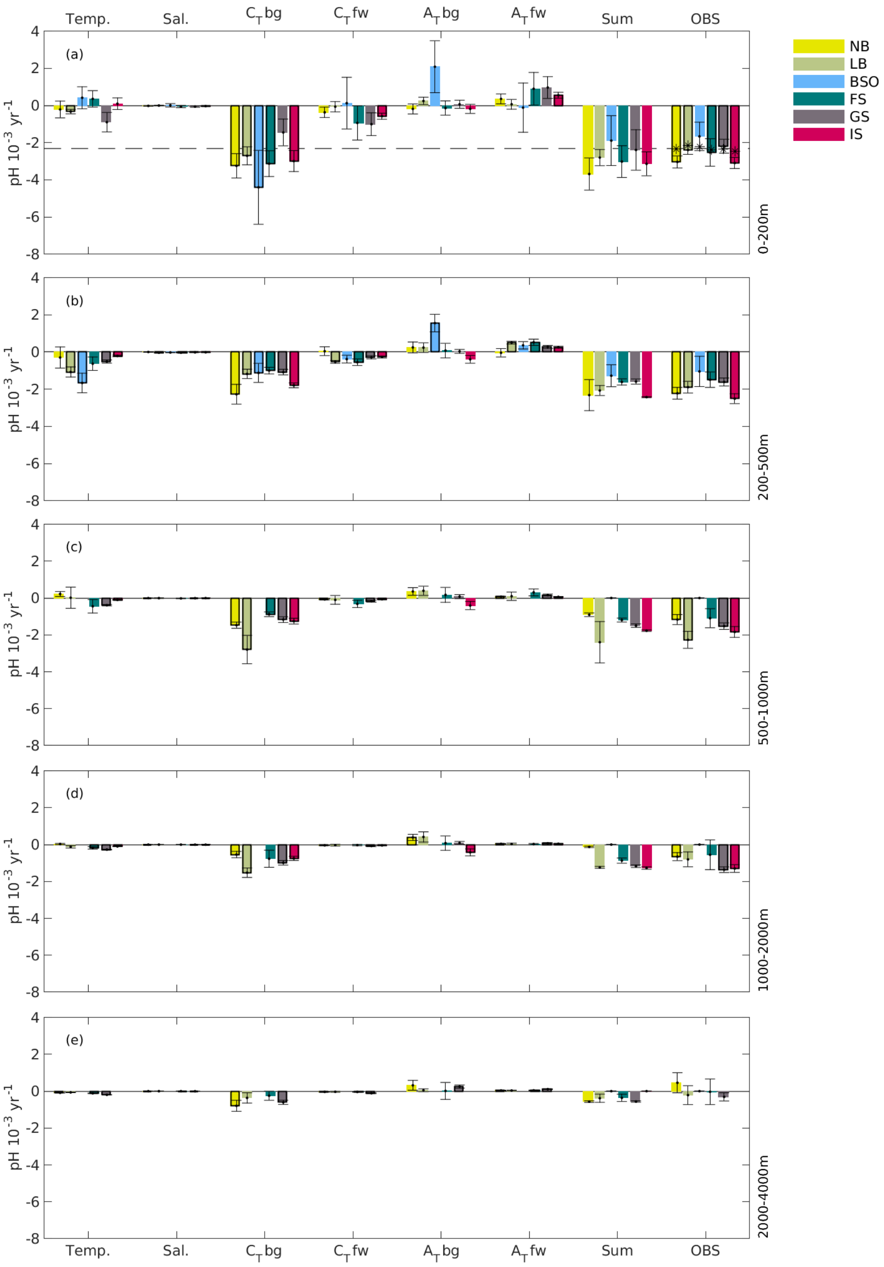

Figure 13. Contribution of observed changes in temperature, salinity, C_T, A_T to the observed trend in pH (OBS) over the 1981-2019 period. The contribution of C_T, A_T was divided into a freshwater (fw) component and a biogeochemical (bg) component. Bars showing trends that are significantly different from zero are outlined with a black line. 'Sum' indicates the total trend in pH calculated as the sum of the trends associated with these ~~four~~ six driving factors. The dashed line and black asterisks indicate the pH trends expected from the change in atmospheric CO_2 during the same period for the whole area and for the separate basins, respectively.

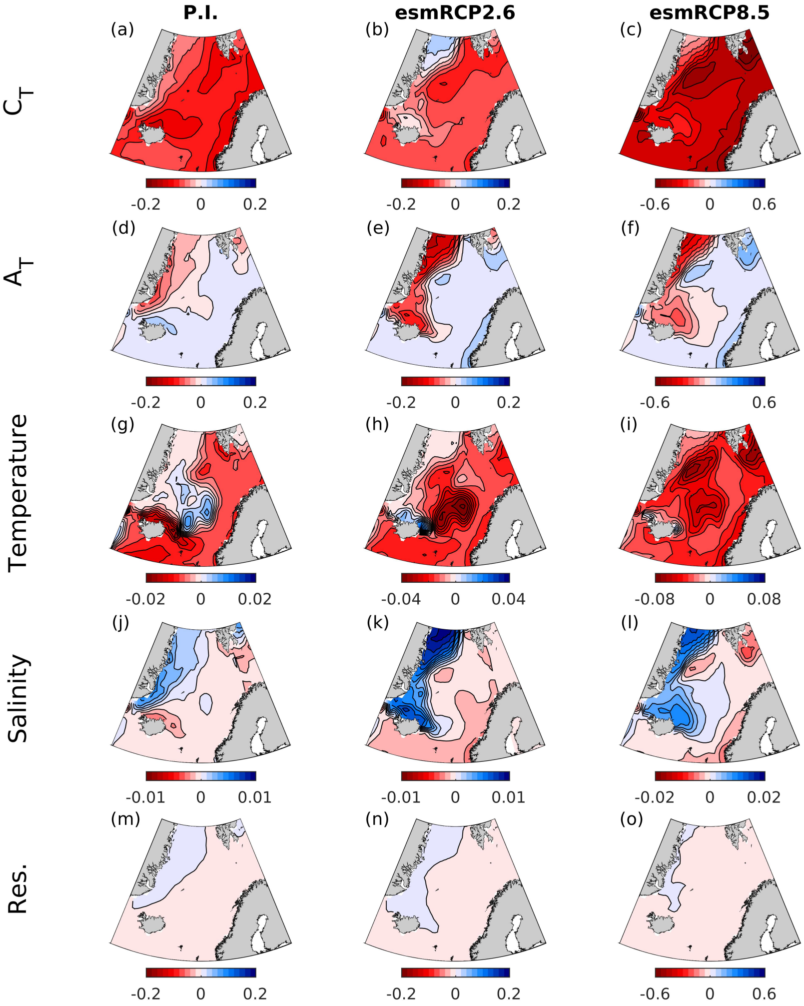

Figure 14. Contribution of modelled changes in surface C_T, A_T, temperature, and salinity, to the change in pH between 1850-1859 and 1996-2005 (P.I.), and 1996-2005 and 2090-2099 (esmRCP2.6 and esmRCP8.5). 'Res.' shows the residual between the total change in pH, calculated as the sum of the trends associated with these four driving factors, and the actual change shown in Figs. 5,9,11.

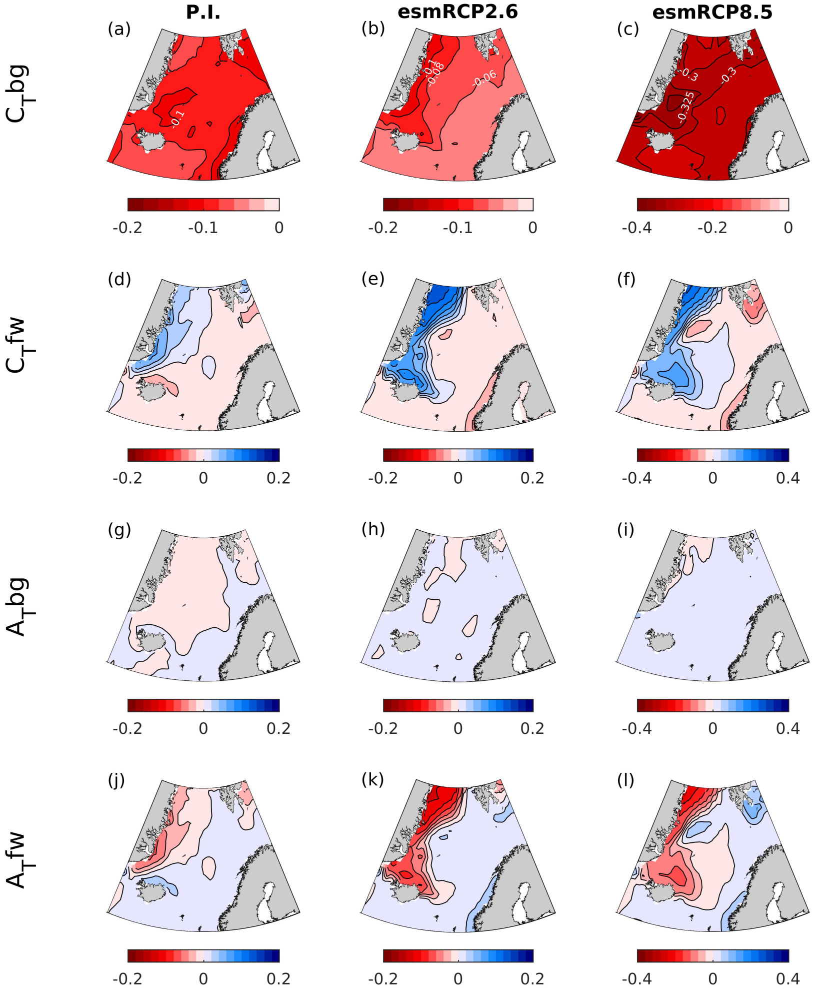

Figure 15. Contribution of the biogeochemical and freshwater components of C_T and of A_T ($A_T$bgc and $A_T$fw) to the change in pH between 1850-1859 and 1996-2005 (P.I.), and 1996-2005 and 2090-2099 (esmRCP2.6 and esmRCP8.5). Res. shows the residual between the total change in C_T and A_T, calculated as the sum of the freshwater and biogeochemical components, and the actual change shown in Fig. 15

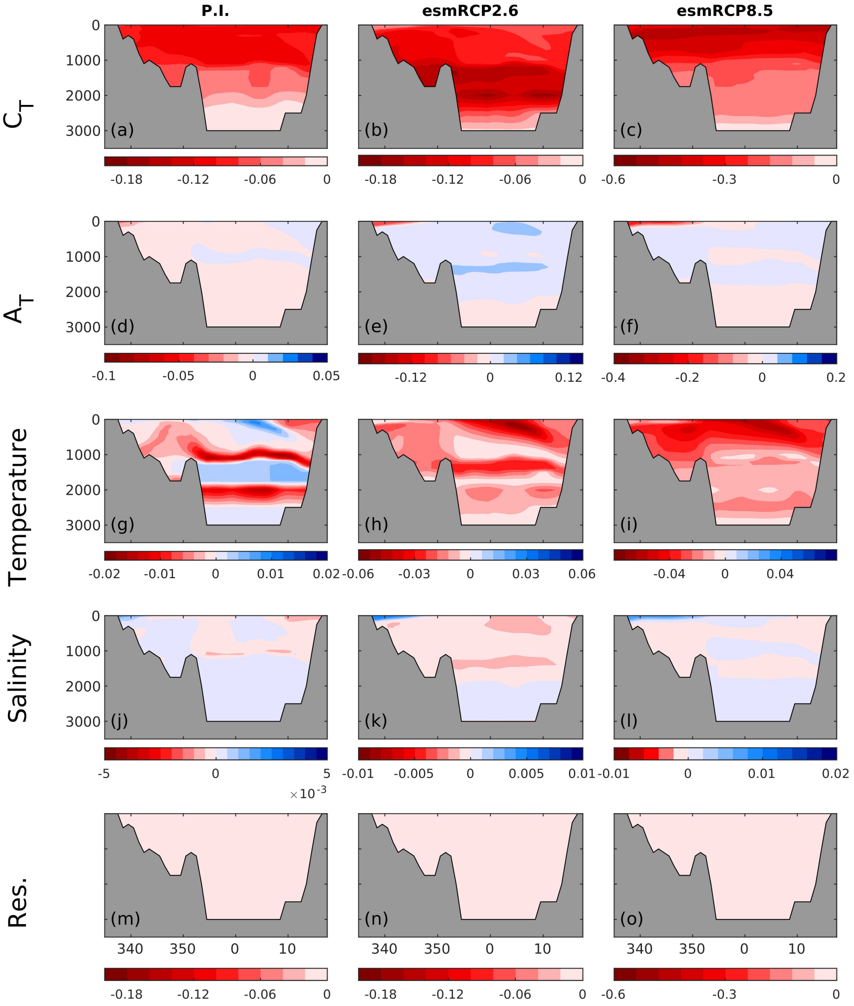

Figure 16. Contribution of modelled changes in surface temperature, salinity, C_T, A_T to the change in pH between 1850-1859 and 1996-2005 (P.I.), and 1996-2005 and 2090-2099 (esmRCP2.6 and esmRCP8.5) at the depth section at 70°N. Res. shows the residual between the total change in pH, calculated as the sum of the trends associated with these four driving factors, and the actual change shown in Figs. 6,10.

are ~~larger~~stronger. This is related to a faster increase in the seawater $p\mathrm{CO}_2$ compared with that of the atmosphere (Fig. ~~S18~~S21), meaning that the $p\mathrm{CO}_2$ undersaturation of the Norwegian Basin and the Iceland Sea is ~~diminishing. The significance of these results are, however, sensitive to the choice of months, i.e. , trends calculated with data from April-September, or July-August, give different results. The~~ has decreased. We note that this diminishing undersaturation is sensitive to seasons. In the Norwegian basin there is no significant decrease if using data from only April to September and June to August, respectively. In the Iceland Sea the decreasing undersaturation is absent for April-September, but it becomes stronger than the annual mean if using data only from June-August. The sensitivity to the choice of seasons indicates that the strong positive trend in the air-sea $p\mathrm{CO}_2$ ~~that we see~~ difference as seen in our dataset can ~~therefore~~ be a result of seasonal undersampling, and that this should be verified with a larger dataset. Notwithstanding, diminishing $p\mathrm{CO}_2$ undersaturation ~~have~~ has been observed in earlier studies of the North Atlantic (Lefèvre et al., 2004; Olsen et al., 2006; Ólafsson et al., 2009; Metzl et al., 2010; Skjelvan et al., 2014), and could be a result of a change in any of the mechanisms underlying the $p\mathrm{CO}_2$ ~~under saturation~~ undersaturation in surface waters of the Nordic Seas (see Sect. 1), including cooling of northward flowing Atlantic waters, primary production and the outflow of $p\mathrm{CO}_2$ undersaturated waters from the Arctic Ocean. ~~Considering that the data we have used are biased towards the productive season, it is possible that parts of the increase in the degree of $p\mathrm{CO}_2$ saturation comes from a reduction in the efficiency of the biological pump (i.e. biological CO_2 consumption). Lefèvre et al. (2004) observed a stronger increase in the seawater $p\mathrm{CO}_2$ during summer compared with winter in the North Atlantic subpolar gyre, which they suggested to be a result of a decrease in productivity.~~ One other possible mechanism was suggested in Olsen et al. (2006) and Anderson and Olsen (2002), where they associated the fast increase in seawater $p\mathrm{CO}_2$ with a large advective supply of anthropogenic carbon from the south and corresponding changes in the buffer capacity (see also Terhaar et al. (2020b)).

The main driver of the present-day (1981-2019) pH decrease in the ~~surface~~ upper layer is increasing C_T, which ~~is partly offset by A~~primarily is caused by biogeochemical processes (C_T~~increases (see also Fig. S4~~bgc), including increasing anthropogenic carbon, along with a small freshwater contribution ($\mathrm{C}_T$fw) caused by an increasing salinity (Fig. S2). The ~~effect of increasing A~~increasing salinity also results in an increasing A_T ~~is strongest in the Barents Sea Opening that, together with an apparent cooling, explain the low, non-significant, pH decline observed there~~ (Fig. ~~7). The overall increase in~~ S4). As seen in Fig. 13, the freshwater components of C_T and A_T ~~is partly a consequence of increasing salinities in~~ are of equal size but opposite sign, and there is therefore no net effect of freshwater fluxes on the pH change (see Sarmiento and Gruber (2006) for a theoretical explanation). Also the thermodynamic effect of increasing salinity on pH is negligible. This increasing salinity of the Nordic Seas ~~in the past decades (Fig. S2, S19), which also have been observed in many studies and has been explained to be~~ is a result of changes in the inflowing Atlantic Water related to subpolar gyre strength (Holliday et al., 2008; Lauvset et al., 2018). The ~~increasing salt content does not only affect A_T, but also equally C_T. This effect is , however, about the same magnitude as the~~ contribution of the biogeochemical component of A_T ~~driver, but in opposite direction~~ is generally negligible, except in the Barents Sea Opening where it explains the lack of a significant pH decline (Fig. ~~S19). The~~ 7). In our dataset, the effect of changes in temperature on pH in the ~~surface~~ upper layer is relatively small. In contrast to several studies pointing towards a warming of the Nordic Seas (e.g. Holliday et al., 2008; Blindheim and Østerhus, 2013; Lauvset et al., 2018; Ruiz-Barradas et al., 2018), the Barents Sea Opening, the ~~Eastern~~ eastern Fram Strait and the Iceland Sea ~~here show a tendency, although~~

~~insignificant, towards a cooling, which slightly increases pH. The ambiguous effect of temperature in surface waters is a result~~ show no significant change in temperature. This might be an artefact of unequal distribution of sampling over the seasons. When calculating trends with all available temperature data, not only ~~the ones that accompanied~~ those accompanying the C$_T$ and A$_T$ data, we obtain a clear warming signal (not shown). ~~In an attempt to estimate the effect of seasonal under sampling on our surface pH trends, we also calculated the trends and their drivers by using data from the productive season (April-September) only. The pH trends obtained from these data are not significantly different from the ones in Fig. . However, the trend in the Barents Sea Opening is now of similar size as in the other regions. The temperature has now a reinforcing effect on the pH decline. This suggest that the weak apparent trend in pH in Fig. is a result of a seasonal undersampling of temperature.~~

In deeper layers, there is an overall increase in C$_T$, A$_T$ (except in the Iceland Sea), salinity, and temperature. Although the effect of increasing C$_T$bgc is reduced away from the surface as a consequence of the gradual isolation of deeper waters from the atmosphere, it remains the main driver of pH change down to 2000 m~~, with a few exceptions~~. The significant trends of C$_T$bgc at the 1000-2000 m depth level in the Greenland Sea could be a consequence of the deep winter mixing that has been shown to reach down to 1500 m in this region (Brakstad et al., 2019). In the ~~200-500 m layer in the~~ other regions of the Nordic Seas the winter mixed layers have not been documented to reach these depths (Ólafsson, 2003; Skjelvan et al., 2014; Våge et al., 2015, e.g.). However, intermediate water masses of the Greenland Sea has been shown to spread horizontally in the Nordic Seas, which could also explain the significant trends in the Norwegian and Lofoten Basin and ~~the Barents Sea Opening, there is an increase in temperature, leading to a pH decline that is almost as large as that from the C$_T$ increase. In~~ in the Icealand Sea (Blindheim, 1990; Blindheim and Rey, 2004; Messias et al., 2008; Jeansson et al., 2017). The effect of the biogeochemical component of A$_T$ is negligible in deep waters, except for in the Barents Sea Opening, where the increase of A$_T$bgc in the 200-500 m layer is as large as in the surface layer, and in the 1000-2000 m layer in the Norwegian Basin, where there is an increase in A$_T$~~that almost~~ bgc that nearly cancels the effect of increasing C$_T$~~. Below 2000 m, the effects of changes in A$_T$ are of similar size as the effect of changes in C$_T$ in all basins. As for the surface layer, part of the C$_T$ and A$_T$ increase can be explained by increasing salinites, but there is also a biogeochemical component (Fig. S19). The uncertainties in the freshwater and biogeochemical components are, however, large, making the decomposition uncertain. The warming seen in the deep waters is likely a result of the decreased deep-water formation in the Greenland Sea and the following increased exchange with warmer Arctic deep waters (e.g. Østerhus and Gammelsrød, 1999; Blindheim and Rey, 2004; Karstensen et al., 2005; Somavilla et al., 2013). The relatively strong trends in C$_T$ and pH in the upper 2000m of the Greenland and Iceland seas could be a consequence of deep winter mixing (Våge et al., 2015; Brakstad et al., 2019). However, the convection in the Iceland Sea has only been documented to reach depths of 200-400 m (Ólafsson, 2003; Våge et al., 2015). The signal in the deep Iceland Sea is therefore likely a result of spreading of intermediate waters from the Greenland Sea (Messias et al., 2008; Jeansson et al., 2017). Also in the Norwegian Basin there is a significant trend down to 2000 m, although weaker than in the other basins. This is likely also a result of advection from the Greenland Sea (Blindheim, 1990; Blindheim and Rey, 2004; Jeansson et al., 2017). The strong trends in C$_T$ in the Lofoten Basin could be a result of a combination of the persistent eddy in this area (dominating the upper 1000 m), and advection of intermediate water from the Greenland Sea at about 1000-1500 m (Jeansson et al., 2017).~~

~~The water-masses in the 2000-4000 m range are increasingly dominated by old Arctic deep waters (e.g. Somavilla et al., 2013). With ages of around or more than 200 years (Jutterström and Jeansson, 2008; Stöven et al., 2016), they have been isolated from the increasing anthropogenic CO_2, which explains the weak trends at these depths.~~

bgc. The exceptionally strong trends in A_T~~in the surface~~ bgc in the upper and the 200-500 m layer in the Barents Sea Opening are intriguing. Considering that the strong $A_T$bgc trend also exists in the 200-500 m layer, it is likely not a result of seasonal undersampling. ~~Further, the salinity decomposition in Fig. S19 in the Supplementary material suggest that it is not a result of changing salinity, but rather of biogeochemical processes. While this decomposition gives clear results in the 200-500 m layer, the uncertainty of the freshwater component is as large as the biogeochemical component in the surface layer, making the decomposition, and therefore the role of changes in freshwater content and biogeochemical processes, uncertain. This is a result of the uncertainty in the salinity trend (Fig. S2), which could be caused by the presence of the relatively fresh, Norwegian Coastal Current that has been shown to occasionally, under specific wind conditions, spread into the Barents Sea Opening Olsen et al. (2003).~~ One biogeochemical process that could have a potential impact the Barents Sea $A_T$bgc trend is the recurrent blooms of calcifying coccolithophorids (Giraudeau et al., 2016), which consumes A_T during growth, and releases A_T when their shells are decomposed. There ~~is an indication~~ are indications of an increase in their presence in the Barents Sea (Giraudeau et al., 2016; Oziel et al., 2020). In which direction this would impact the A_T depends on horizontal advection, remineralization and burial, and deserves separate dedicated process studies. The freshwater components of C_T and A_T are mainly detectable in the upper 500 m. As for the surface, the thermodynamic effect of salinity changes on pH are neglibible in the deep water. The warming seen in deep waters, that has a negative contribution on the pH trend, is an additional indication of that the absence of a temperature trend in the upper layer is a result of seasonal undersampling. In deep waters, the warming signal do not only come from local vertical mixing. There is also an indication of decreased deep-water formation in the Greenland Sea, which has caused an increased exchange with warmer Arctic deep waters (e.g. Østerhus and Gammelsrød, 1999; Blindheim and Rey, 2004; Karstensen et al., 2005; Somavilla et al., 2013). Below 2000 m, there are barely any detectable changes in the various pH drivers. The water masses at these depths are increasingly dominated by old Arctic deep waters (e.g. Somavilla et al., 2013). With ages exceeding 200 years (Jutterström and Jeansson, 2008; Stöven e have been isolated from the increasing anthropogenic CO_2, which explains the weak trends at these depths.

~~Contribution of modelled changes in surface C_T, A_T, temperature, and salinity, to the change in pH between 1850-1859 and 1996-2005 (P.I.), and 1996-2005 and 2090-2099 (RCP2.6 and RCP8.5). Res. shows the residual between the total change in pH, calculated as the sum of the trends associated with these four driving factors, and the actual change shown in Figs. 5,9,11.~~

~~Contribution of modelled changes in surface temperature, salinity, C_T, A_T to the change in pH between 1850-1859 and 1996-2005 (P.I.), and 1996-2005 and 2090-2099 (RCP2.6 and RCP8.5) at the depth section at 70°N. Res. shows the residual between the total change in pH, calculated as the sum of the trends associated with these four driving factors, and the actual change shown in Figs. 6,10.~~

5.2.2 Past and future drivers

For past and future changes, the drivers of surface pH change show similar spatial patterns over all time periods, except for temperature (Fig. 14). ~~As for the present day changes, the main driver of pH change~~ The main driver is an increase in C_T, which is larger in Atlantic Water than in polar waters. ~~The larger increase in~~ This is explained by the dilution of C_T in ~~the Atlantic Water, which is in agreement with what has been observed over the last 2-3 decades (Olsen et al., 2006), can partly be related to their higher buffer capacity (Sect. 2). In polar waters , C_T is additionally diluted~~ polar waters by the increased freshwater export from the Arctic Ocean ~~(Shu et al., 2018) that to varying~~ (Fig. 15, Shu et al., 2018) that to some degree counteracts the effect of atmospheric CO_2 uptake. ~~The increasing freshwater export also results in a dilution of A~~A similar freshwater effect has recently been observed also in the Arctic Ocean (Woosley and Millero, 2020). The biogeochemical component of the C_T ~~and salinity~~ driver (Fig. 15), which is primarily the effect of increasing anthropogenic carbon, is larger in polar waters ~~that have, respectively, a negative and positive contribution to the pH trend. While the~~ for the changes from present to future in both the esmRCP2.6 and esmRCP8.5 scenarios, in agreement with is what is expected from their lower buffer capacity (Sect. 2). The effect of A_T ~~dilution is on~~ is most prominent in polar waters, where a reduced A_T concentration contribute to a pH decrease that is of the same order of magnitude as ~~the effect of~~ that driven by C_T~~dilution, the effect of the reduction in salinity is minor~~. From the freshwater decomposition in Fig. 15, we see that the A_T changes are mainly driven by freshwater fluxes, and that contributions from the biogeochemical component are negligible. A_T dilution has also been shown to be important in the future in the Arctic ocean in several CMIP6-models (Terhaar et al., 2021). However, as discussed earlier, the net effect of these freshwater fluxes on pH are minor, as the dilution of A_T and C_T is similar, but have opposite effects on pH (compare Fig. 15d-f with 15j-k). The increasing freshwater export also results in a dilution of salinity in polar waters that has a positive contribution to the pH trend. The Atlantic Waters show a tendency towards increasing ~~A_T and~~ salinity that partly ~~reduces/amplify~~ amplifies the decrease in pH. ~~The temperature~~ Temperature has an overall negative effect on the pH trend as a result of an overall warming. From ~~past to present, present to future RCP2~~pre-industrial to present-day, and present-day to future esmRCP2.6, the temperature increase is almost ~~non-existing~~ non-existent in polar waters, indicating that it has been shielded from warming through the presence of sea ice. In some smaller regions there is even a sign of a cooling, which could be a result of an increased presence of polar waters due to the increasing freshwater export.

The combined effect of these drivers explain the zonal gradients in the pH decrease that ~~we saw~~ are described in Sect. 5.3 and 5.5. From past to ~~present,~~ present-day the largest pH decrease ~~take~~ takes place in the Atlantic Water due to a stronger ~~uptake~~ increase of anthropogenic carbon and a stronger warming in these waters. From present-day to future the acidification becomes larger in polar waters compared to Atlantic Water due to the stronger increase of anthropogenic carbon in these waters. The increasing freshwater export from the Arctic ~~, and the dilution of A~~that is seen in all time periods is of importance when regarding C_T ~~, plays an important role in the eastern Nordic Seas, but it does not override the acidification rate in the Atlantic Water. From present-future, the freshwater export and dilution of~~ and A_T ~~plays a bigger role, and the acidification becomes larger in polar waters compared to Atlantic Water~~concentrations separately, but their combined effect on pH is negligible. For the changes from ~~past-present, and present to future RCP2~~past to present-day and present-day to future esmRCP2.6 ~~,~~ the zonal gradient in Ω_{Ar} ~~drops~~ trend follows that of pH, showing the importance of the ~~competing effect of A_T dilution in polar waters, and C~~C_T ~~uptake in Atlantic Water, respectively. In RCP8~~driver. It is reinforced by the spatially variations in the warming, i.e., the stronger warming in the Atlantic Water compared polar waters results in a relatively stronger drop in Ω_{Ar} in polar waters. In the esmRCP8.5 ~~, there is~~future, Ω_{Ar}, in contrast to pH, exhibit a larger drop in the ~~easter part~~Atlantic Water. This can be explained by the ~~larger~~ relatively small changes in temperature ~~, which affects Ω_{Ar} in the opposite direction.~~

~~In the historical run and all three future projections of NorESM1-ME, the change in surface ocean $p\mathrm{CO_2}$ differs from the change in the atmosphere (Fig. S14). From past to present, there is an increase in the undersaturation, i.e. the positive trend in the oceanic $p\mathrm{CO_2}$ lags the trend in the atmosphere. This means that the pH decrease is less than that expected from the increase in atmospheric $\mathrm{CO_2}$. The lag continues into all the future scenarios, but from around 2040 and onward the oceanic $p\mathrm{CO_2}$ increases faster than that of the atmosphere, resulting in a decreasing undersaturation. In RCP2.6 and 4.5 this gives rise to, on average, stronger decreases in pH (from 1996-2005 to 2090-2099) than expected from the rise in atmospheric $\mathrm{CO_2}$. In RCP8.5, however, the difference between the end-of-the century ocean and atmospheric $p\mathrm{CO_2}$ is still larger than the present day, meaning that the decrease in pH is less than expected. As detailed above there are several mechanisms underlying undersaturation of surface ocean $p\mathrm{CO_2}$~~ in this region compared to the rest of the Nordic Seas, ~~but further analyses of these, including their potential future changes, is beyond the scope of this paper~~which affect Ω_{Ar} in the opposite direction compared to pH.

Below the surface layer, C_T is also the main driver of past and future pH changes (Fig. 16). The change from pre-industrial to ~~present~~ present-day indicates a gradually weaker impact of C_T with depth, except for a tongue at about 1000 m depth that connects to the surface in the Iceland sea. This is most likely related to the deep water formation in this region that spreads at depth. The end-of-the-century C_T increase ~~under the RCP2~~for the esmRCP2.6 scenario is larger in the deep than in the surface layer, resulting in the stronger pH reduction at mid-depths as seen in Fig. 10. This mid-depth layer with a strong acidification is partly a result of the higher atmospheric $\mathrm{CO_2}$ concentrations in the middle of the 21st century ~~,~~in combination with the rapid ventilation of the water column in this area, i.e., when these waters were at surface they were exposed to peak atmospheric $\mathrm{CO_2}$. However, the large C_T increase in deep waters is also partly explained by increased remineralization, as indicated by a $\sim$1 ml $\mathrm{O_2}$ $\mathrm{l^{-1}}$ increase in the apparent oxygen utilization (AOU) at depths of 1800-2100 m ~~in both RCP2~~throughout the Nordic Seas in both esmRCP2.6 and ~~RCP8~~esmRCP8.5 (not shown)~~throughout the Nordic Seas. Assuming Redfield (~~. Assuming a Redfield ratio of $\mathrm{O_2}$:C=132:106~~)~~, this corresponds to a change in C_T of $\sim$30 μmol kg^{-1}, which results to a pH decrease of $\sim$0.1 at the alkalinity in question. Impacts of changes in A_T, salinity and temperature, are relatively modest at depth.

The residual between the sum of the four drivers and the actual pH change is small (Figs. 14 and 16) and can be attributed to approximations involved in the decomposition, including the approximations of the partial derivatives, the assumption of a linear trend and the use of temporal means (Takahashi et al., 1993; Lenton et al., 2012; Lauvset et al., 2015). ~~These assumptions are least appropriate for the RCP8.5 scenario, where the changes are largest, and therefore the residual is especially large for this scenario.~~ Although the absolute numbers related to the drivers should be taken with care, this decomposition still gives a good estimate of the relative importance of temperature, salinity, C_T, and A_T on pH changes.

5.3 ~~Implications for cold-water corals~~

~~Number of observed reef sites per 50 m depth interval together with the aragonite saturation horizons (solid lines) in the Nordic Seas for past (1850-1879), present (1980-2005) and future (2070-2099) under the emission-driven RCP2.6, RCP4.5 and RCP8.5 scenarios calculated from the GLODAPv2 climatology and NorESM1-ME simulations. The dashed lines show the uncertainty (σ_2). The red shading shows the projection uncertainty as estimated from our ESM ensemble for RCP8.5. (a) and maps showing aragonite saturation state of bottom waters (calculated from the GLODAPv2 climatology and NorESM1-ME simulations) together with positions of observed reefs (b-f).~~

~~Cold-water corals build their structures out of aragonite, which is the more soluble form of calcium carbonate. To some degree, living corals can compensate for aragonite undersaturation in seawater and increase their internal pH by 0.3-0.6 (McCulloch et al., 2012; Allison et al., 2014). For some time these corals can therefore continue to calcify in waters with Ω_{Ar}<1, however, the calcification rates and breaking strength of the structures of the most abundant coral organism, *Lophelia pertusa*, is reduced under such conditions (Hennige et al., 2015). Furthermore, dead coral structures, which compose a major part of the reefs, cannot resist corrosive waters and experience increased dissolution rates in a situation with Ω_{Ar}<1. Cold-water coral reefs, along with their ecosystems, are therefore likely to collapse if the water they live in becomes undersaturated in aragonite. It has been estimated that globally about 70% of the deep sea corals will be below the aragonite saturation horizon by the end-of-the-century under high-emission-scenarios (Guinotte et al., 2006; Zheng and Cao, 2014).~~

~~Most of the reef sites that have been identified in the Nordic Seas (321 out of the 324 within the region defined in Fig. 1) are at depths of 0-500 m~~ In the historical run and all three future projections of NorESM1-ME, the change in surface ocean $p\mathrm{CO}_2$ differs from the change in the atmosphere (Fig. ~~12, see also Buhl-Mortensen et al. (2015)). The current aragonite saturation horizon is at 2000 m, with uncertainty range 1750-2500 m. Note that the uncertainty range of the depth of the saturation horizon is not equally distributed around the mean because the uncertainty analysis is done for the saturation state, from which the depth distribution is calculated. From observations we also see that the waters in the depth range 1000-2000 m are close to being undersaturated in aragonite (Sect.5.4).In the emission-driven RCP2.6 scenario, NorESM1-ME projects that the aragonite saturation horizon will shoal to 1100 m (uncertainty: 900-1300 m) by the end of the century. In the emission-driven RCP4.5 scenario, the saturation horizon is projected to shoal to 600 m depth (uncertainty: 400-800 m) by the end of this century. This implies that the deepest observed reefs will be exposed to corrosive waters, and thus experience elevated costs of calcification and dissolution of dead structures. The majority (315 out of 324) of the coral sites in the Nordic Seas are, however, found at shallower depths than the projected saturation horizon with its uncertainty, although the margins are small. Also García-Ibáñez et al. (2021) suggested that cold-water corals in the subpolar North Atlantic will be exposed to corrosive waters if the 2-degree goal (which is the aim of RCP2.6) is not met. In the RCP8.5 scenario, NorESM1-ME projects the whole water column to be undersaturated in aragonite at the end of this century, such that all cold-water coral reefs in the Nordic Seas will be exposed to corrosive waters. Because of the low Ω_{Ar} in surface waters, the uncertainty of Ω_{Ar} related to mapping, measurements and dissociation constants does not result in any uncertainty in the saturation horizon in this scenario (i.e. Ω_{Ar} < 1 in the surface waters also when taking into account the uncertainties). For RCP8.5~~ S16). From pre-industrial to present-day, there is an increase in the undersaturation, i.e., the ~~NorESM1-ME results are consistent with our CMIP5 model ensemble that suggests that the future saturation horizon lies in the range of 0 and 100 m. Comparison with the CMIP5 ensemble is not possible for RCP2~~increase in the oceanic pCO$_2$ lags behind the increase in the atmosphere. This means that the pH decrease is less than that expected from the increase in atmospheric CO$_2$. The lag continues into all the future scenarios, but from around 2040 and onward, the oceanic pCO$_2$ increases faster than that of the atmosphere, resulting in a decreasing undersaturation. In esmRCP2.6 and ~~RCP4~~esmRCP4.5 ~~because few of the models have performed emission-driven runs under these scenarios. However, NorESM1-ME simulates among the stronger drops in pH in all depth layers considered in Fig. S5, and have also been shown be in the upper end of absorption of anthropogenic carbon in the Arctic Ocean (Terhaar et al., 2020a), suggesting that out estimates of the future saturation horizon lies in the upper bound of possible future states~~this causes stronger decreases in pH (from 1996-2005 to 2090-2099) than expected from the rise in atmospheric CO$_2$. In esmRCP8.5, however, the difference between the end-of-the century ocean and atmospheric pCO$_2$ is still larger than the present-day, meaning that the decrease in pH is less than expected. As detailed above there are several mechanisms underlying undersaturation of surface ocean pCO$_2$ in the Nordic Seas, but further analyses of these, including their potential future changes, is beyond the scope of this paper.

6 Summary and Conclusions

We have provided a detailed analysis of spatial and temporal variations of past, ~~present~~ present-day and future acidification, and its drivers, in the Nordic Seas. We have further assessed the potential impacts of this acidification on aragonite saturation and cold-water coral reefs. This work builds on (Skjelvan et al., 2014), who estimated pH trends, and their drivers, for various sub-regions of the Nordic Seas from observational data sampled between 1981 and 2013. Here we have added data from the Iceland Sea and from later years, to obtain the greatest possible temporal and spatial coverage. We have additionally made an analysis of past and future pH changes by the use of the gridded GLODAP climatolgy and ESM-simulations, to put the observed changes into the context of long-term climate change. In contrast to previous studies that have assessed the future pH changes in the Nordic Seas for single scenarios (Bellerby et al., 2005; Skogen et al., 2014, 2018), we here analyse output from one mitigation scenario, one stabilization scenario and one high-emission scenario. To our knowledge, no previous studies have presented past pH changes in the Nordic Seas.

pH changes and its potential ecosystem impacts

From 1850 to 1980 both the model simulation of NorESM1-ME and observational data, together with the GLODAPv2 pre-industrial estimate, suggest that the pH of Nordic Seas surface waters has dropped by 0.06, which is similar to the pH decrease ~~of~~ in the global surface ocean. During this period, the aragonite saturation horizon has slightly shallowed, but has remained well below the depths of known cold-water coral habitats. During ~~the last 39 years covered by this study~~1981-2019, when regular sampling of carbon system variables have been made in the region, the pH of the Nordic Seas ~~surface waters~~ upper layer has decreased at a rate of -2.79±0.3 10^{-3} yr^{-1} on average, resulting in a pH decline of 0.11~~between 1981 and 2019. This decrease is stronger than the decrease observed for the global ocean of -1.80±0.4 10^{-3} yr^{-1} for the period 1991-2011~~

~~(Lauvset et al., 2015)~~. The pH reductions are significant all over the Nordic Seas ~~surface waters~~upper layer (0-200 m), except in the Barents Sea Opening where the lack of significant change is a result of a strong increase in A$_T$. In some regions the acidification is detectable down to 2000 m, which we attribute to the deep water formation ~~an how these water-masses spreads at depth, and the~~ and spreading of these water masses at depth. The waters at 1000-2000 m throughout the Nordic Seas ~~have approached~~ are now close to aragonite undersaturation. Our results are in overall agreement with Skjelvan et al. (2014), but the longer timeseries result in statistically significant ($p<0.05$) trends in even more regions and depth layers. An additional pH drop of 0.1-0.4 in the surface waters is projected until the end of the 21st century, depending on the emission scenario. In the high-emission scenario, ~~RCP8~~esmRCP8.5, all cold-water coral reefs will be exposed to corrosive waters by the end of the 21st century, threatening not only their existence, but also that of their associated ecosystems. This is confirmed by an ~~CMIP5-ensemble of 7 models, whose members~~ ensemble of 6 CMIP5 models, who all agree on these consequences. The NorESM1-ME simulations suggest that some cold-water corals will be exposed to undersaturation also under the ~~RCP4~~esmRCP4.5 scenario, and that this only can be avoided by keeping the emissions within the limits prescribed in the ~~RCP2~~esmRCP2.6 scenario. ~~In comparison to our ESM-ensemble,~~ Because NorESM1-ME tends to simulate a relatively strong decline of pH and shallow saturation horizons ~~. These results can therefore~~ in comparison to our ESM-ensemble for esmRCP8.5, our estimated aragonite saturation horizons for esmRCP2.6 and esmRCP4.5 should be considered as ~~careful estimates~~ the shallow, lower bound of possible future states. Our estimates of the future pH and Ω_{Ar} in the Nordic Seas add more possible future states to the ones presented for the A1B and RCP4.5 scenarios by Skogen et al. (2014, 2018).

pH drivers

The acidification during the last 39 years is, in all sub-regions, mainly driven by increasing C$_T$ ~~coming from the uptake of anthropogenic carbon~~ in response to the rising anthropogenic carbon concentrations. This is in agreement with the results for the period of 1981-2013 from Skjelvan et al. (2014), who calculated the drivers of pH change for the Norwegian Basin and the Greenland Sea. The effects of increasing C$_T$ ~~is~~ are slightly opposed by increasing A$_T$~~, which partly comes as~~. The increasing A$_T$ is partly a result of ~~the increasing salinities, i.e.~~ a "~~the~~ salinification" ~~,~~ of the Nordic Seas. ~~While in the deep waters there is~~ However, this salinification also results in a decrease in C$_T$, which counteracts the effect of the freshwater-driven increase in A$_T$. The net effect of C$_T$ and A$_T$ on increasing pH is therefore a result of biogeochemical processes. We find a clear warming signal in deep waters, which has contributed to the decreasing pH~~, the impact of temperature in the surface is ambiguous, and even shows a cooling in some places~~. In the upper 200 m, however, there is no clear temperature change. We find this ~~apparent cooling~~ to be a result of seasonal undersampling, which further complicates a comparison of the changes in sea surface pCO$_2$ to the atmospheric one. In the Barents Sea Opening, there is an exceptionally strong increase in A$_T$, which we cannot relate to increasing salinity. The reasons behind this strong increase is then either a result of biogeochemical processes, or can also be a result sampling issues. Unfortunately, we cannot pin this down with the dataset we have, and this remains as an open question for future investigations.

~~Also for~~ For past and future changes, we also find increasing C$_T$ ~~is~~ to be the main driver of pH change in the Nordic Seas~~, but here we can~~. This is in agreement with Skogen et al. (2014), but we distinguish some regional differences related to ~~the different water-masses. In the Atlantic Water, the pH change is mainly driven by~~ different water masses. Increasing temperatures, that amplifiy the effect of increasing C_T~~and temperatures, and slightly opposed by increasing A_T related to a salinification, as we also see in our observational dataset for the period of 1981-2019. In polar waters~~, have the largest impact in Atlantic Water in changes from pre-industrial to present-day and present-day to the future esmRCP2.6. The absence of a warming signal in polar waters is a result of the shielding effect of sea-ice. In esmRCP8.5, however, the warming is more uniform over the Nordic Seas, which most likely is a result of the significantly reduced sea ice cover. In both past and future scenarios, there is a clear signal of an increasing freshwater export from the Arctic ~~which has an important impact on the acidification through dilution of~~ Ocean that dilutes C_T, A_T, and salinity ~~. The dilution of C~~in polar waters, and there is a tendency to increasing salinity in the Atlantic Water, that also leads to increasing C_T ~~slightly opposes the effect of uptake of anthropogenic carbon, which increases the relative impact of decreasing~~ and A_T~~on the pH drop. The absence of this freshwater signal in our observational dataset might be a result of the relatively short time scale, but it is also possible that our regions are located to far to the East~~. The total effect of this change in freshwater content on pH is negligible as the effect of changing C_T and A_T oppose each other, and because the thermal effect of salinity is minor in comparison to the other drivers.

Data availability. The GLODAPv2.2019 data and GLODAPv2 mapped climatologies are available for download at https://www.glodap.info/index.php/merged-and-adjusted-data-product-v2-2019/ and https://www.glodap.info/index.php/mapped-data-product/ , respectively.

The data from Ocean Weather station M from 2001-2007 is available in GLODAPv2.2019. Data from the time period 2008-2019 will be available in the next GLODAP version.

The data from the time-series station in the Iceland Sea can be obtained from the NCEI database (Ólafsson, 2012; Ólafsdóttir et al., 2020)

The data from the Norwegian ocean acidification monitoring program (2011-2012 Tilførselsprogrammet and 2013-2019 Havforsuringsprogrammet) (Chierici et al., 2019a), and from the eastern Fram Strait (Chierici and Fransson, 2019) is available at the Norwegian Marine Data Centre (NMDC).

The ESM simulations can be downloaded at https://esgf-node.llnl.gov/search/cmip5/

The cold-water coral positions have been derived from data that is made available under the European Marine Observation Data Network (EMODnet) Seabed Habitats initiative (www.emodnet-seabedhabitats.eu), financed by the European Union under Regulation (EU) No 508/2014 of the European Parliament and of the Council of 15 May 2014 on the European Maritime and Fisheries Fund.

Author contributions. AO, FF and FF designed the research. FF, FF, and AO performed the data-analysis with inputs from NG, IS, MC and EJ. FF lead the writing of the manuscript with inputs from all co-authors. JT designed, tested, and performed the NorESM1-ME model simulations.

Competing interests. The authors declare that they have no conflict of interest.

Disclaimer. TEXT

Acknowledgements. F. Fransner was funded by the Bjerknes Centre for Climate Research and by the Research Council of Norway through the project The Nansen Legacy (RCN # 276730). F. Fröb was funded by the Bjerknes Centre for Climate Research. JT acknowledges funding from Research Council of Norway (Reef-Futures no. 295349 and Columbia no. 275268). NG acknowledges funding from the Research Council of Norway (IMPOSE, 294930). SKL acknowledges funding from the Research Council of Norway (NorArgo2, 269753). This work is a contribution to the project INTAROS. This project has received funding from the European Union’s Horizon 2020 research and innovation programme under grant agreement No 727890. High-performance computing and storage resources were provided by the Norwegian infrastructure for computational science (through projects nn1002k and ns1002k).The Norwegian Ocean Acidification Monitoring Program is funded by the Norwegian Environmental Agency through project no. 17078007. The ~~flagship program1000~~Norwegian program 1000Monitoring ocean acidification in Norwegian waters” ~~within~~ is supported by the Norwegian Environmental Agency and the Institute of Marine Research and with contributions flagship program "Ocean acidification and ecosystem effects in northern waters" at the FRAM-High North Research Centre for Climate and ~~the Environment.~~ Environment.

We acknowledge the World Climate Research Programme’s Working Group on Coupled Modelling, which is responsible for CMIP, and we thank the climate modeling groups for producing and making available their model output. For CMIP, the U.S. Department of Energy’s Program for Climate Model Diagnosis and Intercomparison provides coordinating support and led development of software infrastructure in partnership with the Global Organization for Earth System Science Portals.

References

Allison, N., Cohen, I., Finch, A., Erez, J., and Tudhope, A.: Corals concentrate dissolved inorganic carbon to facilitate calcification, Nature Communications, 5, https://doi.org/doi:10.1038/ncomms6741, 2014.

Anderson, L. G.: Dissolved inorganic carbon, pH, alkalinity, temperature, salinity and other variables collected from discrete sample and profile observations using CTD, bottle and other instruments from the LANCE in the Barents Sea from 1986-07-19 to 1986-07-26 (NCEI Accession 0113910). NOAA National Centers for Environmental Information. Dataset., https://doi.org/10.3334/cdiac/otg.carina_58la19860719, dataset, 2013a.

Anderson, L. G.: Dissolved inorganic carbon, pH, alkalinity, temperature, salinity and other variables collected from discrete sample and profile observations using CTD, bottle and other instruments from the ODEN in the Arctic Ocean, Barents Sea and others from 2002-04-20 to 2002-06-06 (NCEI Accession 0113590). NOAA National Centers for Environmental Information., https://doi.org/10.3334/cdiac/otg.carina_77dn20020420, dataset, 2013b.

Anderson, L. G. and Olsen, A.: Air–sea flux of anthropogenic carbon dioxide in the North Atlantic, Geophysical Research Letters, 29, 16–1–16–4, https://doi.org/10.1029/2002GL014820, https://agupubs.onlinelibrary.wiley.com/doi/abs/10.1029/2002GL014820, 2002.

Anderson, L. G., Blindheim, J., and Rey, F.: Dissolved inorganic carbon, pH, alkalinity, temperature, salinity and other variables collected from discrete sample and profile observations using CTD, bottle and other instruments from the JOHAN HJORT in the North Greenland Sea and Norwegian Sea from 1997-04-14 to 1997-05-22 (NCEI Accession 0113563). NOAA National Centers for Environmental Information., https://doi.org/10.3334/cdiac/otg.carina_58jh19970414, dataset, 2013a.

Anderson, L. G., Johannessen, T., and Rey, F.: Dissolved inorganic carbon, pH, alkalinity, temperature, salinity and other variables collected from discrete sample and profile observations using CTD, bottle and other instruments from the JOHAN HJORT in the North Greenland Sea and Norwegian Sea from 1998-08-01 to 1998-08-23 (NCEI Accession 0113758). NOAA National Centers for Environmental Information., https://doi.org/10.3334/cdiac/otg.carina_58jh19980801, dataset, 2013b.

Arora, V. K., Scinocca, J. F., Boer, G. J., Christian, J. R., Denman, K. L., Flato, G. M., Kharin, V. V., Lee, W. G., and Merryfield, W. J.: Carbon emission limits required to satisfy future representative concentration pathways of greenhouse gases, Geophysical Research Letters, 38, https://doi.org/https://doi.org/10.1029/2010GL046270, https://agupubs.onlinelibrary.wiley.com/doi/abs/10.1029/2010GL046270, 2011.

Bellerby, R. G. J. and Smethie, William M., J.: Dissolved inorganic carbon, alkalinity, temperature, salinity and other variables collected from discrete sample and profile observations using CTD, bottle and other instruments from the KNORR in the Barents Sea, North Atlantic Ocean and others from 2002-05-30 to 2002-07-01 (NCEI Accession 0113569). NOAA National Centers for Environmental Information., https://doi.org/10.3334/cdiac/otg.carina_316n20020530, dataset, 2013.

Bellerby, R. G. J., Olsen, A., Furevik, T., and Anderson, L. G.: Response of the Surface Ocean CO2 System in the Nordic Seas and Northern North Atlantic to Climate Change, pp. 189–197, American Geophysical Union (AGU), https://doi.org/https://doi.org/10.1029/158GM13, https://agupubs.onlinelibrary.wiley.com/doi/abs/10.1029/158GM13, 2005.

Bentsen, M., Bethke, I., Debernard, J. B., Iversen, T., Kirkevåg, A., Seland, Ø., Drange, H., Roelandt, C., Seierstad, I. A., Hoose, C., and Kristjánsson, J. E.: The Norwegian Earth System Model, NorESM1-M – Part 1: Description and basic evaluation of the physical climate, Geoscientific Model Development, 6, 687–720, https://doi.org/10.5194/gmd-6-687-2013, https://gmd.copernicus.org/articles/6/687/2013/, 2013.

Bleck, R. and Smith, L. T.: A wind-driven isopycnic coordinate model of the north and equatorial Atlantic Ocean: 1. Model development and supporting experiments, Journal of Geophysical Research: Oceans, 95, 3273–3285, https://doi.org/10.1029/JC095iC03p03273, https://agupubs.onlinelibrary.wiley.com/doi/abs/10.1029/JC095iC03p03273, 1990.

Blindheim, J.: Arctic intermediate water in the Norwegian sea, Deep Sea Research Part A. Oceanographic Research Papers, 37, 1475 – 1489, https://doi.org/https://doi.org/10.1016/0198-0149(90)90138-L, http://www.sciencedirect.com/science/article/pii/019801499090138L, 1990.

Blindheim, J. and Østerhus, S.: The Nordic Seas, Main Oceanographic Features, pp. 11–37, American Geophysical Union (AGU), https://doi.org/10.1029/158GM03, https://agupubs.onlinelibrary.wiley.com/doi/abs/10.1029/158GM03, 2013.

Blindheim, J. and Rey, F.: Water-mass formation and distribution in the Nordic Seas during the 1990s, ICES Journal of Marine Science, 61, 846–863, https://doi.org/10.1016/j.icesjms.2004.05.003, https://doi.org/10.1016/j.icesjms.2004.05.003, 2004.

Bockmon, E. E. and Dickson, A. G.: An inter-laboratory comparison assessing the quality of seawater carbon dioxide measurements, Marine Chemistry, 171, 36–43, https://doi.org/https://doi.org/10.1016/j.marchem.2015.02.002, https://www.sciencedirect.com/science/article/pii/S0304420315000213, 2015.

Booth, B. B. B., Bernie, D., McNeall, D., Hawkins, E., Caesar, J., Boulton, C., Friedlingstein, P., and Sexton, D. M. H.: Scenario and modelling uncertainty in global mean temperature change derived from emission-driven global climate models, Earth System Dynamics, 4, 95–108, https://doi.org/10.5194/esd-4-95-2013, https://esd.copernicus.org/articles/4/95/2013/, 2013.

Bopp, L., Resplandy, L., Orr, J. C., Doney, S. C., Dunne, J. P., Gehlen, M., Halloran, P., Heinze, C., Ilyina, T., Séférian, R., Tjiputra, J., and Vichi, M.: Multiple stressors of ocean ecosystems in the 21st century: projections with CMIP5 models, Biogeosciences, 10, 6225–6245, https://doi.org/10.5194/bg-10-6225-2013, https://bg.copernicus.org/articles/10/6225/2013/, 2013.

Brakstad, A., Våge, K., Håvik, L., and Moore, G. W. K.: Water Mass Transformation in the Greenland Sea during the Period 1986–2016, Journal of Physical Oceanography, 49, 121–140, https://doi.org/10.1175/JPO-D-17-0273.1, https://doi.org/10.1175/JPO-D-17-0273.1, 2019.

Brewer, P. G., Takahashi, T., and Williams, R. T.: Partial pressure (or fugacity) of carbon dioxide, dissolved inorganic carbon (DIC), total alkalinity, water temperature, salinity, dissolved oxygen concentration and other variables collected from discrete sample and profile observations during R/V Knorr TTO-NAS cruises in the North Atlantic Ocean from 1981-04-01 to 1981-10-19 (NCEI Accession 0000733). NOAA National Centers for Environmental Information., https://doi.org/10.3334/cdiac/otg.ndp004, dataset, 2010.

Buhl-Mortensen, L., Olafsdottir, S. H., Buhl-Mortensen, P., Burgos, J. M., and Ragnarsson, S. A.: Distribution of nine cold-water coral species (Scleractinia and Gorgonacea) in the cold temperate North Atlantic: effects of bathymetry and hydrography, Hydrobiologia, 759, 39–61, https://doi.org/10.1007/s10750-014-2116-x, https://doi.org/10.1007/s10750-014-2116-x, 2015.

Caldeira, K. and Wickett, M. E.: Anthropogenic carbon and ocean pH, Nature, 425, 365–365, https://doi.org/10.1038/425365a, https://doi.org/10.1038/425365a, 2003.

Chafik, L. and Rossby, T.: Volume, Heat, and Freshwater Divergences in the Subpolar North Atlantic Suggest the Nordic Seas as Key to the State of the Meridional Overturning Circulation, Geophysical Research Letters, 46, 4799–4808, https://doi.org/10.1029/2019GL082110, https://agupubs.onlinelibrary.wiley.com/doi/abs/10.1029/2019GL082110, 2019.

Chierici, M. and Fransson, A.: Seasonal variability of the marine CO_2 system and nutrients in the Atlantic water inflow to the Arctic Ocean in 2014, https://doi.org/10.21335/NMDC-154415697, dataset, 2019.

Chierici, M., Sørensen, K., Johannessen, T., Børsheim, K., A.Olsen, Yakushev, E., Omar, A., and Blakseth, T.: Tillførselprogrammet 2011, Overvåking av havsforsuring av norske farvann. Rapport, Klif, TA2936-2012, Tech. rep., 2012.

Chierici, M., Sørensen, K., Johannessen, T., Børsheim, K., A.Olsen, Yakushev, E., Omar, A., Skjelvan, I., Norli, M., , and Lauvset, S.: Tillførselprogrammet 2012, Overvåking av havsforsuring av norske farvann. Rapport, Klif, TA3043-2013, Tech. rep., 2013.

Chierici, M., Skjelvan, I., Bellerby, R., M. Norli, L. F., Hodal, H., Børsheim, K., Lauvset, S., Johannessen, T., Sørensen, K., and Yakushev, E.: Overvåking av havforsuring av norske farvann. Rapport, Miljødirektoratet M-218, Tech. rep., 2014.

Chierici, M., Skjelvan, I., Norli, M., Lødemel, H., Lunde, L., Sørensen, K., Yakushev, E., Bellerby, R., King, A., Lauvset, S., Johannessen, T., and Børsheim, K.: Overvåking av havforsuring i norske farvann i 2014, Rapport, Miljødirektoratet, M-354, Tech. rep., 2015.

Chierici, M., Skjelvan, I., Norli, M., Børsheim, K., Lauvset, S., Lødemel, H., Sørensen, K., King, A., Kutti, T., Renner, A., Omar, A., and Johannessen, T.: Overvåking av havforsuring i norske farvann i 2015, Rapport, Miljødirektoratet, M-573, Tech. rep., 2016.

Chierici, M., Skjelvan, I., Norli, M., Jones, E., Børsheim, K., Lauvset, S., Lødemel, H., Sørensen, K., King, A., and Johannessen, T.: Overvåking av havforsuring i norske farvann i 2016, Rapport, Miljødirektoratet, M-776, Tech. rep., 2017.

Chierici, M., Jones, E., and Lødemel, H. H.: Interannual variability of the marine CO_2 system and nutrients in the Norwegian Sea from 2011 to 2017, https://doi.org/10.21335/NMDC-1939716216, dataset, 2019a.

Chierici, M., Vernet, M., Fransson, A., and Børsheim, K. Y.: Net Community Production and Carbon Exchange From Winter to Summer in the Atlantic Water Inflow to the Arctic Ocean, Frontiers in Marine Science, 6, 528, https://doi.org/10.3389/fmars.2019.00528, https://www.frontiersin.org/article/10.3389/fmars.2019.00528, 2019b.

Dai, A., Luo, D., Song, M., and Liu, J.: Arctic amplification is caused by sea-ice loss under increasing CO2, Nature Communications, 10, 121, https://doi.org/10.1038/s41467-018-07954-9, https://doi.org/10.1038/s41467-018-07954-9, 2019.

Dickson, A., Sabine, C., and Christian, J. e.: Guide to best practices for ocean CO2 measurement., PICES Special Publication 3; IOCCP Report 8, 2007.

Dickson, A. G.: Standard potential of the reaction: AgCl(s) + 12H2(g) = Ag(s) + HCl(aq), and and the standard acidity constant of the ion HSO4- in synthetic sea water from 273.15 to 318.15 K, The Journal of Chemical Thermodynamics, 22, 113 – 127, https://doi.org/https://doi.org/10.1016/0021-9614(90)90074-Z, http://www.sciencedirect.com/science/article/pii/002196149090074Z, 1990.

Dickson, R. R. and Brown, J.: The production of North Atlantic Deep Water: Sources, rates, and pathways, Journal of Geophysical Research: Oceans, 99, 12 319–12 341, https://doi.org/10.1029/94JC00530, https://agupubs.onlinelibrary.wiley.com/doi/abs/10.1029/94JC00530, 1994.

Doney, S. C., Fabry, V. J., Feely, R. A., and Kleypas, J. A.: Ocean Acidification: The Other CO_2 Problem, Annual Review of Marine Science, 1, 169–192, https://doi.org/10.1146/annurev.marine.010908.163834, https://doi.org/10.1146/annurev.marine.010908.163834, pMID: 21141034, 2009.

Doney, S. C., Busch, D. S., Cooley, S. R., and Kroeker, K. J.: The Impacts of Ocean Acidification on Marine Ecosystems and Reliant Human Communities, Annual Review of Environment and Resources, 45, null, https://doi.org/10.1146/annurev-environ-012320-083019, https://doi.org/10.1146/annurev-environ-012320-083019, 2020.

Doo, S. S., Kealoha, A., Andersson, A., Cohen, A. L., Hicks, T. L., Johnson, Z. I., Long, M. H., McElhany, P., Mollica, N., Shamberger, K. E. F., Silbiger, N. J., Takeshita, Y., and Busch, D. S.: The challenges of detecting and attributing ocean acidification impacts on marine ecosystems, ICES Journal of Marine Science, https://doi.org/10.1093/icesjms/fsaa094, https://doi.org/10.1093/icesjms/fsaa094, fsaa094, 2020.

Dufresne, J.-L., Foujols, M.-A., Denvil, S., Caubel, A., Marti, O., Aumont, O., Balkanski, Y., Bekki, S., Bellenger, H., Benshila, R., Bony, S., Bopp, L., Braconnot, P., Brockmann, P., Cadule, P., Cheruy, F., Codron, F., Cozic, A., Cugnet, D., de Noblet, N., Duvel, J.-P., Ethé, P., Fairhead, L., Fichefet, T., Flavoni, S., Friedlingstein, P., Grandpeix, J.-Y., Guez, L., Guilyardi, E., Hauglustaine, D., Hourdin, F., Idelkadi, A., Ghattas, J., Joussaume, S., Kageyama, M., Krinner, G., Labetoulle, S., Lahellec, A., Lefebvre, M.-P., Lefevre, F., Levy, C., Li, Z. X., Lloyd, J., Lott, F., Madec, G., Mancip, M., Marchand, M., Masson, S., Meurdesoif, Y., Mignot, J., Musat, I., Parouty, S., Polcher, J., Rio, C., Schulz, M., Swingedouw, D., Szopa, S., Talandier, C., Terray, P., Viovy, N., and Vuichard, N.: Climate change projections using the IPSL-CM5 Earth System Model: from CMIP3 to CMIP5, Clim. Dynamics, 40, 2123–2165, https://doi.org/10.1007/s00382-012-1636-1, 2013.

Dunne, J. P., John, J. G., Adcroft, A. J., Griffies, S. M., Hallberg, R. W., Shevliakova, E. N., Stouffer, R. J., Cooke, W., Dunne, K. A., Harrison, M. J., Krasting, J. P., Malyshev, S. L., Milly, P. C. D., Phillips, P. J., Sentman, L. T., Samuels, B. L., Spelman, M., Winton, M., Wittenberg, A. T., and Zadeh, N.: GFDL's ESM2 global coupled climate-carbon Earth System Models Part I: Physical Formulation and Baseline Simulation Characteristics, J. Climate, 25, https://doi.org/10.1175/JCLI-D-11-00560.1, 2013a.

Dunne, J. P., John, J. G., Adcroft, A. J., Griffies, S. M., Hallberg, R. W., Shevliakova, E. N., Stouffer, R. J., Cooke, W., Dunne, K. A., Harrison, M. J., Krasting, J. P., Malyshev, S. L., Milly, P. C. D., Phillips, P. J., Sentman, L. T., Samuels, B. L., Spelman, M., Winton, M., Wittenberg, A. T., and Zadeh, N.: GFDL's ESM2 global coupled climate-carbon Earth System Models Part II: Carbon System Formulation and Baseline Simulation Characteristics, J. Climate, 26, https://doi.org/10.1175/JCLI-D-12-00150.1, 2013b.

Fassbender, A. J., Sabine, C. L., and Palevsky, H. I.: Nonuniform ocean acidification and attenuation of the ocean carbon sink, Geophysical Research Letters, 44, 8404–8413, https://doi.org/https://doi.org/10.1002/2017GL074389, https://agupubs.onlinelibrary.wiley.com/doi/abs/10.1002/2017GL074389, 2017.

Fassbender, A. J., Orr, J. C., and Dickson, A. G.: Technical note: Interpreting pH changes, Biogeosciences, 18, 1407–1415, https://doi.org/10.5194/bg-18-1407-2021, https://bg.copernicus.org/articles/18/1407/2021/, 2021.

Frankignoulle, M.: A complete set of buffer factors for acid/base CO2 system in seawater, Journal of Marine Systems, 5, 111–118, https://doi.org/https://doi.org/10.1016/0924-7963(94)90026-4, https://www.sciencedirect.com/science/article/pii/0924796394900264, 1994.

Friedlingstein, P., Meinshausen, M., Arora, V. K., Jones, C. D., Anav, A., Liddicoat, S. K., and Knutti, R.: Uncertainties in CMIP5 Climate Projections due to Carbon Cycle Feedbacks, Journal of Climate, 27, 511 – 526, https://doi.org/10.1175/JCLI-D-12-00579.1, https://journals.ametsoc.org/view/journals/clim/27/2/jcli-d-12-00579.1.xml, 2014.

Friedlingstein, P., O'Sullivan, M., Jones, M. W., Andrew, R. M., Hauck, J., Olsen, A., Peters, G. P., Peters, W., Pongratz, J., Sitch, S., Le Quéré, C., Canadell, J. G., Ciais, P., Jackson, R. B., Alin, S., Aragão, L. E. O. C., Arneth, A., Arora, V., Bates, N. R., Becker, M., Benoit-Cattin, A., Bittig, H. C., Bopp, L., Bultan, S., Chandra, N., Chevallier, F., Chini, L. P., Evans, W., Florentie, L., Forster, P. M., Gasser, T., Gehlen, M., Gilfillan, D., Gkritzalis, T., Gregor, L., Gruber, N., Harris, I., Hartung, K., Haverd, V., Houghton, R. A., Ilyina, T., Jain, A. K., Joetzjer, E., Kadono, K., Kato, E., Kitidis, V., Korsbakken, J. I., Landschützer, P., Lefèvre, N., Lenton, A., Lienert, S., Liu, Z., Lombardozzi, D., Marland, G., Metzl, N., Munro, D. R., Nabel, J. E. M. S., Nakaoka, S.-I., Niwa, Y., O'Brien, K., Ono, T., Palmer, P. I., Pierrot, D., Poulter, B., Resplandy, L., Robertson, E., Rödenbeck, C., Schwinger, J., Séférian, R., Skjelvan, I., Smith, A. J. P., Sutton, A. J., Tanhua, T., Tans, P. P., Tian, H., Tilbrook, B., van der Werf, G., Vuichard, N., Walker, A. P., Wanninkhof, R., Watson, A. J., Willis, D., Wiltshire, A. J., Yuan, W., Yue, X., and Zaehle, S.: Global Carbon Budget 2020, Earth System Science Data, 12, 3269–3340, https://doi.org/10.5194/essd-12-3269-2020, https://essd.copernicus.org/articles/12/3269/2020/, 2020.

Friis, K., Körtzinger, A., and Wallace, D. W. R.: The salinity normalization of marine inorganic carbon chemistry data, Geophysical Research Letters, 30, https://doi.org/https://doi.org/10.1029/2002GL015898, https://agupubs.onlinelibrary.wiley.com/doi/abs/10.1029/2002GL015898, 2003.

Fröb, F., Olsen, A., Becker, M., Chafik, L., Johannessen, T., Reverdin, G., and Omar, A.: Wintertime fCO2 Variability in the Subpolar North Atlantic Since 2004, Geophysical Research Letters, 46, 1580–1590, https://doi.org/https://doi.org/10.1029/2018GL080554, https://agupubs.onlinelibrary.wiley.com/doi/abs/10.1029/2018GL080554, 2019.

Frölicher, T. L., Rodgers, K. B., Stock, C. A., and Cheung, W. W. L.: Sources of uncertainties in 21st century projections of potential ocean ecosystem stressors, Global Biogeochemical Cycles, 30, 1224–1243, https://doi.org/https://doi.org/10.1002/2015GB005338, https://agupubs.onlinelibrary.wiley.com/doi/abs/10.1002/2015GB005338, 2016.

García-Ibáñez, M. I., Bates, N. R., Bakker, D. C., Fontela, M., and Velo, A.: Cold-water corals in the Subpolar North Atlantic Ocean exposed to aragonite undersaturation if the 2 °C global warming target is not met, Global and Planetary Change, 201, 103 480, https://doi.org/https://doi.org/10.1016/j.gloplacha.2021.103480, https://www.sciencedirect.com/science/article/pii/S0921818121000655, 2021.

Gattuso, J.-P. and Hansson, L.: Ocean acidification: background and history, In Ocean Acidification, ed. J-P Gattuso, L Hansson, pp. 1–20, Oxford University Press, Oxford, UK, 2011.

Giorgetta, M. A., Jungclaus, J., Reick, C. H., Legutke, S., Bader, J., Bóttinger, M., Brovkin, V., Crueger, T., Esch, M., Fieg, K., Glushak, K., Gayler, V., Haak, H., Hollweg, H.-D., Ilyina, T., Kinne, S., Kornblueh, L., Matei, D., Mauritsen, T., Mikolajewicz, U., Mueller, W., Notz, D., Pithan, F., Raddatz, T., Rast, S., Redler, R., Roeckner, E., Schmidt, H., Schnur, R., Segschneider, J., Six, K. D., Stockhause, M., Timmreck, C., Wegner, J., Widmann, H., Wieners, K.-H., Claussen, M., Marotzke, J., and Stevens, B.: Climate and carbon cycle changes from 1850 to 2100 in MPI-ESM simulations for the Coupled Model Intercomparison Project phase 5, Journal of Advances in Modeling Earth Systems, 5, 572–597, https://doi.org/10.1002/jame.20038, 2013.

Giraudeau, J., Hulot, V., Hanquiez, V., Devaux, L., Howa, H., and Garlan, T.: A survey of the summer coccolithophore community in the western Barents Sea, Journal of Marine Systems, 158, 93–105, https://doi.org/https://doi.org/10.1016/j.jmarsys.2016.02.012, https://www.sciencedirect.com/science/article/pii/S0924796316300021, 2016.

Guinotte, J. M., Orr, J., Cairns, S., Freiwald, A., Morgan, L., and George, R.: Will human-induced changes in seawater chemistry alter the distribution of deep-sea scleractinian corals?, Frontiers in Ecology and the Environment, 4, 141–146, https://doi.org/10.1890/1540-9295(2006)004[0141:WHCISC]2.0.CO;2, 2006.

He, Y.-C., Tjiputra, J., Langehaug, H. R., Jeansson, E., Gao, Y., Schwinger, J., and Olsen, A.: A Model-Based Evaluation of the Inverse Gaussian Transit-Time Distribution Method for Inferring Anthropogenic Carbon Storage in the Ocean, Journal of Geophysical Research: Oceans, 123, 1777–1800, https://doi.org/https://doi.org/10.1002/2017JC013504, https://agupubs.onlinelibrary.wiley.com/doi/abs/10.1002/2017JC013504, 2018.

Hennige, S. J., Wicks, L. C., Kamenos, N. A., Perna, G., Findlay, H. S., and Roberts, J. M.: Hidden impacts of ocean acidification to live and dead coral framework, Proceedings of the Royal Society B: Biological Sciences, 282, 20150 990, https://doi.org/10.1098/rspb.2015.0990, https://royalsocietypublishing.org/doi/abs/10.1098/rspb.2015.0990, 2015.

Holliday, N. P., Hughes, S. L., Bacon, S., Beszczynska-Möller, A., Hansen, B., Lavín, A., Loeng, H., Mork, K. A., Østerhus, S., Sherwin, T., and Walczowski, W.: Reversal of the 1960s to 1990s freshening trend in the northeast North Atlantic and Nordic Seas, Geophysical Research Letters, 35, https://doi.org/10.1029/2007GL032675, https://agupubs.onlinelibrary.wiley.com/doi/abs/10.1029/2007GL032675, 2008.

Jeansson, E., Olsen, A., Eldevik, T., Skjelvan, I., Omar, A. M., Lauvset, S. K., Nilsen, J. E. Ø., Bellerby, R. G. J., Johannessen, T., and Falck, E.: The Nordic Seas carbon budget: Sources, sinks, and uncertainties, Global Biogeochemical Cycles, 25, https://doi.org/10.1029/2010GB003961, https://agupubs.onlinelibrary.wiley.com/doi/abs/10.1029/2010GB003961, 2011.

Jeansson, E., Olsen, A., and Jutterström, S.: Arctic Intermediate Water in the Nordic Seas, 1991–2009, Deep Sea Research Part I: Oceanographic Research Papers, 128, 82 – 97, https://doi.org/https://doi.org/10.1016/j.dsr.2017.08.013, http://www.sciencedirect.com/science/article/pii/S0967063716300668, 2017.

Jeansson, E., Olsen, A., Lauvset, S. K., Brakstad, A., Jackson, K., Lunde, L. F., He, Y., and Onarheim, T.: Discrete profile measurements of dissolved inorganic carbon, total alkalinity, other hydrographic and chemical data obtained during the R/V G.O. Sars Repeat Hydrography Cruise in the Greenland Sea and Iceland Sea: GO-SHIP Section 75N (EXPOCODE 58GS20160802), from 2016-08-02 to 2016-08-12 (NCEI Accession 0174834). NOAA National Centers for Environmental Information., https://doi.org/10.25921/3kjg-ak47., dataset, 2018.

Jiang, L.-Q., Carter, B. R., Feely, R. A., Lauvset, S. K., and Olsen, A.: Surface ocean pH and buffer capacity: past, present and future, Scientific Reports, 9, 18 624, https://doi.org/10.1038/s41598-019-55039-4, https://doi.org/10.1038/s41598-019-55039-4, 2019.

Johannessen, T.: Dissolved inorganic carbon, alkalinity, temperature, salinity and other variables collected from discrete sample and profile observations using CTD, bottle and other instruments from the HAKON MOSBY in the North Greenland Sea from 1996-11-21 to 1996-11-30 (NCEI Accession 0113544). NOAA National Centers for Environmental Information., https://doi.org/10.3334/cdiac/otg.carina_58aa19961121, dataset, 2013a.

Johannessen, T.: Dissolved inorganic carbon, alkalinity, temperature, salinity and other variables collected from discrete sample and profile observations using CTD, bottle and other instruments from the HAKON MOSBY in the North Greenland Sea and Norwegian Sea from 1997-02-25 to 1997-03-24 (NCEI Accession 0113545). NOAA National Centers for Environmental Information., https://doi.org/10.3334/cdiac/otg.carina_58aa19970225, dataset, 2013b.

Johannessen, T. and Golmen, L. G.: Dissolved inorganic carbon, alkalinity, temperature, salinity and other variables collected from discrete sample and profile observations using CTD, bottle and other instruments from the HAKON MOSBY in the North Greenland Sea and Norwegian Sea from 1994-08-26 to 1994-09-10 (NCEI Accession 0113542). NOAA National Centers for Environmental Information., https://doi.org/10.3334/cdiac/otg.carina_58aa19940826, dataset, 2013.

Johannessen, T. and Olsen, A.: Dissolved inorganic carbon, alkalinity, temperature, salinity and other variables collected from discrete sample and profile observations during the G.O. SARS cruise along GO-SHIP Repeat Section A75N (EXPOCODE 58GS200309) in the North Atlantic Ocean, North Greenland Sea and Norwegian Sea from 2003-09-22 to 2003-10-13 (NCEI Accession 0113752). NOAA National Centers for Environmental Information., https://doi.org/10.3334/cdiac/otg.carina_58gs20030922, dataset, 2013.

Johannessen, T. and Simonsen, K. .: Dissolved inorganic carbon, alkalinity, temperature, salinity and other variables collected from discrete sample and profile observations using CTD, bottle and other instruments from the HAKON MOSBY in the North Greenland Sea and Norwegian Sea from 1998-03-08 to 1998-03-24 (NCEI Accession 0113546). NOAA National Centers for Environmental Information., https://doi.org/10.3334/cdiac/otg.carina_58aa19980308, dataset, 2013.

Johannessen, T., Skjelvan, I., and Rey, F.: Dissolved inorganic carbon, alkalinity, temperature, salinity and other variables collected from discrete sample and profile observations using CTD, bottle and other instruments from the JOHAN HJORT in the North Greenland Sea and Norwegian Sea from 1994-05-25 to 1994-06-06 (NCEI Accession 0113954). NOAA National Centers for Environmental Information., https://doi.org/10.3334/cdiac/otg.carina_58jh19940525, dataset, 2013a.

Johannessen, T., Skjelvan, I., and Watson, A. J.: Dissolved inorganic carbon, alkalinity, temperature, salinity and other variables collected from discrete sample and profile observations using CTD, bottle and other instruments from the JAMES CLARK ROSS in the North Greenland Sea and Norwegian Sea from 1996-07-20 to 1996-08-22 (NCEI Accession 0113757). NOAA National Centers for Environmental Information. Dataset., https://doi.org/10.3334/cdiac/otg.carina_74jc19960720., dataset, 2013b.

Johannessen, T., Soiland, H., Thingstad, T. F., Bellerby, R. G. J., and Olsen, A.: Dissolved inorganic carbon, alkalinity, temperature, salinity and other variables collected from discrete sample and profile observations using CTD, bottle and other instruments from the G.O. SARS in the Barents Sea, North Atlantic Ocean and others from 2009-05-28 to 2009-08-11 (NCEI Accession 0114433). NOAA National Centers for Environmental Information., https://doi.org/10.25921/3q88-gs40, dataset, 2013c.

Jones, E., Chierici, M., Skjelvan, I., M. Norli, K. B., Lødemel, H., Kutti, T., Sørensen, K., King, A., Jackson, K., and de Lange, T.: Monitoring of the ocean acidification in Norwegian seas in 2017, Report, Miljødirektoratet, M-1072, Tech. rep., 2018.

Jones, E., Chierici, M., Skjelvan, I., Norli, M., Børsheim, K., Lødemel, H., Sørensen, K., King, A., Lauvset, S., Jackson, K., de Lange, T., Johannsessen, T., and Mourgues, C.: Monitoring ocean acidification in Norwegian seas in 2018, Rapport, Miljødirektoratet, M-1417, Tech. rep., 2019.

Jones, E., Chierici, M., Skjelvan, I., Norli, M., Frigstad, H., Børsheim, K., Lødemel, H., Kutti, T., King, A., Sørensen, K., Lauvset, S., Jackson-Misje, K., Apelthun, L., de Lange, T., Johannsessen, T., Mourgues, C., and Bellerby, R.: Monitoring ocean acidification in Norwegian seas in 2019, Rapport, Miljødirektoratet, M-1735, Tech. rep., 2020.

Jones, E. P., Azetsu-Scott, K., Aagaard, K., Carmack, E., and Swift, J. H.: Dissolved inorganic carbon, alkalinity, temperature, salinity and other variables collected from discrete sample and profile observations using CTD, bottle and other instruments from the LOUIS S. ST. LAURENT in the Arctic Ocean, Beaufort Sea and North Greenland Sea from 1994-07-24 to 1994-09-01 (NCEI Accession 0113983).NOAA National Centers for Environmental Information., https://doi.org/10.3334/cdiac/otg.carina_18sn19940724, dataset, 2013.

Jutterström, S. and Jeansson, E.: Anthropogenic carbon in the East Greenland Current, Progress in Oceanography, 78, 29 – 36, https://doi.org/https://doi.org/10.1016/j.pocean.2008.04.001, http://www.sciencedirect.com/science/article/pii/S0079661108000876, 2008.

Karstensen, J., Schlosser, P., Wallace, D. W. R., Bullister, J. L., and Blindheim, J.: Water mass transformation in the Greenland Sea during the 1990s, Journal of Geophysical Research: Oceans, 110, https://doi.org/https://doi.org/10.1029/2004JC002510, https://agupubs.onlinelibrary.wiley.com/doi/abs/10.1029/2004JC002510, 2005.

Keeling, C. D., Brix, H., and Gruber, N.: Seasonal and long-term dynamics of the upper ocean carbon cycle at Station ALOHA near Hawaii, Global Biogeochemical Cycles, 18, https://doi.org/https://doi.org/10.1029/2004GB002227, https://agupubs.onlinelibrary.wiley.com/doi/abs/10.1029/2004GB002227, 2004.

Kutti, T., Bergstad, O. A., Fosså, J. H., and Helle, K.: Cold-water coral mounds and sponge-beds as habitats for demersal fish on the Norwegian shelf, Deep Sea Research Part II: Topical Studies in Oceanography, 99, 122 – 133, https://doi.org/https://doi.org/10.1016/j.dsr2.2013.07.021, http://www.sciencedirect.com/science/article/pii/S0967064513002956, biology and Geology of Deep-Sea Coral Ecosystems: Proceedings of the Fifth International Symposium on Deep Sea Corals, 2014.

Kwiatkowski, L. and Orr, J. C.: Diverging seasonal extremes for ocean acidification during the twenty-first century, Nature Climate Change, 8, 141–145, https://doi.org/10.1038/s41558-017-0054-0, https://doi.org/10.1038/s41558-017-0054-0, 2018.

Kwiatkowski, L., Torres, O., Bopp, L., Aumont, O., Chamberlain, M., Christian, J. R., Dunne, J. P., Gehlen, M., Ilyina, T., John, J. G., Lenton, A., Li, H., Lovenduski, N. S., Orr, J. C., Palmieri, J., Santana-Falcón, Y., Schwinger, J., Séférian, R., Stock, C. A., Tagliabue, A., Takano, Y., Tjiputra, J., Toyama, K., Tsujino, H., Watanabe, M., Yamamoto, A., Yool, A., and Ziehn, T.: Twenty-first century ocean warming, acidification, deoxygenation, and upper-ocean nutrient and primary production decline from CMIP6 model projections, Biogeosciences, 17, 3439–3470, https://doi.org/10.5194/bg-17-3439-2020, https://bg.copernicus.org/articles/17/3439/2020/, 2020.

Lauvset, S. K., Gruber, N., Landschützer, P., Olsen, A., and Tjiputra, J.: Trends and drivers in global surface ocean pH over the past 3 decades, Biogeosciences, 12, 1285–1298, https://doi.org/10.5194/bg-12-1285-2015, https://bg.copernicus.org/articles/12/1285/2015/, 2015.

Lauvset, S. K., Key, R. M., Olsen, A., van Heuven, S., Velo, A., Lin, X., Schirnick, C., Kozyr, A., Tanhua, T., Hoppema, M., Jutterström, S., Steinfeldt, R., Jeansson, E., Ishii, M., Perez, F. F., Suzuki, T., and Watelet, S.: A new global interior ocean mapped climatology: the $1^\circ \times 1^\circ$ GLODAP version 2, Earth System Science Data, 8, 325–340, https://doi.org/10.5194/essd-8-325-2016, https://essd.copernicus.org/articles/8/325/2016/, 2016.

Lauvset, S. K., Brakstad, A., Våge, K., Olsen, A., Jeansson, E., and Mork, K. A.: Continued warming, salinification and oxygenation of the Greenland Sea gyre, Tellus A: Dynamic Meteorology and Oceanography, 70, 1–9, https://doi.org/10.1080/16000870.2018.1476434, https://doi.org/10.1080/16000870.2018.1476434, 2018.

Lauvset, S. K., Carter, B. R., Pèrez, F. F., Jiang, L.-Q., Feely, R. A., Velo, A., and Olsen, A.: Processes Driving Global Interior Ocean pH Distribution, Global Biogeochemical Cycles, 34, e2019GB006 229, https://doi.org/https://doi.org/10.1029/2019GB006229, https://agupubs.onlinelibrary.wiley.com/doi/abs/10.1029/2019GB006229, e2019GB006229 2019GB006229, 2020.

Lefèvre, N., Watson, A. J., Olsen, A., Ríos, A. F., Pérez, F. F., and Johannessen, T.: A decrease in the sink for atmospheric CO$_2$ in the North Atlantic, Geophysical Research Letters, 31, https://doi.org/10.1029/2003GL018957, https://agupubs.onlinelibrary.wiley.com/doi/abs/10.1029/2003GL018957, 2004.

Lenton, A., Metzl, N., Takahashi, T., Kuchinke, M., Matear, R. J., Roy, T., Sutherland, S. C., Sweeney, C., and Tilbrook, B.: The observed evolution of oceanic pCO2 and its drivers over the last two decades, Global Biogeochemical Cycles, 26, https://doi.org/https://doi.org/10.1029/2011GB004095, https://agupubs.onlinelibrary.wiley.com/doi/abs/10.1029/2011GB004095, 2012.

Lewis, E. and Wallace, D. W. R.: Program Developed for CO$_2$ System Calculations, ORNL/CDIAC-105. Carbon Dioxide Information Analysis Center, Oak Ridge National Laboratory, US Department of Energy, Oak Ridge, Tennessee., 1998.

Long, M. C., Lindsay, K., Peacock, S., Moore, J. K., and Doney, S. C.: Twentieth-century oceanic carbon uptake and storage in CESM1(BGC), J. Climate, 26, 6775–6800, https://doi.org/http://dx.doi.org/10.1175/JCLI-D-12-00184.1, 2013.

Lovenduski, N. S., Gruber, N., Doney, S. C., and Lima, I. D.: Enhanced CO2 outgassing in the Southern Ocean from a positive phase of the Southern Annular Mode, Global Biogeochemical Cycles, 21, https://doi.org/https://doi.org/10.1029/2006GB002900, https://agupubs.onlinelibrary.wiley.com/doi/abs/10.1029/2006GB002900, 2007.

Lueker, T. J., Dickson, A. G., and Keeling, C. D.: Ocean pCO$_2$ calculated from dissolved inorganic carbon, alkalinity, and equations for K1 and K2: validation based on laboratory measurements of CO$_2$ in gas and seawater at equilibrium, Marine Chemistry, 70, 105 – 119, https://doi.org/https://doi.org/10.1016/S0304-4203(00)00022-0, http://www.sciencedirect.com/science/article/pii/S0304420300000220, 2000.

Maier-Reimer, E., Kriest, I., Segschneider, J., and Wetzel, P.: The HAMburg Ocean Carbon Cycle Model HAMOCC5.1 - Technical Description Release 1.1.Berichte zur Erdsystemforschung, 14., Tech. rep., 2005.

Malmberg, S. A. and Désert, J.: Hydrographic conditions in North Icelandic waters and annual air temperature in Iceland, ICES CM 1999/LM:14,21pp, 1999.

Manno, C., Bednaršek, N., Tarling, G. A., Peck, V. L., Comeau, S., Adhikari, D., Bakker, D. C., Bauerfeind, E., Bergan, A. J., Berning, M. I., Buitenhuis, E., Burridge, A. K., Chierici, M., Flöter, S., Fransson, A., Gardner, J., Howes, E. L., Keul, N., Kimoto, K., Kohnert, P., Lawson, G. L., Lischka, S., Maas, A., Mekkes, L., Oakes, R. L., Pebody, C., Peijnenburg, K. T., Seifert, M., Skinner, J., Thibodeau, P. S., Wall-Palmer, D., and Ziveri, P.: Shelled pteropods in peril: Assessing vulnerability in a high CO2 ocean, Earth-Science

Reviews, 169, 132–145, https://doi.org/https://doi.org/10.1016/j.earscirev.2017.04.005, https://www.sciencedirect.com/science/article/pii/S0012825216302495, 2017.

Marcussen, C.; Anderson, L. G.: Discrete profile measurements of carbon dioxide, hydrographic and chemical data during the R/V Oden Lomonosov Ridge off Greenland (LOMROG) expedition (EXPOCODE 77DN20070812) in the Arctic Ocean from 2007-08-12 to 2007-09-19 (NCEI Accession 0170966). NOAA National Centers for Environmental Information., https://doi.org/10.7289/v52n50jb., dataset, 2018.

McCulloch, M., Trotter, J., Montagna, P., Falter, J., Dunbar, R., Freiwald, A., Försterra, G., López Correa, M., Maier, C., Rüggeberg, A., and Taviani, M.: Resilience of cold-water scleractinian corals to ocean acidification: Boron isotopic systematics of pH and saturation state up-regulation, Geochimica et Cosmochimica Acta, 87, 21 – 34, https://doi.org/https://doi.org/10.1016/j.gca.2012.03.027, http://www.sciencedirect.com/science/article/pii/S001670371200169X, 2012.

Meehl, G., Stocker, T., Collins, W., Friedlingstein, P., Gaye, A., Gregory, J., Kitoh, A., Knutti, R., Murphy, J., A. Noda, S. R., I.G. Watterson, A. W., and Zhao, Z.-C.: Global Climate Projections. In: Climate Change 2007: The Physical Science Basis. Contribution of Working Group I to the Fourth Assessment Report of the Intergovernmental Panel on Climate Change [Solomon, S., D. Qin, M. Manning, Z. Chen, M. Marquis, K.B. Averyt, M. Tignor and H.L. Miller (eds.)]. Cambridge University Press, Cambridge, United Kingdom and New York, NY, USA., 2007.

Meinshausen, M., Smith, S. J., Calvin, K., Daniel, J. S., Kainuma, M. L. T., Lamarque, J.-F., Matsumoto, K., Montzka, S. A., Raper, S. C. B., Riahi, K., Thomson, A., Velders, G. J. M., and van Vuuren, D. P. P.: The RCP greenhouse gas concentrations and their extensions from 1765 to 2300, Climatic Change, 109, 213, https://doi.org/10.1007/s10584-011-0156-z, https://doi.org/10.1007/s10584-011-0156-z, 2011.

Messias, M.-J., Watson, A., Johannessen, T., Oliver, K., Olsson, K., Fogelqvist, E., Olafsson, J., Bacon, S., Balle, J., Bergman, N., Budéus, G., Danielsen, M., Gascard, J.-C., Jeansson, E., Olafsdottir, S., Simonsen, K., Tanhua, T., Van Scoy, K., and Ledwell, J.: The Greenland Sea tracer experiment 1996–2002: Horizontal mixing and transport of Greenland Sea Intermediate Water, Progress in Oceanography, 78, 85 – 105, https://doi.org/https://doi.org/10.1016/j.pocean.2007.06.005, http://www.sciencedirect.com/science/article/pii/S0079661108000852, 2008.

Metzl, N., Corbière, A., Reverdin, G., Lenton, A., Takahashi, T., Olsen, A., Johannessen, T., Pierrot, D., Wanninkhof, R., Ólafsdóttir, S. R., Olafsson, J., and Ramonet, M.: Recent acceleration of the sea surface fCO_2 growth rate in the North Atlantic subpolar gyre (1993–2008) revealed by winter observations, Global Biogeochemical Cycles, 24, https://doi.org/10.1029/2009GB003658, https://agupubs.onlinelibrary.wiley.com/doi/abs/10.1029/2009GB003658, 2010.

Middelburg, J. J., Soetaert, K., and Hagens, M.: Ocean Alkalinity, Buffering and Biogeochemical Processes, Reviews of Geophysics, 58, e2019RG000 681, https://doi.org/https://doi.org/10.1029/2019RG000681, https://agupubs.onlinelibrary.wiley.com/doi/abs/10.1029/2019RG000681, e2019RG000681 2019RG000681, 2020.

NOAA National Geophysical Data Center: ETOPO1 1 Arc-Minute Global Relief Model. NOAA National Centers for Environmental Information., doi:10.7289/V5C8276M, dataset, 2020.

Nondal, G., Bellerby, R. G. J., Olsen, A., Johannessen, T., and Olafsson, J.: Optimal evaluation of the surface ocean CO2 system in the northern North Atlantic using data from voluntary observing ships, Limnology and Oceanography: Methods, 7, 109–118, https://doi.org/https://doi.org/10.4319/lom.2009.7.109, https://aslopubs.onlinelibrary.wiley.com/doi/abs/10.4319/lom.2009.7.109, 2009.

Ólafsdóttir, S. R., Benoit-Cattin, A., and Danielsen, M.: Dissolved inorganic carbon (DIC), total alkalinity, temperature, salinity, nutrients and dissolved oxygen collected from discrete samples and profile observations during the R/Vs Arni Fridriksson and Bjarni Saemundsson time series IcelandSea (LN6) cruises in the North Atlantic Ocean from 2014-02-18 to 2019-10-31 (NCEI Accession 0209074), https://doi.org/10.25921/qhed-3h84, dataset, 2020.

Ólafsson, J.: Winter mixed layer nutrients in the Irminger and Iceland Seas,1990-2000, ICES Marine Science Symposia, 219, 2003.

Ólafsson, J.: Partial pressure (or fugacity) of carbon dioxide, dissolved inorganic carbon, temperature, salinity and other variables collected from discrete samples, profile and time series profile observations during the R/Vs Arni Fridriksson and Bjarni Saemundsson time series IcelandSea (LN6) cruises in the North Atlantic Ocean from 1985-02-22 to 2013-11-26 (NCEI Accession 0100063), https://doi.org/10.3334/cdiac/otg.carina_icelandsea, dataset, 2012.

Ólafsson, J., Ólafsdóttir, S., Benoit-Cattin, A., Danielsen, M., Arnarson, T. S., and Takahashi, T.: Rate of Iceland Sea acidification from time series measurements, Biogeosciences, 6, 2661–2668, 2009.

Ólafsson, J., Lee, K., Ólafsdóttir, S. R., Benoit-Cattin, A., Lee, C.-H., and Kim, M.: Boron to salinity ratios for Atlantic, Arctic and Polar Waters: A view from downstream, Marine Chemistry, 224, 103 809, https://doi.org/https://doi.org/10.1016/j.marchem.2020.103809, http://www.sciencedirect.com/science/article/pii/S0304420320300633, 2020a.

Ólafsson, J., Ólafsdóttir, S. R., Takahashi, T., Danielsen, M., and Arnarson, T. S.: Enhancement of the North Atlantic CO_2 sink by Arctic Waters, Biogeosciences Discussions, 2020, 1–21, https://doi.org/10.5194/bg-2020-313, https://bg.copernicus.org/preprints/bg-2020-313/, 2020b.

Olsen, A. and Omar, A. M.: Dissolved inorganic carbon, alkalinity, temperature, salinity and other variables collected from discrete sample and profile observations using Alkalinity titrator, CTD and other instruments from the G.O. SARS in the North Greenland Sea and Norwegian Sea from 2006-07-21 to 2006-08-05 (NCEI Accession 0105859). NOAA National Centers for Environmental Information., https://doi.org/10.3334/cdiac/otg.clivar_75n_2006, dataset, 2013.

Olsen, A., Johannessen, T., and Rey, F.: On the nature of the factors that control spring bloom development at the entrance to the Barents Sea and their interannual variability, Sarsia, 88, 379–393, https://doi.org/10.1080/00364820310003145, https://doi.org/10.1080/00364820310003145, 2003.

Olsen, A., Omar, A. M., Bellerby, R. G. J., Johannessen, T., Ninnemann, U., Brown, K. R., Olsson, K. A., Olafsson, J., Nondal, G., Kivimäe, C., Kringstad, S., Neill, C., and Olafsdottir, S.: Magnitude and origin of the anthropogenic CO_2 increase and 13C Suess effect in the Nordic seas since 1981, Global Biogeochemical Cycles, 20, https://doi.org/10.1029/2005GB002669, https://agupubs.onlinelibrary.wiley.com/doi/abs/10.1029/2005GB002669, 2006.

Olsen, A., Brown, K. R., Chierici, M., Johannessen, T., and Neill, C.: Sea-surface CO_2 fugacity in the subpolar North Atlantic, Biogeosciences, 5, 535–547, https://doi.org/10.5194/bg-5-535-2008, https://bg.copernicus.org/articles/5/535/2008/, 2008.

Olsen, A., Omar, A. M., and Johannessen, T.: Dissolved inorganic carbon, alkalinity, temperature, salinity and other variables collected from discrete sample and profile observations using CTD, bottle and other instruments from the HAKON MOSBY in the North Atlantic Ocean, North Greenland Sea and Norwegian Sea from 2001-05-27 to 2001-06-19 (NCEI Accession 0113754). NOAA National Centers for Environmental Information., https://doi.org/10.3334/cdiac/otg.carina_58aa20010527, dataset, 2013.

Olsen, A., Lange, N., Key, R. M., Tanhua, T., Álvarez, M., Becker, S., Bittig, H. C., Carter, B. R., Cotrim da Cunha, L., Feely, R. A., van Heuven, S., Hoppema, M., Ishii, M., Jeansson, E., Jones, S. D., Jutterström, S., Karlsen, M. K., Kozyr, A., Lauvset, S. K., Lo Monaco, C., Murata, A., Pérez, F. F., Pfeil, B., Schirnick, C., Steinfeldt, R., Suzuki, T., Telszewski, M., Tilbrook, B., Velo, A., and Wanninkhof, R.: GLODAPv2.2019 – an update of GLODAPv2, Earth System Science Data, 11, 1437–1461, https://doi.org/10.5194/essd-11-1437-2019, https://essd.copernicus.org/articles/11/1437/2019/, 2019.

Omar, A. M. and Olsen, A.: Dissolved inorganic carbon, alkalinity, temperature, salinity and other variables collected from discrete sample and profile observations using CTD, bottle and other instruments from the HAKON MOSBY in the Barents Sea, North Greenland Sea and Norwegian Sea from 1999-10-03 to 1999-10-11 (NCEI Accession 0113888). NOAA National Centers for Environmental Information., https://doi.org/10.3334/cdiac/otg.carina_58aa19991003., dataset, 2013.

Omar, A. M. and Skogseth, R.: Dissolved inorganic carbon, alkalinity, temperature, salinity and other variables collected from discrete sample and profile observations using CTD, bottle and other instruments from the HAKON MOSBY in the Barents Sea and Norwegian Sea from 2001-08-22 to 2001-08-29 (NCEI Accession 0113887). NOAA National Centers for Environmental Information., https://doi.org/10.3334/cdiac/otg.carina_58aa20010822, dataset, 2013.

Omar, Abdirahman M.; Østerhus, S.: Dissolved inorganic carbon, alkalinity, temperature, salinity and other variables collected from discrete sample and profile observations using CTD, bottle and other instruments from the HAKON MOSBY in the Barents Sea from 2000-09-23 to 2000-10-03 (NCEI Accession 0113886). NOAA National Centers for Environmental Information, https://doi.org/10.3334/cdiac/otg.carina_58aa20000923, dataset, 2013.

Orr, J. C.: Recent and future changes in ocean carbonate chemistry, In Ocean Acidification, ed. J-P Gattuso, L Hansson, pp. 41–66, Oxford University Press, Oxford, UK, 2011.

Orr, J. C., Fabry, V. J., Aumont, O., Bopp, L., Doney, S. C., Feely, R. A., Gnanadesikan, A., Gruber, N., Ishida, A., Joos, F., Key, R. M., Lindsay, K., Maier-Reimer, E., Matear, R., Monfray, P., Mouchet, A., Najjar, R. G., Plattner, G.-K., Rodgers, K. B., Sabine, C. L., Sarmiento, J. L., Schlitzer, R., Slater, R. D., Totterdell, I. J., Weirig, M.-F., Yamanaka, Y., and Yool, A.: Anthropogenic ocean acidification over the twenty-first century and its impact on calcifying organisms, Nature, 437, 681–686, https://doi.org/10.1038/nature04095, https://doi.org/10.1038/nature04095, 2005.

Orr, J. C., Epitalon, J.-M., Dickson, A. G., and Gattuso, J.-P.: Routine uncertainty propagation for the marine carbon dioxide system, Marine Chemistry, 207, 84–107, https://doi.org/https://doi.org/10.1016/j.marchem.2018.10.006, https://www.sciencedirect.com/science/article/pii/S030442031830149X, 2018.

Østerhus, S. and Gammelsrød, T.: The Abyss of the Nordic Seas Is Warming, Journal of Climate, 12, 3297–3304, https://doi.org/10.1175/1520-0442(1999)012<3297:TAOTNS>2.0.CO;2, https://doi.org/10.1175/1520-0442(1999)012<3297:TAOTNS>2.0.CO;2, 1999.

Oziel, L., Baudena, A., Ardyna, M., Massicotte, P., Randelhoff, A., Sallée, J.-B., Ingvaldsen, R. B., Devred, E., and Babin, M.: Faster Atlantic currents drive poleward expansion of temperate phytoplankton in the Arctic Ocean, Nature Communications, 11, 1705, https://doi.org/10.1038/s41467-020-15485-5, https://doi.org/10.1038/s41467-020-15485-5, 2020.

Pegler, K., Graf, G., and Pfannkuche, O.: Partial pressure (or fugacity) of carbon dioxide, dissolved inorganic carbon, alkalinity, temperature, salinity and other variables collected from discrete sample and profile observations using CTD, bottle and other instruments from the METEOR in the North Atlantic Ocean, North Greenland Sea and Norwegian Sea from 1992-07-01 to 1992-08-31 (NCEI Accession 0113985). NOAA National Centers for Environmental Information., https://doi.org/10.3334/cdiac/otg.carina_06mt19920701, dataset, 2013.

Perez, F. F., Fontela, M., García-Ibáñez, M. I., Mercier, H., Velo, A., Lherminier, P., Zunino, P., de la Paz, M., Alonso-Pérez, F., Guallart, E. F., and Padin, X. A.: Meridional overturning circulation conveys fast acidification to the deep Atlantic Ocean, Nature, 554, 515–518, https://doi.org/10.1038/nature25493, https://doi.org/10.1038/nature25493, 2018.

Raven, J., Caldeira, K., Elderfield, H., Hoegh-Guldberg, O., Liss, P., Riebesell, U., Shepherd, J., Turley, C., and Watson, A.: Ocean acidification due to increasing atmospheric carbon dioxide, Policy document, The Royal Society, London Pp. 1–68, 2005.

Ruiz-Barradas, A., Chafik, L., Nigam, S., and Häkkinen, S.: Recent subsurface North Atlantic cooling trend in context of Atlantic decadal-to-multidecadal variability, Tellus A: Dynamic Meteorology and Oceanography, 70, 1–19, https://doi.org/10.1080/16000870.2018.1481688, https://doi.org/10.1080/16000870.2018.1481688, 2018.

Sarmiento, J. L. and Gruber, N.: Ocean Biogeochemical Dynamics, chap. 8, pp. 318–358, Princeton University Press, Princeton, Woodstock, 2006.

Schauer, U., Jones, E. M., Ulfsbo, A., Hansell, D. A., Smethie, William M., J., Rabe, B., and van Ooijen, J. C.: Discrete, profile measurements of the dissolved inorganic carbon (DIC), total alkalinity, pH on total scale and other hydrographic and chemical data obtained during the PS-94, ARK-XXIX/3, TransArc-II cruise onboard the R/V Polarstern (EXPOCODE 06AQ20150817) in the central Arctic Ocean from 2015-08-17 to 2015-10-15 (NCEI Accession 0170256). NOAA National Centers for Environmental Information., https://doi.org/10.7289/v5319t5z, dataset, 2018.

Shu, Q., Qiao, F., Song, Z., Zhao, J., and Li, X.: Projected Freshening of the Arctic Ocean in the 21st Century, Journal of Geophysical Research: Oceans, 123, 9232–9244, https://doi.org/10.1029/2018JC014036, https://agupubs.onlinelibrary.wiley.com/doi/abs/10.1029/2018JC014036, 2018.

Skjelvan, I., Falck, E., Rey, F., and Kringstad, S. B.: Inorganic carbon time series at Ocean Weather Station M in the Norwegian Sea, Biogeosciences, 5, 549–560, https://doi.org/10.5194/bg-5-549-2008, https://bg.copernicus.org/articles/5/549/2008/, 2008.

Skjelvan, I., Johannessen, T., and Anderson, L. G.: Dissolved inorganic carbon, alkalinity, temperature, salinity and other variables collected from discrete sample and profile observations using CTD, bottle and other instruments from the HAKON MOSBY in the North Greenland Sea and Norwegian Sea from 1994-02-24 to 1994-03-17 (NCEI Accession 0113541). NOAA National Centers for Environmental Information. Dataset., https://doi.org/10.3334/cdiac/otg.carina_58aa19940224, dataset, 2013.

Skjelvan, I., Jeansson, E., Chierici, M., Omar, A., Olsen, A., Lauvset, S., and Johannessen, T.: Havforsuring og opptak av antropogent karbon i de Nordiske hav [Ocean acidification and uptake of anthropogenic carbon in the Nordic Seas], 1981-2013. Miljødirektoratet, Rapport M244-2014, Tech. rep., 2014.

Skjelvan, I., Jones, E., Chierici, M., Frigstad, H., Børsheim, K., Lødemel, H., Kutti, T., King, A., Sørensen, K., Omar, A., Bellerby, R., Christensen, G., Marty, S., Protsenko, E., Mengeot, C., Valestrand, L., Norli, M., Jackson-Misje, K., Apelthun, L., de Lange, T., Johannessen, T., and Mourgues., C.: Monitoring of the ocean acidification in Norwegian seas in 2020, Report, Miljødirektoratet, M-2056, Tech. rep., 2021.

Skogen, M. D., Olsen, A., Børsheim, K. Y., Sandø, A. B., and Skjelvan, I.: Modelling ocean acidification in the Nordic and Barents Seas in present and future climate, Journal of Marine Systems, 131, 10–20, https://doi.org/https://doi.org/10.1016/j.jmarsys.2013.10.005, https://www.sciencedirect.com/science/article/pii/S092479631300211X, 2014.

Skogen, M. D., Hjøllo, S. S., Sandø, A. B., and Tjiputra, J.: Future ecosystem changes in the Northeast Atlantic: a comparison between a global and a regional model system, ICES Journal of Marine Science, 75, 2355–2369, https://doi.org/10.1093/icesjms/fsy088, https://doi.org/10.1093/icesjms/fsy088, 2018.

Somavilla, R., Schauer, U., and Budéus, G.: Increasing amount of Arctic Ocean deep waters in the Greenland Sea, Geophysical Research Letters, 40, 4361–4366, https://doi.org/10.1002/grl.50775, https://agupubs.onlinelibrary.wiley.com/doi/abs/10.1002/grl.50775, 2013.

Stöven, T., Tanhua, T., Hoppema, M., and von Appen, W.-J.: Transient tracer distributions in the Fram Strait in 2012 and inferred anthropogenic carbon content and transport, Ocean Science, 12, 319–333, https://doi.org/10.5194/os-12-319-2016, https://os.copernicus.org/articles/12/319/2016/, 2016.

Takahashi, T., Olafsson, J., Goddard, J. G., Chipman, D. W., and Sutherland, S. C.: Seasonal variation of CO_2 and nutrients in the high-latitude surface oceans: A comparative study, Global Biogeochemical Cycles, 7, 843–878, https://doi.org/10.1029/93GB02263, https://agupubs.onlinelibrary.wiley.com/doi/abs/10.1029/93GB02263, 1993.

Takahashi, T., Sutherland, S. C., Sweeney, C., Poisson, A., Metzl, N., Tilbrook, B., Bates, N., Wanninkhof, R., Feely, R. A., Sabine, C., Olafsson, J., and Nojiri, Y.: Global sea–air CO2 flux based on climatological surface ocean pCO2, and seasonal biological and temperature effects, Deep Sea Research Part II: Topical Studies in Oceanography, 49, 1601–1622, https://doi.org/https://doi.org/10.1016/S0967-0645(02)00003-6, https://www.sciencedirect.com/science/article/pii/S0967064502000036, the Southern Ocean I: Climatic Changes in the Cycle of Carbon in the Southern Ocean, 2002.

Tanhua, Toste; Hoppema, M.: Dissolved Inorganic Carbon (DIC), Total Alkalinity, Oxygen and other Hydrographic and Chemical Data Obtained During the R/V Polarstern Cruise ARKXXVII/1 (EXPOCODE 06AQ20120614) along the CLIVAR Repeat Section 75N in the North Atlantic Ocean from 2012-06-14 to 2012-07-15 (NCEI Accession 0162432). NOAA National Centers for Environmental Information., dataset, 2017.

Taylor, K. E., Stouffer, R. J., and Meehl, G. A.: An Overview of CMIP5 and the Experiment Design, Bulletin of the American Meteorological Society, 93, 485–498, https://doi.org/10.1175/BAMS-D-11-00094.1, https://doi.org/10.1175/BAMS-D-11-00094.1, 2012.

Terhaar, J., Kwiatkowski, L., and Bopp, L.: Emergent constraint on Arctic Ocean acidification in the twenty-first century, Nature, 582, 379–383, https://doi.org/10.1038/s41586-020-2360-3, https://doi.org/10.1038/s41586-020-2360-3, 2020a.

Terhaar, J., Tanhua, T., Stöven, T., Orr, J. C., and Bopp, L.: Evaluation of Data-Based Estimates of Anthropogenic Carbon in the Arctic Ocean, Journal of Geophysical Research: Oceans, 125, e2020JC016 124, https://doi.org/https://doi.org/10.1029/2020JC016124, https://agupubs.onlinelibrary.wiley.com/doi/abs/10.1029/2020JC016124, e2020JC016124 10.1029/2020JC016124, 2020b.

Terhaar, J., Torres, O., Bourgeois, T., and Kwiatkowski, L.: Arctic Ocean acidification over the 21st century co-driven by anthropogenic carbon increases and freshening in the CMIP6 model ensemble, Biogeosciences, 18, 2221–2240, https://doi.org/10.5194/bg-18-2221-2021, https://bg.copernicus.org/articles/18/2221/2021/, 2021.

Tjiputra, J. F., Assmann, K., and Heinze, C.: Anthropogenic carbon dynamics in the changing ocean, Ocean Science, 6, 605–614, https://doi.org/10.5194/os-6-605-2010, https://os.copernicus.org/articles/6/605/2010/, 2010.

Tjiputra, J. F., Roelandt, C., Bentsen, M., Lawrence, D. M., Lorentzen, T., Schwinger, J., Seland, Ø., and Heinze, C.: Evaluation of the carbon cycle components in the Norwegian Earth System Model (NorESM), Geoscientific Model Development, 6, 301–325, https://doi.org/10.5194/gmd-6-301-2013, https://gmd.copernicus.org/articles/6/301/2013/, 2013.

Tjiputra, J. F., Grini, A., and Lee, H.: Impact of idealized future stratospheric aerosol injection on the large-scale ocean and land carbon cycles, Journal of Geophysical Research: Biogeosciences, 121, 2–27, https://doi.org/https://doi.org/10.1002/2015JG003045, https://agupubs.onlinelibrary.wiley.com/doi/abs/10.1002/2015JG003045, 2016.

Turley, C. M., Roberts, J. M., and Guinotte, J. M.: Corals in deep-water: will the unseen hand of ocean acidification destroy cold-water ecosystems?, Coral Reefs, 26, 445–448, https://doi.org/10.1007/s00338-007-0247-5, https://doi.org/10.1007/s00338-007-0247-5, 2007.

Uppström, L. R.: The boron/chlorinity ratio of deep-sea water from the Pacific Ocean, Deep Sea Research and Oceanographic Abstracts, 21, 161 – 162, https://doi.org/https://doi.org/10.1016/0011-7471(74)90074-6, http://www.sciencedirect.com/science/article/pii/0011747174900746, 1974.

van Heuven, S., Pierrot, D., Rae, J., Lewis, E., and Wallace, D.: MATLAB Program Developed for CO_2 System Calculations, ORNL/CDIAC-105b. Carbon Dioxide Information Analysis Center, Oak Ridge National Laboratory, US Department of Energy, Oak Ridge, Tennessee., 2011.

van Vuuren, D. P., Edmonds, J., Kainuma, M., Riahi, K., Thomson, A., Hibbard, K., Hurtt, G. C., Kram, T., Krey, V., Lamarque, J.-F., Masui, T., Meinshausen, M., Nakicenovic, N., Smith, S. J., and Rose, S. K.: The representative concentration pathways: an overview, Climatic Change, 109, 5, https://doi.org/10.1007/s10584-011-0148-z, https://doi.org/10.1007/s10584-011-0148-z, 2011a.

van Vuuren, D. P., Stehfest, E., den Elzen, M. G. J., Kram, T., van Vliet, J., Deetman, S., Isaac, M., Klein Goldewijk, K., Hof, A., Mendoza Beltran, A., Oostenrijk, R., and van Ruijven, B.: RCP2.6: exploring the possibility to keep global mean temperature increase below 2°C, Climatic Change, 109, 95, https://doi.org/10.1007/s10584-011-0152-3, https://doi.org/10.1007/s10584-011-0152-3, 2011b.

Våge, K., Pickart, R. S., Spall, M. A., Moore, G., Valdimarsson, H., Torres, D. J., Erofeeva, S. Y., and Nilsen, J. E. Ø.: Revised circulation scheme north of the Denmark Strait, Deep Sea Research Part I: Oceanographic Research Papers, 79, 20 – 39, https://doi.org/https://doi.org/10.1016/j.dsr.2013.05.007, http://www.sciencedirect.com/science/article/pii/S0967063713001040, 2013.

Våge, K., Moore, G., Jónsson, S., and Valdimarsson, H.: Water mass transformation in the Iceland Sea, Deep Sea Research Part I: Oceanographic Research Papers, 101, 98 – 109, https://doi.org/https://doi.org/10.1016/j.dsr.2015.04.001, http://www.sciencedirect.com/science/article/pii/S0967063715000680, 2015.

Wallace, D. W. R. and Deming, J.: Dissolved inorganic carbon, alkalinity, temperature, salinity and other variables collected from discrete sample and profile observations using CTD, bottle and other instruments from the USCGC POLAR SEA in the North Greenland Sea from 1992-07-15 to 1992-08-14 (NCEI Accession 0115687). NOAA National Centers for Environmental Information., https://doi.org/10.3334/cdiac/otg.carina_32l919920715, dataset, 2014.

Woosley, R. J. and Millero, F. J.: Freshening of the western Arctic negates anthropogenic carbon uptake potential, Limnology and Oceanography, 65, 1834–1846, https://doi.org/https://doi.org/10.1002/lno.11421, https://aslopubs.onlinelibrary.wiley.com/doi/abs/10.1002/lno.11421, 2020.

Wu, Y., Hain, M. P., Humphreys, M. P., Hartman, S., and Tyrrell, T.: What drives the latitudinal gradient in open-ocean surface dissolved inorganic carbon concentration?, Biogeosciences, 16, 2661–2681, https://doi.org/10.5194/bg-16-2661-2019, https://bg.copernicus.org/articles/16/2661/2019/, 2019.

Yukimoto, S., Yoshimura, H., and Hosaka, M.: Meteorological Research Institute-Earth System Model v1 (MRI-ESM1)—Model Description.Technical Report of MRI. Ibaraki, Japan, 88 pp., Tech. rep., 2011.

Zeebe, R. and Wolf-Gladrow, D.: CO_2 in Seawater: Equilibrium, Kinetics, Isotopes, vol. 65 of *Elsevier Oceanography Series*, Elsevier Science, 1 edn., 2001.

Zheng, M.-D. and Cao, L.: Simulation of global ocean acidification and chemical habitats of shallow- and cold-water coral reefs, Advances in Climate Change Research, 5, 189–196, https://doi.org/https://doi.org/10.1016/j.accre.2015.05.002, https://www.sciencedirect.com/science/article/pii/S1674927815000210, including special topic on China's carbon emissions peaking, 2014.